1-1-2015

Efficient Utilization of Solar Energy in Dye-Sensitized Solar Cells and in the Photocatalytic Reduction of Carbon Dioxide

Aron Joel Huckaba
University of Mississippi

EFFICIENT UTILIZATION OF SOLAR ENERGY IN DYE-SENSITIZED SOLAR CELLS AND IN THE PHOTOCATALYTIC REDUCTION OF CARBON DIOXIDE

A Dissertation
presented in partial fulfillment of requirements
for the degree of Doctor of Philosophy
in the Department of Chemistry and Biochemistry
The University of Mississippi

By

ARON J. HUCKABA

May 2015

ABSTRACT

One of the most important questions humanity will face in the next 100 years is going to be "What will happen when oil runs out?" This dissertation describes efforts to utilize solar energy to improve renewable energy technology in two ways: First, through the improvement of dye sensitized solar cells by the improvement of D-π-A dye subunits, the development of practical sensitizers, and progress towards stable, tunable redox shuttles. A novel indolizine donor subunit was synthesized that was shown to be the strongest reported donor. Dyes made from this novel donor and devices using the I^-/I_3^- reached up to 5.4% efficiency. This donor was then systematically improved by the addition of non-conjugated substituents, which acted as good surface blocking groups and thus facilitated high performance during device testing. Dyes made using this donor and devices using the I^-/I_3^- redox shuttle reached up to 6.7% efficiency. Second, this thesis describes efforts to close the carbon cycle through utilization of solar energy in CO_2 reduction. The described efforts regard the improvement of known catalysts through increased stability and performance, and of the use of a simulated solar spectrum to improve the practicality of photocatalytic CO_2 reduction. By the substitution of a pyridyl chelating group for an N-Heterocyclic Carbene (NHC) ligand, the synthesized complexes were more stable while still absorbing visible light. The synthesized complexes operated as photocatalysts with *or without* a photosensitizer, making this the fourth reported series of non-sensitized photocatalysts for CO_2 reduction.

DEDICATION

This dissertation is dedicated to everyone who helped me towards the goal of achieving my doctorate. I want to especially thank my wife, Amy, whose love and support made this achievement possible.

LIST OF ABBREVIATIONS AND SYMBOLS

B.C.	Before Christ
PV	Photovoltaic
U.S.	United States
DSC	Dye-Sensitized Solar Cell(s)
η	Power Conversion Efficiency
FF	Fill Factor
V_{oc}	Open Circuit Voltage
J_{sc}	Short Circuit Current
I_0	Intensity of Incident Light
CT	Charge Transfer
PCE	Power Conversion Efficiency
HOMO	Highest Occupied Molecular Orbital
LUMO	Lowest Unoccupied Molecular Orbital
UV	Ultraviolet
NIR	Near-IR
TPA	Triphenylamine
D-π-A	Donor-π-Bridge-Acceptor
T-CAA	Thiophene-cyanoacrylic Acid
EDG	Electron-Donating Group
DABCO	1,4-diazabicyclo[2.2.2]octane

NMP	N-Methyl-2-pyrrolidone
Cy	Cyclohexyl
THF	Tetrahydrofuran
KOAc	Potassium Acetate
dppp	1,3-Bis(diphenylphosphino)propane
UV-Vis	Ultraviolet-Visible
λ_{max}	Wavelength of Lowest Energy Absorption
λ_{onset}	Wavelength of Lowest Energy Absorption Onset
ε	Molar Absorptivity
$E_{(0\text{-}0)}$	Optical Bandgap
$E_{(S+/S)}$	Ground State Oxidation Potential
$E_{(S+/S^*)}$	Excited State Oxidation Potential
NHE	Normal Hydrogen Electrode
EWG	Electron-Withdrawing Group
$\Delta\lambda_{onset}$	Change in the Wavelength of Lowest Energy Absorption Onset
ΔG_{reg}	Gibbs' Free Energy of Regeneration
ΔG_{inj}	Gibbs' Free Energy of Injection
IR	Infrared
DFT	Density Functional Theory
TD-DFT	Time Dependent Density Functional Theory

η_{eff}	Electron Injection Efficiency
τ_{TiO2}	Excited State Lifetime on TiO_2
τ_{sol}	Excited State Lifetime in solution
CDCA	Chenodeoxycholic Acid
MeCN	Acetonitrile
IPCE	Incident Photon-to-Electric Conversion Efficiency
EAS	Electrophilic Aromatic Substitution
HWE	Horner-Wadsworth-Emmonds
DSSC	Dye-Sensitized Solar Cell
LED	Light Emitting Diode
TLC	Thin Layer Chromatography
NMR	Nuclear Magnetic Resonance
LDA	Lithium Diisopropyl Amide
Pyr	Pyridine
CPDT	4H-cyclopenta[2,1-b:3,4-b]dithiophene
BDT	Benzo[1,2-b:4,5-b']dithiophene
DMF	N,N-dimethylformamide
EtOAc	Ethyl Acetate
Et_2O	Diethyl Ether
DBU	1,8-Diazabicyclo[5.4.0]undec-7-ene
CB	Conduction Band

MeOH	Methanol
SiO_2	Silica Gel
KOtBu	Potassium tert-butoxide
D-A-π-A	Donor-Acceptor-π-Bridge-Acceptor
D-π-A-A	Donor-π-Bridge-Acceptor-Acceptor
AIBN	Azobisisobutyronitrile
BuLi	Butyl Lithium
EDOT	3,4-ethylenedioxythiophene
DMAD	Dimethylactylenedicarboxylate
MLCT	Metal-to-Ligand Charge Transfer
EBT	Eriochrome Black T
EBB	Eriochrome Blue Black B
SET	Single Electron Transfer
J_{lim}	Limiting Current Density
ε_p	Porosity
F	Faraday
D_o	Diffusion Coefficient
$[R^+]$	Concentration of Oxidized Redox Shuttle
l	Electrolyte Diffusion Difference
U_{rec}	Recombination
k_{rec}	Recombination Rate

n_s	Concentration of Free Electrons at the Electrode Surface
NHC	N-Heterocyclic Carbene
bpy	2,2'-bipyridyl
Φ_{CO}	Quantum Yield of CO
BIH	1,3-dimethyl-2-phenyl-2,3-dihydro-1H-benzo[d]imidazole
PS	Photosensitizer
TON	Turnover Number
TEA	Triethylamine
TEOA	Triethanolamine
CV	Cyclic Volttametry *or* Cyclic Voltammogram
TMEDA	tetramethylethylenediamine
dipic	pyridine dipicolinate
NP	Nanoparticle
GC	Gas Chromatography
HPLC	High-Performance Liquid Chromatography
DMA	N,N'-dimethylacetamide
DMSO	Dimethylsulfoxide
BNAH	1-Benzyl-1,4-dihydronicotinamide
T_o	Initial Condition
FID	Flame Ionization Detector
TCD	Thermal Conductivity Detector

ACKNOWLEDGMENTS

I extend all the grateful appreciation I can muster to my advisor, Dr. Jared Delcamp, who trained me, taught me, and invested himself in my success. I would also like to thank my committee members Dr. Nathan Hammer, Dr. Amal Dass, Dr. John Rimoldi, and Dr. Walt Cleland for their time, advice, and collaboration.

I would also like to thank my graduate student colleagues who helped, collorated with, and supported me along the way. Lastly, I'd like to thank the NSF MS EPSCoR program for that allowed me to research full time during my last two years here.

TABLE OF CONTENTS

LIST OF TABLES

LIST OF FIGURES

LIST OF SCHEMES

INTRODUCTION

INTRODUCTION TO THE HISTORY OF ENERGY

Since the discovery of fire, people have searched for sources of energy to improve standards of living or to aid human endeavors. Prior to the 19th century, woody material comprised the most of the world's accessible energy reserves. While early accounts indicate that man utilized coal as early as 1000 B.C.,[1] poor extraction technique left most of the useful material—and the feasibility of coal energy—behind. In the middle of the 19th century, the industrial revolution required more powerful energy sources and thus the movement was built largely on coal, whale oil, and petroleum.

Because whale oil was difficult to obtain and its supply waned with the population of whales, it fell out of use quickly. Better mining and extraction processes have led to the ubiquitous use of coal, natural gas, and petroleum as the modern world's primary sources of fuel. Even so, the overall supply of each resource above is finite. Furthermore, just as whale oil's use met its end with increasing prices and dwindling supply, so too must happen (eventually) to each. The timeline of such a decline is hotly debated at present, but some estimates say oil could run out in the next 100 years. The decline of supply (as well as rising prices) is a major influence in the quest to find renewable energy sources that are feasible for widespread use.

A myriad of renewable energy sources exist, including wind, hydrothermal, geothermal, and solar power. Wood burning is also technically a renewable resource, however, it is not feasible or sustainable for widespread use. Solar energy is very promising in that each year, the sun irradiates the earth with $3x10^{21}$ kJ of energy, which equates to roughly 10,000 times annual global consumption.[2] While much research is concerned with advancing each type of renewable energy source, only solar energy will be discussed here further.

Humans have utilized solar energy (excluding agriculture) purely as a heat source even as early as the 7th century B.C. with the invention of the magnifying glass. Perhaps the most famous early use of the suns thermal power came in the 2nd century B.C. As the story goes, a fleet of Roman ships besieged Syracuse and Archimedes used bronze shields to focus the sun's power into a highly intense beam to set fire to the wooden ships (Note: No definite proof of this feat exists, however, it is possible to set fire to wooden ships in the same manner at a distance of 50m).[3]

Solar power went largely underutilized until 1839 when Edmond Bacquerel discovered that an electrolytic cell's electricity generation increased when exposed to light. This phenomenon was termed the photoelectric effect. It would be another 115 years until scientists brought forth a solar cell able to power everyday electrical appliances-- the Si photovoltaic (PV) cell developed by Fuller, Chapin, and Pearson of Bell Laboratories. It is useful to note that photovoltaics found use immediately for space application, as early satellites did not need much power and panels were not very heavy. Terrestrial cells, however, were developed much more slowly.

The early (1956) terrestrial cells were capable of nearly 2% efficiency and 10W on a bright day. Ten years later, efficiency crept to 5% with Sharp outfitting Ogami Island Japan's lighthouses with the largest (225 W) solar module of the time.[3b] The energy generated from these systems has been estimated to be about $100/Watt. The energy crisis of the 1970s further spurred the pursuit of affordable solar technology, with 6% modules being sold for nearly $20/Watt (in large quantities). In the middle of the 1970s, the U.S. government began investing in solar power application and through purchasing nearly 200 kW, by 1979 the efficiency had improved to 8.4% and the price to $12-$18/Watt.[3b]

With the start of the 1980s, funding had begun to diminish for fundamental solar cell development. Many manufacturing innovations had increased the durability dramatically, and engineering of the crystalline Si wafers also led to large increases in efficiency (up to 10% in 1985). By the end of 1997, further engineering innovation led to the announcement of a commercial module with 15% efficiency, and in 2004 it was announced that a 16% efficiency module was being produced. Projections indicate that module prices should continue to fall with increased scale of manufacture and decreasing silicon wafer widths,[3b] a rate that so far has followed Swanson's Law.[4] Whether the price decrease continues that trend remains to be seen, however, it should be noted that Swanson himself questioned if the continued trend would continue much farther past 2012.[4]

While Si PV modules exhibit efficiencies now greater than 16% at a commercial level (for research cell efficiencies, see Figure 1), the initial cost of installation is prohibitive. The reason for the high initial cost of production is that most manufacturing processes require large

energy and time input to produce high quality cells. The modules are also fragile, as the best performing devices are single Si crystals. As long as the panel does not suffer damage, modules can operate indefinitely with a median 0.5% decrease in power output per year.[5]

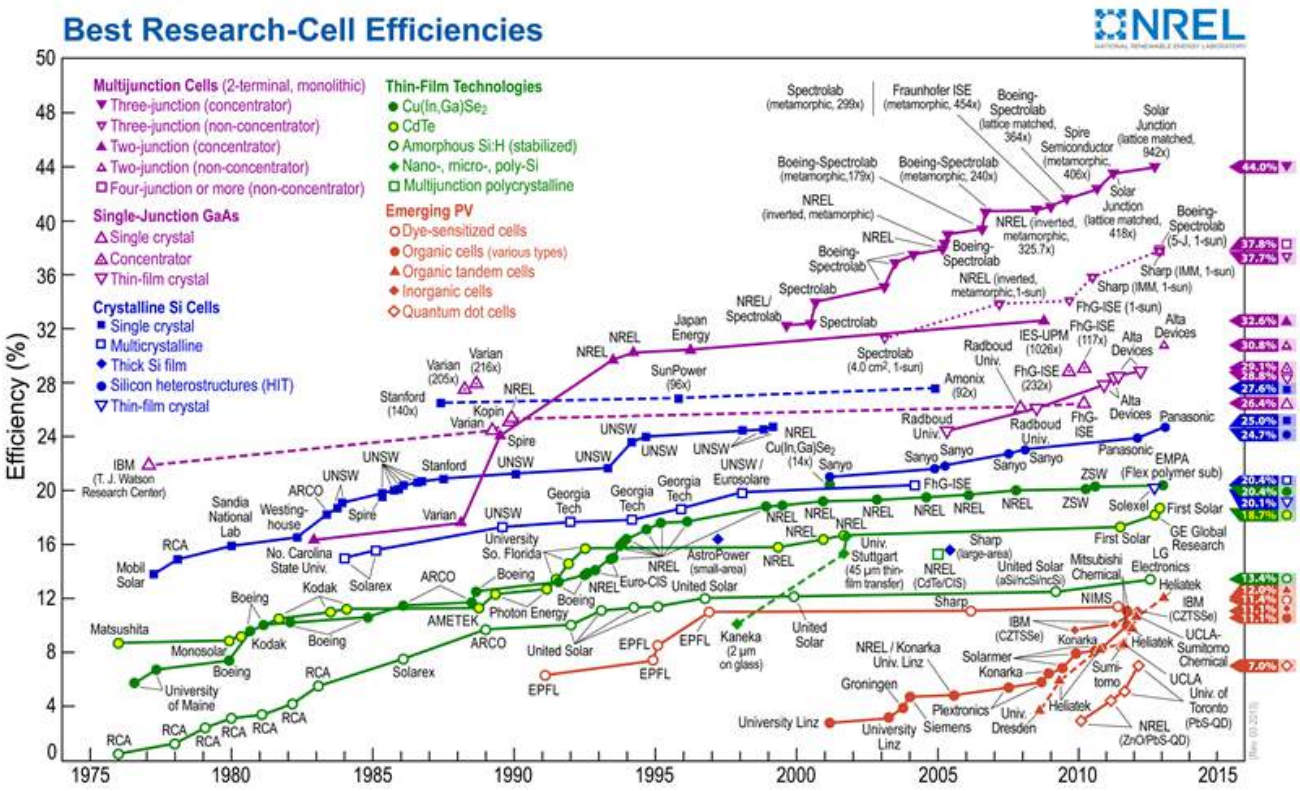

Figure 1. A graph of the best research-cell efficiencies, compiled by the National Renewable Energy Laboratories. This plot is courtesy of the National Renewable Energy Laboratory, Golden, CO.

As showcased above, manufacturing advances over the first 50 years of production have led to the increase in viability of Si photovoltaics for large-scale use. However, solid-state photoelectrochemical cells like Si PV are not the only hope for solar energy. In fact, the opinion

of nanocrystalline or conductive polymer devices are improving due to their potentially low fabrication cost, flexibility, and tinting capability (useful for transparent or near-transparent architectural or device applications). The rest of this work's solar photovoltaics focus will be on dye-sensitized solar cells (DSC).

INTRODUCTION TO DYE SENSITIZED SOLAR CELLS

The concept of a dye-sensitized cell came about in 1883 with Vogel's discovery that silver halide emulsions could absorb visible light past 460 nm with the addition of a sensitizing dye. This description was important in regards to photography; however, four years later Moser used the same principle to construct a photoelectrochemical cell from erythrosine and silver halide electrodes. It would be another eighty years before the sensitization process (in both photography and photoelectrochemical cells) was confirmed to include primarily electron transfer from dye to semiconductor.[2]

The modern era of DSC started in 1991 with Grätzel and O'Regan's first communication of a 7.2% eifficiency cell based on dye-sensitized colloidal-TiO_2 films.[6] A schematic of the principle of operation of a DSC is shown in Figure 2. In a DSC, dye molecules adsorbed onto the TiO_2 film's surface absorb light and subsequently inject an electron into the TiO_2 conduction band. With injection, the dye is oxidized and is regenerated to the ground state by the redox electrolyte. With regeneration of the dye, the redox electrolyte becomes oxidized and is in turn regenerated by electrons from the counter electrode, which completes the circuit. The overall efficiency of the DSC (η) is determined by the following (simplified) equation:

$$\eta = (FF \times V_{oc} \times J_{sc})/I_0 \qquad (1)$$

where FF is the fill factor, V_{oc} is the open circuit voltage, and J_{sc} is the short circuit current. The expanded equations for each term, the kinetics governing each, and the relevant issues in maximizing all three will not be covered here, however, each has been covered in reviews by Hagfeldt[7] and Grätzel.[8] While attempts to use dye-sensitized cells had been undertaken before

Grätzel and O'Regan's publication, efficiencies had been too low to render DSC a viable competitor to Si PV cells. In their publication, the two authors addressed two very important problems.

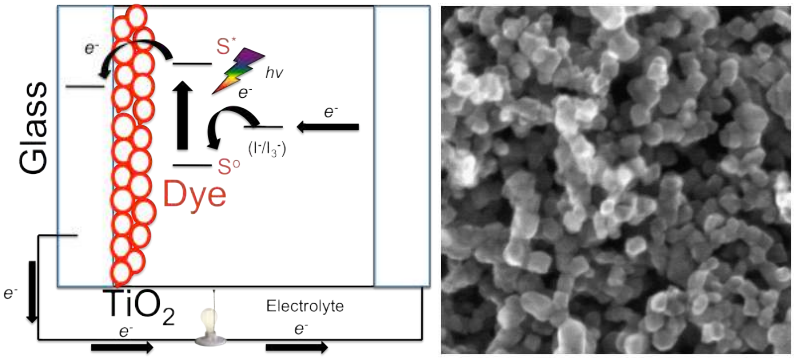

Figure 2. *Left:* Principle of operation of a DSC. *Right:* Transmission electron micrograph of nanometer-sized anatase TiO_2 colloid used for DSC. Reprinted with permission from Gratzel, M. *Journal of Photochemistry and Photobiology C: Photochemistry Reviews* **2003**, 4, 145. Copyright 1991 Elsevier.[6,7,8]

The first was that of light harvesting. With smooth surfaces, a monomolecular layer of sensitizing dye absorbed less than 1% of available light. By using a sintered nanometer-sized TiO_2 semiconductor film, the surface area was greatly improved, which allowed for much greater quantities of dye to be adsorbed while also remaining in contact with the electrolyte solution. A transmission electron micrograph of the surface of the mesoporous TiO_2 film described is presented in Fig 2.[6]

The second important problem to be addressed was that of dye stability. Previous attempts to sensitize semiconductor films had utilized dyes such as Rose Bengal, which brought the efficiencies of these early DSC to less than 1%. The dye proposed for use by Grätzel and

O'Regan was a Ru metal-complex dye anchored to the TiO_2 surface with carboxylic acid functionalities (Figure 3).[6] The Ru dye's longest wavelength (lowest energy) absorption is the result of charge transfer (CT), in which the ground-state of the molecule contains no charged species (other than the metal ion) but the excited state harbors both a discreet positive and negative charge. The CT absorption band drives electron injection, as the discreet negative charge lies very near the TiO_2 surface, while the discreet positive charge lies far from the surface.

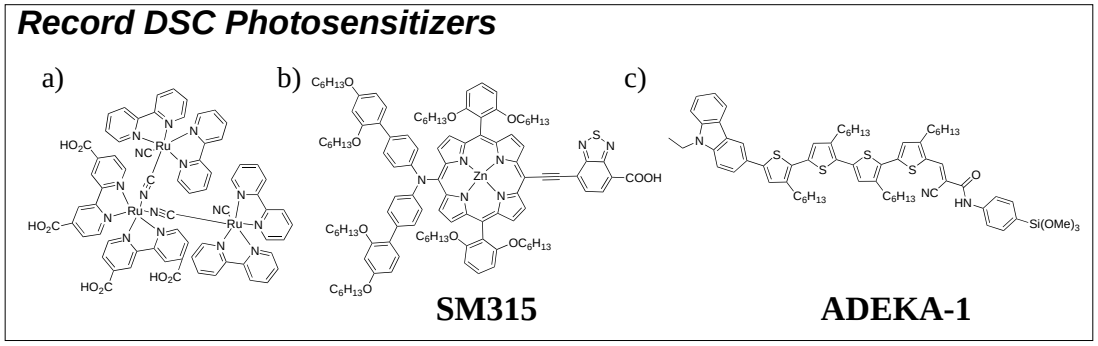

Figure 3. Chemical structures of a) Grätzel's trimeric Ru dye, b) current metalized dye record-holder **SM315**, and c) current organic dye record-holder **ADEKA-1**.

Since the seminal article, research in DSC has grown considerably and much progress has been achieved. Currently, the best metal containing dye (SM315,[9] Figure 3) exhibited a 13% power conversion efficiency (PCE, equivalent to η), while the best all organic dye (ADEKA-1,[10] Figure 3) exhibited a PCE of 12.5%. Both state-of-the-art dyes highlighted here were published very recently, which demonstrates the continued need and utility of high quality synthetic dyes. Future potential dye targets should ideally conform to a set of parameters designed to give DSC the leg up it needs to be a feasible solar energy technology.

First, the ideal photosensitizer should absorb all light in the standard solar AM 1.5 spectrum[11] up to a wavelength of 920 nm. The sun's solar spectrum extends much further than 920 nm, but energetically the dyes are theoretically limited to about this wavelength. Second, the dye must contain (at least one) functional group capable of allowing adsorption onto a TiO_2 surface, such as carboxylate, phosphate, silylalkoxy, or sulfonate groups. Third, the dye must inject absorbed photons into the TiO_2 conduction band with a quantum yield of unity. Fourth, the dye must have energy levels (HOMO and LUMO) that are well matched for electron injection from the excited state and regeneration from the ground-state. Lastly, the ideal dye should be stable to at least 10^8 turnover cycles, which equates to 20 years of continual device operation.[7,12]

These dye guidelines allow for synthetic chemists to understand the benchmarks by which the greater community will judge their work and planning that is represented by the efficiencies their dyes reach.[13] For the DSC portion of this work, the emphasis will be on dye synthesis, as the dye inside of a DSC is the most costly and also the most responsible for device performance. Thus, the development of highly performing, synthetically simple dyes will allow DSC to overtake Si-PV as the best option for solar energy.

INTRODUCTION TO PHOTOCATALYTIC CARBON DIOXIDE REDUCTION

Since at least May 2006, the amount of carbon dioxide in earth's atmosphere has become a polarizing political figure, due to its implication in global warming. The debate (the political nature of which and the arguments from both sides are outside the scope of this work) surrounding the level of CO_2 in Earth's atmosphere centers on the gas's origin. As an integral part of the carbon cycle, CO_2 is needed to ensure each of Earth's ecosystems has enough carbon to sustain it. While the carbon cycle is a natural phenomenon known since the days of Priestley and Lavoisier, man's contribution to the atmospheric total is the debated factor. As illustrated in Figure 4, the amount of CO_2 in the atmosphere has increased each year since the Scripps Institution of Oceanography has started monitoring in 1958.

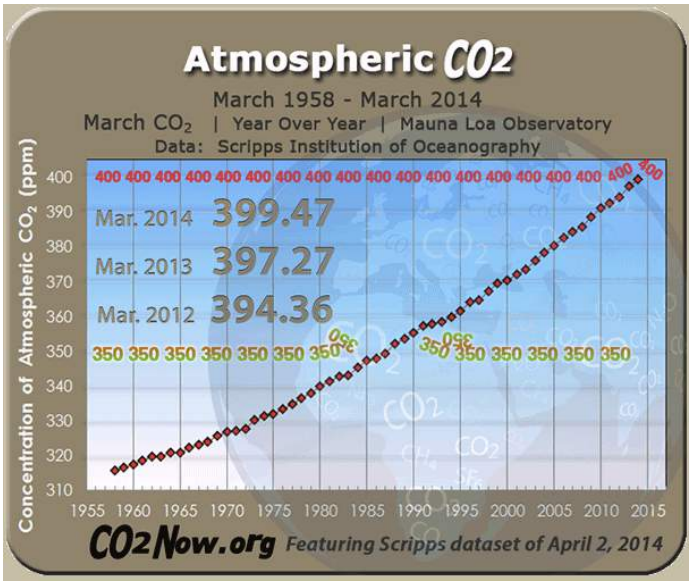

Figure 4. Carbon dioxide level in Earth's atmosphere in March 2014 as reported by Scripps Institution of Oceanography.

According to a recent measurement in May 2014, CO_2 resides in the atmosphere at 401.18 ppm.[14] This level is 51.18 ppm above 350 ppm, or what many experts consider as a safe level of atmospheric CO_2. Because this work's aim ultimately hopes to reduce the amount of CO_2 by developing catalysts that can react CO_2 at its source (while also generating useful chemical intermediates or liquid fuels), determining how far from a safe level we are is important.

Taking the mass of Earth's atmosphere as 5.132×10^{18} kg, then the total mass of CO_2 in the atmosphere is 2,068 Tt.[15] It follows then that the mass of CO_2 we need to remove from the atmosphere (as of May 2014) to return to 350 ppm is 262 Tt of CO_2. This figure, while accurate, is also misleading (aside from the problem of CO_2 concentration continuing to rise), as 262 Tt of any solid or liquid would be at best intractable. This, then, means that any process converting CO_2 into another chemical needs to take into account the problem of scale in order to be practical or useful. Simple organometallic chemistry would suggest that using Grignard reagents or lithiated hydrocarbons might be a useful way to remove CO_2, but aside from needing vast quantities of these extremely reactive reagents, the products of these stoichiometric reactions (meaning reactant and product ratios are whole number integers) are solid ionic salts and liquids.

In order to mitigate the problems of scale, then, catalytic processes for reducing CO_2 are needed. The energy source for reduction can be electricity (electrocatalysis), solar energy (photocatalysis). In electrical catalysis, electrons provided by the working electrode fuel the catalytic cycle; however, the reaction is also spatially dependent as the requisite electrons can only be transferred to the catalyst within close proximity of the electrode (Figure 5). In photocatalysis, photons fuel the catalytic cycle, and the catalytic cycle is completed by electron

transfer from sacrificial reductant molecules (Figure 5). Currently, no "best" method for CO_2 utilization exists, even though much research on catalytic processes is ongoing throughout the world (only 1% of CO_2 on earth is being used in synthesis).[16] Because of the aforementioned scale issues, the ideal photocatalytic process would draw the required electrons and protons (Figure 5) from H_2O.

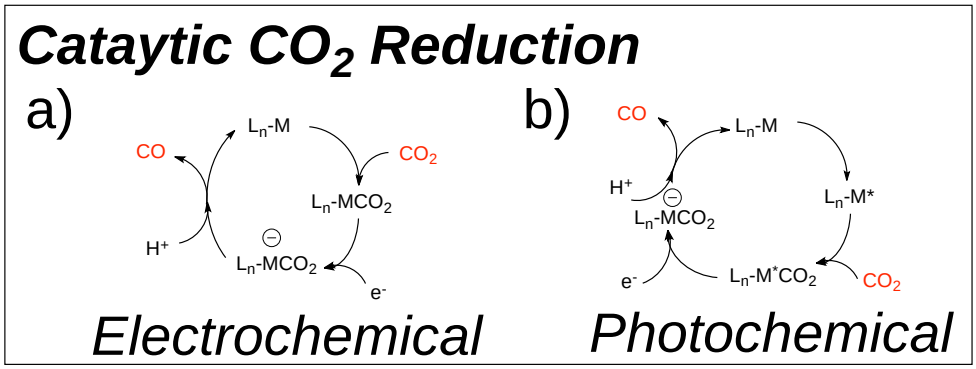

Figure 5. Two general methods for CO_2 reduction: a) electrocatalysis. b) photocatalysis.

All three routes could play important roles in reducing atmospheric CO_2 levels. Catalytic processes can produce valuable chemical feedstocks such as: lactones, carboxylic acids, acrylates, and more.[16-17] Electrocatalytically, CO_2 can be changed selectively into CO, which can be utilized directly in the Fischer-Tropsch process to generate liquid fuels to help offset the energy cost associated with bulk electrolysis. Photocatalytic processes also generate CO and use sunlight as an integral part of the catalytic cycle. Photocatalysis offers a truly sustainable catalytic process. Because of this marked advantage, it will be the focus of this work.

Perhaps one of the biggest problems facing photocatalytic CO_2 reduction research is that homogeneous catalysts should both absorb visible light and interact with CO_2. Transition metal complexes often have color, however, not many transition metal complexes are capable of interacting with CO_2. In fact, there are only three series of metal complexes reported to do both the jobs of absorbing visible light and reducing CO_2 (a literature search will show that porphyrin metal complexes have been reported to reduce CO_2 with UV light and that several electrocatalysts have been photosensitized) (Figure 6). The first to be reported was based on Re (I) bipyridyl complexes,[18] while the others are based on cyclometallated Ir (III) catalysts.[19] The Re catalyst is capable of 27 turnovers in four hours; however, the catalyst is not active after that time. Similarly, the Ir catalyst is capable of 40 turnovers in the same amount of time but is inactive thereafter. Thus, the problem of CO_2 photoreduction remains to be solved. In order to do so, new light absorbing, CO_2 interacting catalysts must be synthesized.

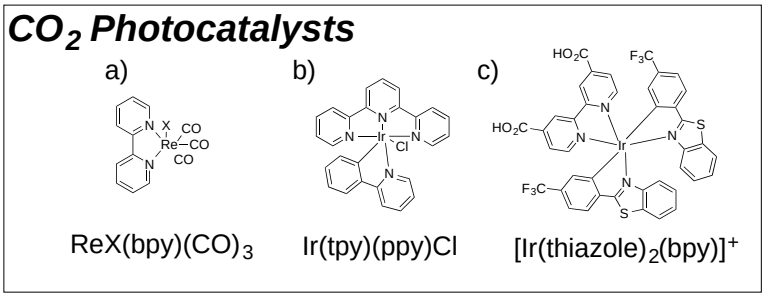

Figure 6. The molecular structures of: a): The first photocatalytic CO_2 reduction catalyst, $ReX(bpy)(CO)_3$. b): Ir(tpy)(ppy)Cl catalyst reported by Ishitani. c): $[Ir(thiazole)_2(bpy)]^+$ catalyst reported by Zhou.

CHAPTER 1

SECTION 1

INDOLIZINE-BASED DONORS AS ORGANIC SENSITIZER COMPONENTS FOR DYE-SENSITIZED SOLAR CELLS

INTRODUCTION

Dye-sensitized solar cells (DSCs) have undergone continuous improvements since their introduction in 1991.[2] DSCs have already extended into the solar energy conversion market due to their high solar-to-electric power conversion efficiencies (PCEs) and relative affordability.[3,13] Despite their tremendous success so far, several key aspects of DSCs could benefit from additional improvements, including conversion of near-IR (NIR) photons and price of sensitizers.[20] Often cited as cost-effective alternatives to metal-based sensitizers, organic sensitizers have been a key focus within DSC development.[13] These sensitizers have remarkable tunability and have been demonstrated to productively utilize NIR photons up to 1000 nm.[21] Organic sensitizers have seen continuous improvements leading to PCEs of >12% since the inception of DSCs.[10]

The most common organic dye structure is the proven donor-π bridge-acceptor (D-π-A) configuration. Research with regard to the donor fragment has proven instrumental in increasing organic sensitizer-based DSC PCE values to >10%.[22] High-efficiency NIR absorbing D-π-A dyes require balanced donor and acceptor strengths to avoid non-beneficial energy level perturbations. Frequently, strongly electron deficient motifs (acceptors) result in excited-state

oxidation potentials that are too stabilized for electron injection into the TiO_2 conduction band rendering these dyes non-functional. Accordingly, there is a vast need for stronger organic electron-donor materials to be matched with many of the common electron deficient DSC π-bridge-acceptor motifs.[23] We examined for the first time in DSC devices a fully-conjugated planar nitrogen-containing donor, indolizine, in model visible light absorbing systems.

Nearly all-organic sensitizers with >10% PCE utilize arylamine donors, either as triphenylamine, diphenylamine, or indoline. However, these donor systems are not ideal since the electron donation strength is mitigated by three main factors: (1) weak donation directionality to the dye acceptor, (2) large energy barriers to charge transfer due to the breaking of phenyl resonance stabilization energy to access the dye excited-state, and (3) non-optimal nitrogen lone pair orbital alignment with the dye π-conjugated system due to sterically induced twist angles. These mitigating factors can be substantially reduced through designing planar fully-conjugated nitrogen-containing donor building blocks for dyes, such as indolizine-based donors. For the first time in DSCs, we have examined indolizine in model dye systems (Figure 7). When compared computationally to triphenylamine (TPA) and diphenylamine (or indoline) based donors, dramatic improvements in nitrogen-substituent twist angles are observed. TPA shows a substantial 43^o dihedral angle and indoline shows a significantly improved 23^o dihedral angle. However, indolizine shows an ideal planar nitrogen-substituent bond angle. Additionally, the nitrogen lone-pair of indolizine may donate either into the 6 or 5 member ring and productively deliver the donated electron pair to the π-bridge according to valence bond theory. Given these desirable properties and a remarkably rapid high-yielding donor synthesis (1-step in many cases),

we have prepared a series of model dyes with indolizine donors for comparison to the properties of TPA and indoline donor-based dyes with identical π-bridges and acceptors.

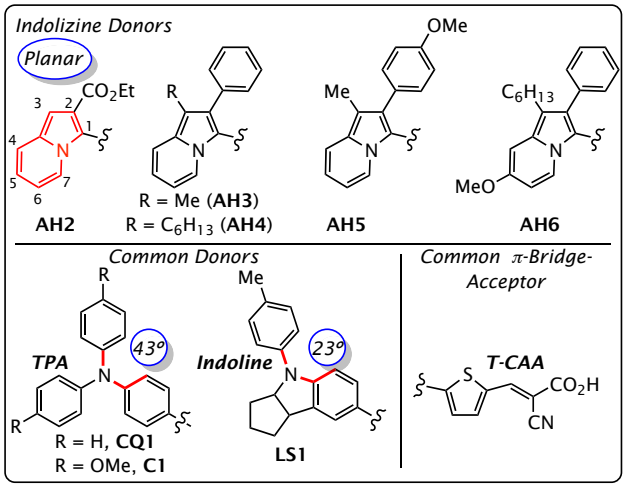

Figure 7. Indolizine-based donors as D-π-A dye components (top) with a common thiophene π-bridge-cyanoacrylic acid acceptor (T-CAA, bottom right). Common all-organic donor functionality (bottom left) with nitrogen-aryl bond dihedral angles calculated after DFT geometry optimization with a B3LYP functional and 6-311G(d,p) basis set.

DYE SYNTHESIS

A range of substituted indolizine donor targets were selected with substituents on both the five and six member rings of the fused system (Figure 7). The selected DSC target indolizine-based dyes keep the π-bridge and acceptor regions constant as thiophene-cyanoacrylic acid (**T-CAA**) throughout the series for simple donor effect comparison (Figure 7). The indolizine donors differ in electron-donating group (EDG) strength at the 2-position, substituent choice on the 6-member ring at the 5-position, and in varying alkyl chain length at the 3-position.

For practical synthetic purposes, we found the 2-position may be substituted with either electron-withdrawing functionality (which adversely effects charge transfer based absorptions)[24] or with aryl substituents to yield stable electron-rich intermediates.

The synthetic route employed for all dyes began with donor formation followed by palladium-catalyzed direct C-H arylation at the Indolizine 2-position then Knovenagle condensation. Concerning donor formation, indolizine **3** was prepared according to literature precedent.[25] Synthesis of indolizine-based dyes **AH3**, **AH4**, **AH5** and **AH6** began with 2-alkylated pyridines which were purchased (2-ethylpyridine), prepared through lithiation-alkylation (**4**), or prepared through Kumada coupling (**6**). The 2-alkyl pyridines were then *N*-alkylated with α-bromoacetophenones and underwent subsequent base-induced cyclization to form intermediates **7**-**10**. The alkylation/cyclization sequence may be conducted in a single step to generate the parent polycyclic donor or as a two-step sequence with simple filtrations to purify the intermediate pyridinium salts (Scheme 1).[26] It is noteworthy that indolizine **10** decomposes significantly within minutes when exposed to air which suggests the indolizine parent system for **AH6** is near the maximum electron donating potential available for handling under ambient conditions. Palladium catalyzed C-H activation of the indolizine donors (**3**, **7**-**10**) with 5-bromo-2-formylthiophene led to aldehyde intermediates **11**-**15**, which underwent Knovenagle condensation with cyanoacetic acid to give the desired dyes **AH2**-**AH6**.[27] These dyes are accessible in remarkably few synthetic steps (3-5 steps total) in up to 39% overall yield.

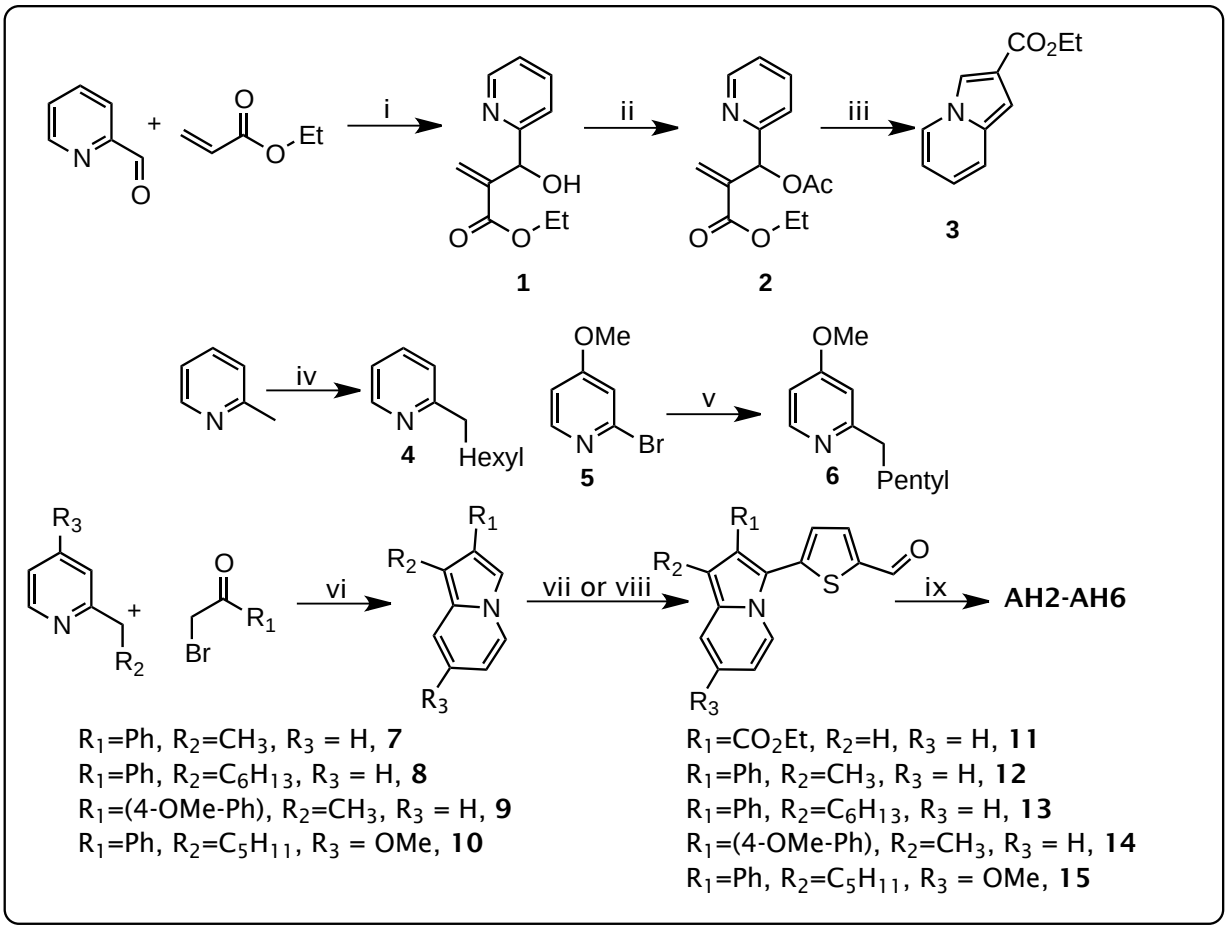

Scheme 1. Synthetic route to dyes **AH2-AH6**. Reaction Conditions: i) DABCO, $CHCl_3$, rt, 91% **1**; ii) Ac_2O, 100ºC, 86% **2**; iii) 120ºC, neat, 76% **3**; iv) *t*-BuLi, THF, -78ºC, then $C_6H_{13}Br$, 50% **4**; v) Mg, I_2, THF, rt to reflux, then Ni(dppp)Cl_2, pentylbromide, 0ºC to reflux, 92% **6**; vi) acetone, reflux, then $NaHCO_3$, H_2O, reflux, 92%-16% intermediate**s 7-10**; vii) R_3 = H, 5-bromothiophene-2-carboxaldehyde, Pd(PPh_3)$_2Cl_2$, KOAc, NMP, 80ºC, 92-44% intermediates **11-14**; viii) R_3 = OMe, Pd(OAc)$_2$, PCy_3, Cs_2CO_3, toluene, 130ºC, 19% intermediate **15**; ix) piperidine, cyanoacetic acid, $CHCl_3$, 90ºC, 84-14%, **AH2-AH6**.

OPTICAL AND ELECTROCHEMICAL PROPERTIES

The optical properties of **AH2-AH6** were analyzed to understand the effect of the indolizine substituents on the UV-Vis absorption properties (Table 1, Figure 2).

Table 1. Optical and electrochemical properties of **AH2-AH6** in dichloromethane solutions.

Dye	λ_{max} (nm)[a]	λ_{onset} (nm)[a]	ε (L mol^{-1}cm^{-1})[a]	$E_{(0\text{-}0)}$ (eV)[b]	$E_{(S+/S)}$ (V)[c]	$E_{(S+/S^*)}$ (V)[d]
AH2	419 (sh)	535	1,250	2.42	1.22	-1.12
AH3	553	633	8,500	2.06	0.99	-0.98
AH4	558	633	11,300	2.06	0.99	-0.98
AH5	562 (sh)	640	5,800	2.06	0.97	-1.00
AH6	592	675	12,500	1.88[g]	0.85	-1.03
CQ1[e]	442	540	25,000	2.27	1.16	-1.11
C1[f]	499	590	27,500	2.16[g]	1.04[h]	-1.12
LS1[i]	523	600	20,000	2.06	1.01	-1.05

[a] Measured in CH_2Cl_2 [b]Measured at the intercept of the absorption and emission curves in CH_2Cl_2. [c] Measured in a 0.1 M Bu_4NPF_6 in CH_2Cl_2 solution with glassy carbon working electrode, Pt reference electrode, and Pt counter electrode with ferrocene as an internal standard. Values are reported versus NHE. [d] Calculated from $E_{(S+/S^*)} = E_{(S+/S)} - E_{(0\text{-}0)}$. [e] Triphenylamine-thiophene-cyanoacrylic acid (CAA) dye, CQ1. See ref. 28. [f] *p*-Dimethoxytriphenylamine-thiophene-CAA dye, C1. See ref. 29. [g] Estimated from the absorption curve onset in CH_2Cl_2. [h] Estimated from the CV voltammogram in CH_2Cl_2. [i] Indoline-thiophene-CAA dye, LS1. See ref. 30.

Substituents at the 2-position of indolizine were found to be electronically active whereas the dyes **AH2**, **AH3** and **AH5** exhibited red-shifted λ_{max} values progressing from electron withdrawing groups (EWGs) to EDGs (ester < *p*H-phenyl < *p*MeO-phenyl) over a range of ~150 nanometers (nm) (Figure 8). Additionally, substituents on the 5-positon of indolizine were found to give a significant red-shift (~50 nm) when comparing H-substituted **AH4** to OMe-substituted **AH6**. The large red-shifted absorptions (75-135 nm $\Delta\lambda_{onset}$ **AH6** *vs.* **CQ1**,[28] **C1**[29] & **LS1**)[30]

observed with the indolizine dye series when compared to other common donor-based dyes illustrates the strong electron donation strength of the indolizine building blocks. The molar absorptivities ranged from 1,000-13,000 $M^{-1}cm^{-1}$ with the short alkyl chain length dyes at the 3-position (**AH2**, **AH3** and **AH5**) yielding the lowest molar absorptivities. **AH2** has a substantially lower molar absorptivity than the remaining indolizine-based dyes which is likely the result of a weakened charge transfer transition due to the addition of an electron deficient ester on the indolizine donor. The highest molar absorptivity indolizine-based dyes, **AH4** and **AH6**, have roughly half the molar absorptivity values observed for the phenylamine based-donors. The indolizine donors are significantly more sterically congested at the donor-π bridge bond than phenyl amine based donors and computationally show larger twist angles about this bond (32° *vs.* ~20°).

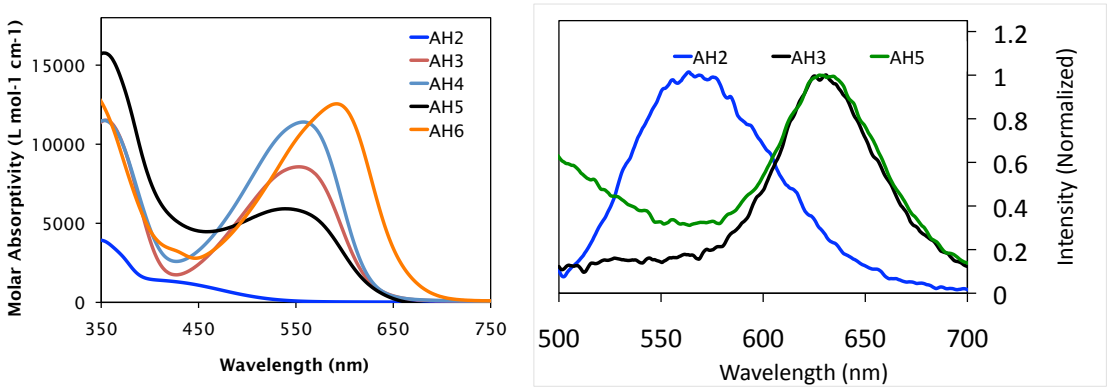

Figure 8. *Left:* Absorption spectra of dyes **AH2-AH6** measured in 0.05% AcOH and $CHCl_3$. *Right:* Emission spectra of of dyes **AH2,3** & **5** in $CHCl_3$.

The increase in wavelength absorption breadth of indolizine donors when compared with triaryl- and diarylamine donors can be rationalized through several factors including amine

planarity (Figure 9), the generation of an aromatically stabilized pyridinium excited-state region upon electron donation (Figure 9a), less competing electron donation directionality due to indolizine being a fully conjugated donor system (Figure 9b), and a lower inherent resonance stabilization energy for the amine donor to overcome than the common benzene resonance stabilization energy (Figure 9c).

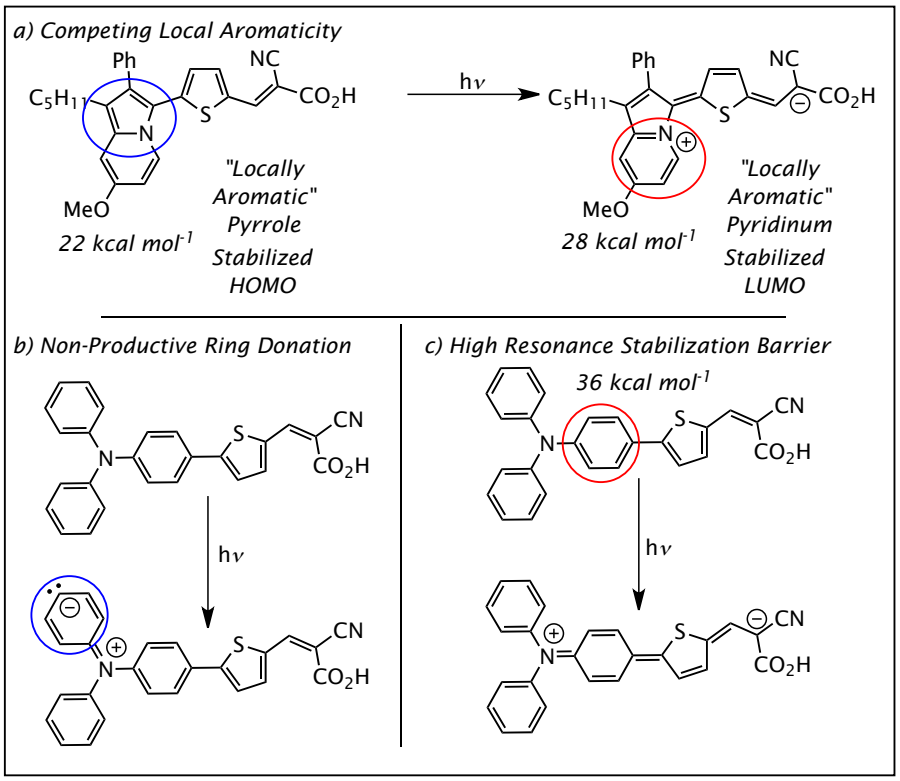

Figure 9. a) Structures of **AH6** in the ground- and excited-state, illustrating the competing local aromaticity between the pyrrole and pyridinium substructures. b) Structure of **CQ1** with a non-productive conjugated pathway illustrated. c) Structure of **CQ1** in the ground- and excited-state illustrating a high-resonance stabilization barrier, which must be overcome for charge transfer to occur.

The excited-state generated pyridinium substructure has a larger aromatic stabilization energy than the ground-state locally aromatic pyrrole (28 kcal mol^{-1} *vs.* 22 kcal mol^{-1}) which likely leads to a substantially lower charge-transfer energy barrier. Proaromatic substructures (i.e. substructures with competing local aromaticity) are rare in donor functionality and most commonly observed with π-bridges and acceptors.

The electrochemical properties of the D-π-A dyes **AH3**-**AH6** were analyzed with regard to DSC device components to evaluate if the dyes are energetically suitable for regeneration from the I^-/I_3^- redox shuttle and electron injection into a mesoporous TiO_2 semiconductor (Table 1). Through cyclic voltammetry (CV), the ground-state oxidation potentials ($E_{(S+/S)}$) of **AH3**-**AH6** are established to range from 0.99 to 0.85 V versus normal hydrogen electrode (NHE) which indicates regeneration from the I^-/I_3^- redox shuttle is favorable (ΔG_{reg} = 500-640 mV). According to the equation $E_{(S+/S^*)} = E_{(S+/S)} - E_{(0\text{-}0)}$ the excited-state oxidation potentials ($E_{(S+/S^*)}$) are determined based on $E_{(S+/S)}$ and the intercept of the absorption and emission curves ($E_{(0\text{-}0)}$) (Figure 8b). The $E_{(S+/S^*)}$ values were found to be favorable for electron injection into the TiO_2 conduction band (ΔG_{inj} = 480 – 530 mV). The oxidation potential of indolizine dyes **AH3**-**AH6** were found to be significantly higher in energy when compared with triphenyl amine and indoline based dye derivatives. The indolizine molecular geometry enhances electron donation strengths leading to a significant destabilizing of the oxidation potential (more strongly than typical donors) *and* the proaromatic pyridinium substructure leads to a unique stabilization of the excited-state oxidation potential. Because the optical band-gap is concomitantly narrowed,

longer absorption wavelengths may be accessed with an atypically low number of conjugated π-bonds relative to typical DSC D-π-A dyes with absorptions reaching ~700 nm.

While $E_{(S+/S)}$ is a good measure of a one-electron donation strength and the ability of the molecule to stabilize a radical cation, we sought to also examine the two-electron donation strengths through a comparison of the **CAA** carbonyl vibrational stretches between dyes. The **CAA** carbonyl stretch shifts to smaller wavenumbers with increasing donor strength and allows for a comparison of a variety of donor groups with identical π-bridges and acceptors. The TPA-based dyes **L1** (identical to **CQ1**) and **C213** (a **C1** analogue) give similar values for this stretch (1683 cm^{-1} for **L1**,[31] 1682 cm^{-1} for **C213**, Table 2).[32] An indoline-based dye gave only a slightly smaller carbonyl vibrational frequency value (1680 cm^{-1}).[33] In comparison, indolizine-based dyes gave an average value of 1646 cm^{-1}, which is significantly smaller (~35 cm^{-1}) than the other donors examined. Additionally, the C-N bond stretch of the **CAA** cyano group was compared between the four donors (Table 2).

Table 2. Electrochemical and spectroscopic vibrational analysis of dyes with varying donor functionalities (with **T-CAA** as bridge and acceptor) as they pertain to electron donation strength.

Dye	Asymm. CO (cm^{-1})	CN (cm^{-1})	$E_{(S+/S)}$ (V)
L1 (CQ1)	1683	2216	1.16
C213 (C1)	1682	2216	1.04
LS1	1680	2220[a]	1.01
AH3	1646	2203	0.98

[a] Estimated from IR absorption figure in Ref. 33.

Both TPA donors (**L1** and **C213**) have the same value (2216 cm^{-1}), while indoline is estimated to be near identical (~2220 cm^{-1}). The indolizine dyes again demonstrated the lowest C-N bond stretch value (2203 cm^{-1}) further illustrating the remarkable two-electron donations strengths.

COMPUTATIONAL STUDIES

For dyes to efficiently inject electrons into the TiO_2 conduction band with minimal back electron transfer for TiO_2 to the oxidized dye, the LUMO should be positions near the dye anchor and significantly separated from the dye HOMO. To examine the orbital geometries, **AH2-AH6** were computationally evaluated using a variety of density functional theory (DFT) methods (B3LYP, VSXC, MN12L, N12, M11L, VSXC, M06L, LC-PBE, PBE0, CAM-B3LYP) and basis sets (6-31G(d,p), 6-311G(2df,2pd)) with dichloromethane polar continuum model (PCM) and no-PCM. The HOMO and LUMO orbitals for each of the dyes show the HOMO primarily localized on the indolizine donor and the LUMO primarily localized on the **T-CAA** motif (Figure 10). The dye LUMO and HOMO orbital arrangements are well situated for efficient electron injection from the dye into the TiO_2 conduction band and diminished back electron transfer from the TiO_2 semiconductor to the oxidized dye, respectively.

A tremendous number of organic dye building blocks are available to tune dye properties. An experimentally accurate computational method for predicting dye absorption spectrum can have a dramatic impact on prioritizing future synthetic dye targets and on the wise utilization of chemical resources. To establish an accurate computational method, time-dependent DFT (TD-DFT) computations were performed to analyze the dye vertical transitions and oscillator strengths (Table 3, Figure 10).

HOMO

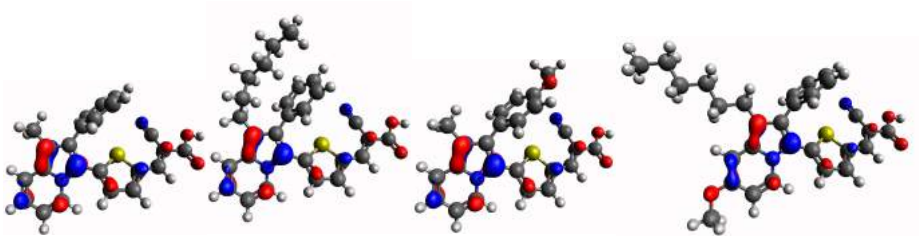

AH3 **AH4** **AH5** **AH6**

LUMO

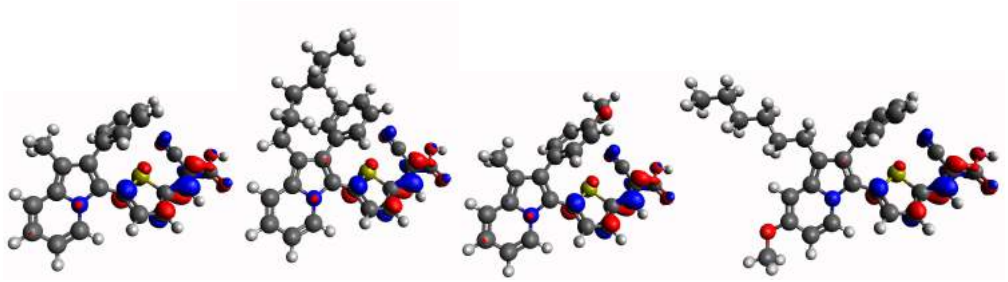

AH3 **AH4** **AH5** **AH6**

Figure 10. HOMO (top) and LUMO (bottom) orbitals for **AH3**, **AH4**, **AH5**, and **AH6** with a set contour value of 0.065. Calculations performed by Dreux and Tschumper.

After extensive calibration (Table 3), DFT/TD-DFT protocols were identified for the computation of the vertical transitions of **AH3-AH6** that could reliably reproduce the experimental λ_{max} (within 10 nm). No-PCM, TD-DFT computations performed with the VSXC functional and 6-311G(2df,2pd) basis set gave very good agreement when using geometries optimized with either the VSXC or B3LYP functionals (within 10 nm or 20 nm, respectively).

Table 3: Deviations ($\Delta\lambda$ in nm where + indicates an overestimation of the experimental λmax) from experimental

λ_{max} values for the most intense vertical transition computed with two different functionals and the 6-311G(2df,2pd) basis set. Calculations performed by Dreux and Tschumper.

		AH3	AH4	AH5	AH6
Experimental Reference (λ_{max} in nm)		553	558	562(sh)	592
TD-DFT	Geometry Optimization	$\Delta\lambda$ in nm			
No-PCM	**No-PCM**				
B3LYP	B3LYP	-44	-52	-62	-63
B3LYP	VSXC	-40	-38	-44	-47
VSXC	B3LYP	+17	+5	-18	-12
VSXC	VSXC	+4	+9	-4	+1
PCM[a]	**No-PCM**				
B3LYP	B3LYP	+2	-6	-19	-11
B3LYP	VSXC	+2	+3	-7	0
VSXC	B3LYP	+68	+53	+29	+40
VSXC	VSXC	+49	+52	+46	+48
PCM[a]	**PCM**[a]				
B3LYP	B3LYP	0	-8	-10	-18
B3LYP	VSXC	+3	+4	-1	-24
VSXC	B3LYP	+57	+43	-10	+21
VSXC	VSXC	+44	+49	+49	+7
Experimental Reference (λ_{max} in nm)		553	558	562(sh)	592

[a]Default solvent parameters for dichloromethane.

While these results were highly accurate, we sought to examine the effects of solvent on the structures and vertical transitions of **AH3-AH6** through the use of an implicit solvation model for dichloromethane. When coupled with PCM, TD-DFT computations performed with the B3LYP functional provided better agreement with the experimental λ_{max} values regardless of

whether the VSXC or B3LYP functional was employed for the geometry optimizations (within 10 nm and 20 nm, respectively for **AH3-AH6)**. This level of agreement is encouraging given the relative simplicity of these computational models, and it suggests the predictive computational analysis of extended conjugation π-bridges could play an important role in the design and development of second generation dye targets based on indolizine donors.

FLUORESCENCE LIFETIME MEASUREMENTS

Electron injection from each of the dyes into the TiO_2 conduction band was found to be geometrically favorable through computational analysis of HOMO/LUMO orbital positions as well as thermodynamically favorable through electrochemical, UV-Vis and emission spectrum analysis. To examine the kinetics for electron injection, fluorescence lifetime studies were undertaken for each of the dyes in solution and on TiO_2 films to evaluate electron injection efficiencies (η_{eff}, where $\eta_{eff} = 1 - \tau_{TiO2}/\tau_{sol}$). Lifetimes of the dyes in dichloromethane solutions (τ_{sol}) were found to be on the order of nanoseconds ranging from 1.6 ns to 0.9 ns (Figure 11, Table 4).

Excited-state lifetimes of the dyes on TiO_2 films (τ_{TiO2}) are predicted to be significantly shorter whereas electrons may be injected from the dye into the TiO_2 CB effectively quenching the fluorescence. Dye-TiO_2 film fluorescence lifetimes were measured under three environmental conditions: (1) with dye and TiO_2 under air, (2) with dye, TiO_2 and known deaggreation agent chenodeoxycholic acid (CDCA) under air, and (3) with dye, TiO_2 and CDCA in a filled acetonitrile cell containing a typical device electrolyte lithium iodide concentration of

0.002 M. τ_{TiO2} was found to be dramatically shorter for all dyes on TiO_2 regardless of environment.

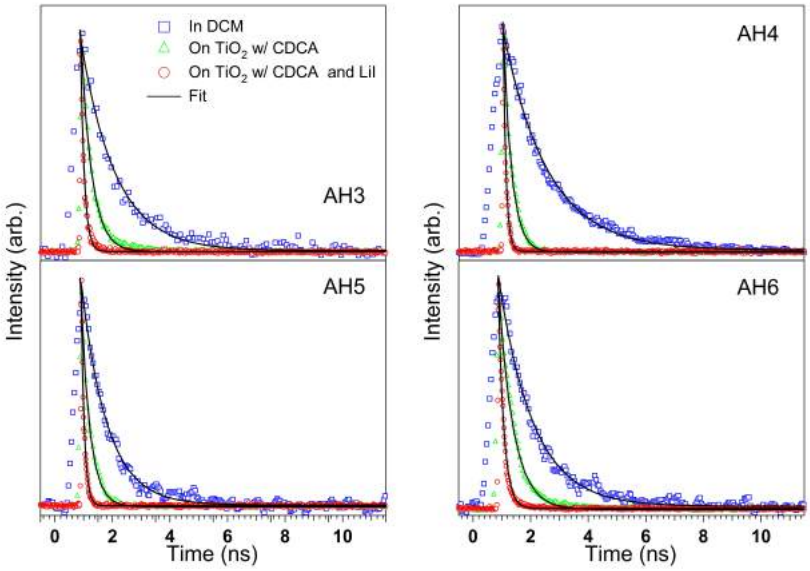

Figure 11. Excited-state fluorescence decay curves for dicholormethane solutions and TiO_2 films sensitized with dyes **AH3-AH6**. Blue square markers are dichloromethane dye solutions, green triangle markers are dyes on TiO_2 films with CDCA under air, red circle markers are dyes on TiO_2 films with CDCA and mock-device electrolyte 0.002 M LiI in acetonitrile. Measurements performed by McNamara and Hammer.

Without any additives, η_{eff} was found to vary between 45-82% according to the following order: **AH4**>**AH3**>**AH5**>**AH6**. Upon introduction of CDCA, a substantial increase in η_{eff} is observed for **AH5** and **AH6** leading to a range of injection efficiencies from 70-82%. The increase in efficiency is likely due to the reduction of intermolecular energy transfer between aggregated dyes on the TiO_2 film, which decreases the rate of electron injection into the TiO_2 conduction band. Upon the addition of an electrolyte containing MeCN and 0.002 M LiI to give

mock-device conditions, η_{eff} increased even further to >84% for each of the dyes where τ_{TiO2} was found to be beyond measureable limits.

Table 4. Excited-state lifetime measurements for dyes **AH3-AH6**. Measurements performed by McNamara and Hammer.

Dye	τ_{sol} [a] (ns)	τ_{TiO2} [b] (ns)	η_{eff} [b] (%)	τ_{TiO2} [c] (ns)	η_{eff} [c] (%)	τ_{TiO2} [d] (ps)	η_{eff} [d] (%)
AH3	1.14	0.30	74	0.30	74	<150	>86
AH4	1.59	0.29	82	0.29	82	<150	>91
AH5	0.93	0.26	63	0.26	72	<150	>84
AH6	1.18	0.65	45	0.35	70	<150	>87

[a] Measurement made using dye dissolved in CH_2Cl_2. [b] Measurement made using dye-sensitized TiO_2 film in air with no additive. [c] Measurement made using dye-sensitized TiO_2 film with added CDCA. [d] Measurement made using dye-sensitized TiO_2 films with added CDCA and 0.002 M LiI in MeCN electrolyte.

PHOTOVOLTAIC PERFORMANCE

Having established the indolizine dye series exhibits suitable characteristics for productive photon-to-electric conversion, dyes **AH3-AH6** were examined in DSC devices with a TiO_2 semiconductor and I^-/I_3^- redox shuttle. From the equation PCE (η) % = $(J_{sc}V_{oc}FF)/I_{(sun)}$ where J_{sc} = short-circuit current, V_{oc} is the open-circuit voltage, *FF* is the fill factor and $I_{(sun)}$ is the incident light intensity, the device performances under AM 1.5 irradiation were analyzed (Table 5).

Table 5. Photovoltaic parameters measured under AM 1.5 incident light. Measurements Performed by Giordano, Nazeeruddin, Zakeeruddin, and Grätzel.

Dye	J_{sc} (mA/cm^2)	V_{oc} (mV)	FF	η (%)
AH3	10.0	680	0.74	5.10
AH4	8.06	560	0.69	3.10
AH5	9.75	668	0.76	4.97
AH6	10.8	670	0.74	5.36
CQ1	10.29	707	0.69	4.99
C1	9.72	787	0.71	5.45
LS1	10.58	650	0.69	4.72

After device optimization with CDCA loadings to diminish aggregation, dye J_{sc} values ranged from 8.1-10.8 mA/cm^2 in the order of **AH6**>**AH3**>**AH5**>**AH4**. **AH6** has the longest wavelength absorption, which led to a significantly larger photocurrent than the remaining dyes. **AH3**, **AH5** and **AH6** demonstrated very similar V_{oc} values (680-668 mV) and *FF* values (0.74-0.76) leading to a close range of PCEs from 5.0%-5.4% with **AH6** demonstrating the overall highest PCE of 5.4%. **AH4** demonstrated the lowest PCE due to lower performance in all parameters. The model indolizine donors employed in these studies utilized few aggregation controlling substituents and TiO_2 surface protecting alkyl chains (only **AH4** and **AH6** have a single alkyl chain longer than methyl) which are known to boost V_{oc} values. When compared to dyes **CQ1**, **C1**, and **LS1**, similar voltages are observed for the no-alkyl chain donor triphenylamine (**CQ1**) and the methyl substituted indoline donor (**LS1**). Superior PCE values were observed for **AH6** when compared with these donors despite a potentially PCE-diminishing lower molar absorptivity and significant aggregation on the TiO_2 film surface. Among the

common donors compared to the **AH6** donor, only the bis(methyloxy)triphenylamine donor of **C1** gives a similar PCE value due to a significantly higher V_{oc}.

The incident photon-to-electron conversion efficiency (IPCE) spectra were measured for each of the dyes (Figure 12). **AH6** had the longest wavelength IPCE onset at ~700 nm which coincides with the largest J_{sc} value observed. The remaining dyes (**AH3**-**AH5**) all have similar IPCE onset values of ~650 nm. Ranging from ~400-475 nm, a significant depression is observed for each of the dyes which mirrors the absorption spectral profiles of these sensitizers (Figure 8) due to their low molar absorptivity (~2,000 $M^{-1}cm^{-1}$) in this region. Overall, these model dyes suffer from low molar absorptivities (13,000-6,000 $M^{-1}cm^{-1}$), which could lead to diminished IPCE values as a result of less light being absorbed on the 10 μm TiO_2 films. Additionally, dye aggregation on TiO_2 led to apparent lower injection efficiencies when fluorescence lifetime measurements were taken. Both of these factors likely contributed to the observed peak maximum IPCE values reaching 70-75% for each of the dyes. However, while the percent IPCE intensity is diminished in these model systems relative to TPA and indoline based analogues (~80% from 400-550 nm), the IPCE breadth is significantly increased for the indolizine-based dyes as a result of absorptions at longer wavelengths (650 nm *vs.* 700 nm onset). TPAs and indolines are two of the most common DSC donors in organic dye designs which are common to nearly all organic sensitizers with greater than 10% PCE.[22,34] Indolizine donors exhibit substantially broader solution absorption spectra (narrowed optical band-gap) compared with these donors (λ_{onset} = 675 nm for **AH6** versus λ_{onset} = 540 nm for TPA-based **CQ1**,[28] 590 nm for diMeO-TPA-based **C1**,[29] and 600 nm for indoline-based **LS1**,[30] Table 1, Figure 12) and

increased performance beyond 650 nm in DSC devices (Figure 13). Significantly, both TPA and indoline derivatives are common to nearly all organic sensitizers with greater than 10% PCE.[22,34]

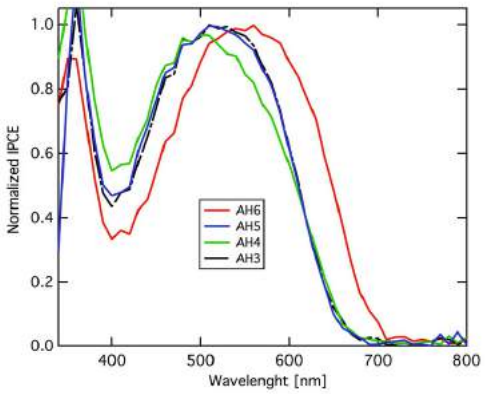

Figure 12. IPCE curves for devices based on **AH3**-**AH6**. Measurements Performed by Giordano, Nazeeruddin, Zakeeruddin, and Grätzel.

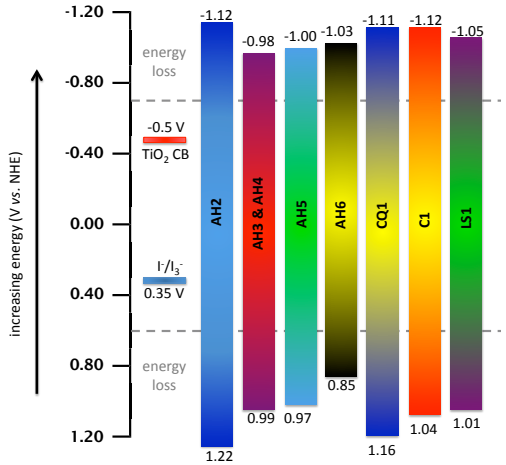

Figure 13. Energy level schematics comparing the optical bandgaps (right) of indolizine (dyes **AH2**-**AH6**), (*o*-H)$_2$TPA (**CQ1**), (*o*-OMe)$_2$TPA (**C1**) and indoline (**LS1**) donors on T-CAA.

While this part has largely outlined the successes of discovering the indolizine donor subunit the advance of indolizine was just as dependent on synthetic failures as it was on the successes. Take, for example, the optimization of the donor heterocycle. Before synthesizing the donor utilized in **AH2**, several other donor heterocycles were synthesized in an attempt to better understand the reactivity of indolzine (Figure 14).

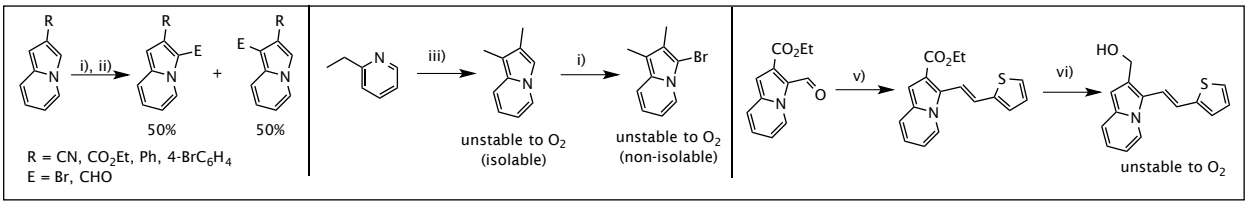

Figure 14. Attempts towards indolizine synthesizers that were not successful. Conditions: i): NBS, DMF, 0ºC to rt, 0.040 g, 30%. ii): DMF, $POCl_3$, DCE, 0ºC to rt, 80%. iii) a): acetone, chloroacetone, reflux. b): $NaHCO_3$, H_2O, reflux, 50% yield. i): NBS, DMF, 0ºC to rt, 0% yield. v): 2-(diethylphosphonato)methylthiophene, NaH, THF, 0ºC to rt, 45% yield. vi): $LiAlH_4$, THF, 0ºC, 38% yield.

The first indolizine dyes we synthesized had EWG at the 2- position, as it was assumed these were needed to form the indolizine heterocycle. Because these first structures had no substituents at either the 3-position or the 1-position, which had the two largest HOMO molecular orbital coefficients in early computation, attempts to substitute the heterocycle by EAS yielded 2:1 mixtures of 1-subtituted or 3-substituted products. Once the need to force selectivity by alkyl substitution had been determined, attempts to synthesize the dimethyl indolizine resulted in heterocycles that were very unstable to O_2. Before embarking upon the synthesis of indolizine **6**, reducing the withdrawing ester group of indolizine **3** after HWE olefin

formation to a donating alkoxy group was attempted. While the olefin starting material was stable to ambient atmosphere, the alcohol product was not.

CONCLUSION

We have synthesized and characterized a series of organic dyes for dye-sensitized solar cells based on the indolizine donor. This donor is shown to have a facile synthesis, remarkable electron donation strength when compared with state-of-the-art organic donors, and promising first generation DSC device performances based on a simple thiophene-CAA bridge-acceptor systems. The IPCE spectrum onset of the low molecular weight indolizine dye **AH6** is within ~25 nm of high performance dyes (10-12.5% PCEs) such as **Y123**,[34c] **YA422,**[33] **C259**[34a] and **ADEKA-1**[10] and is available in a fraction of the synthetic steps and molecular mass.

Given the seemingly unprecedented rapid donor synthesis and the remarkable electron donation strength of indolizine donors when compared with state-of-the-art donor functionalities, studies are underway to computationally determine the origin of the substantial absorption breadth observed from simple indolizine donor-based dyes, increase the π-bridge conjugation length to access high-efficiency dyes, reduce twist angles along the conjugated charge transfer pathway and to incorporate additional film morphology controlling substituents on the donor. Tuning TiO_2 film dye surface coverage has proven highly successful for the Hagfeldt[34] and Grätzel[33,9] donors with regard to slowing electrolyte-TiO_2 recombination pathways, controlling aggregation states, and substantially improving device voltages.

EXPERIMENTAL SECTION

General Information: All commercially obtained reagents were used as received. ^{1}H NMR spectra were recorded on a Bruker Avance-300 (300 MHz), Bruker Avance DRX-500 (500MHzspectrometer and are reported in ppm using solvent as an internal standard ($CDCl_3$ at 7.26 ppm). Data reported as: s = singlet, d = doublet, t = triplet, q = quartet, p = pentet, m = multiplet, b = broad, ap = apparent; coupling constant(s) in Hz; integration. UV-Vis spectra were measured with a Cary 5000 UV-Vis spectrometer. Cyclic voltammograms were measured with a C-H Instruments electrochmeical analyzer.

Photovoltaic Characterization: A 450W xenon lamp (Oriel, USA) was used as a light source to study the current-voltage characteristics of the DSSC. The spectral output of the lamp was filtered using a Schott K113 Tempax sunlight filter (Präzisions Glas & Optik GmbH, Germany) to reduce the mismatch between the simulated and actual solar spectrum to less than 2 %. The Keithley model 2400 digital source meter (Keithley, USA) was used for data acquisition. The photo-active area of 0.16 cm^2 was defined by a black mask of 4x4 mm^2. Incident photon-to-current conversion efficiency measurements were carried from the mono chromated visible photons, from Gemini-180 double monochromator Jobin Yvon Ltd. (UK), powered by a 300 W xenon light source (ILC Technology, USA) superimposed on a 10mW/cm^2 LED light. The monochromatic incident light was passed through a chopper running at 2 Hz frequency and the on / off ratio was measured by an operational amplifier.

Device Fabrication: The photoanode consists of thin TiO_2 electrodes comprising a 9.5 mm mesoporous TiO_2 layer (particle size, 20 nm) and a 5.0 mm TiO_2 scattering layer (particle size, 400 nm).The sintered photoanode was soaked 30 minutes at 70 C in a 40mM $TiCl_4$ water solution and heated again at 500ºC prior sensitization. The complete working electrode was prepared by immersing the 14.5 mm (9.5 mm thick transparent layer + 5.0 mm thick scattering) TiO_2 film into the dye solution for 2 h.The solution is 0.2 mM of dye in THF:ethanol mixture (1:4). The dye:CDCA molar ratio for the optimized device is 1:40 A thermally platinized FTO glass counter electrode and the working electrode were then sealed with a 25 mm thick hot-melt film (Surlyn, Dupont) by heating the system at 100°C. Devices were completed by filling the electrolyte by pre-drilled holes in the counter electrodes and finally the holes were sealed with a Surlyn sheet and a thin glass cover by heating. A black mask (4x4 mm^2) was used in the subsequent photovoltaic studies.

General Computational Details: Numerous combinations of density functional theory (DFT) method, basis set and implicit solvation model were examined in an attempt to identify efficient model chemistries capable of reproducing experimental λ_{max} values for 5 dye molecules (AH2, AH3, AH4, AH5 and AH6). Emphasis was placed on pure density functionals in order to take advantage of the density fitting (DF)[35] procedures available in the Gaussian09[36] software package, but several popular hybrid functionals were also tested. Full geometry optimizations were performed with the B3LYP,[37] VSXC,[38] M06L,[39] M11L,[40] N12,[41] and MN12L[42] functionals in conjunction with two split-valence basis sets of double- and triple-zeta quality (6-31G(d,p) and 6-311G(2df,2pd), respectively). Rather stringent convergence criteria were adopted for the

geometry optimizations (maximum Cartesian force < 1.1×10^{-5} Hartree/bohr). Harmonic vibrational frequencies were also computed to ensure that every gas-phase optimized structure was a minimum at the corresponding level of theory. These gas-phase structures were also re-optimized with the same functionals and basis sets in conjunction with an implicit solvation model to mimic the effects of the experimental solvent. The polarizable continuum model (PCM)[43] was adopted for these computations along with the default parameters for dichloromethane as implemented in Revision D.01 of Gaussian09.

Time-dependent density functional theory (TD-DFT) computations were carried out to compute the vertical transition energies and oscillator strengths for the 10 lowest excited states. Symmetry was explicitly turned off for these computations even though all of the optimized structures belonged to the C_1 point group. In addition to the procedures used to optimize the structures, the TD-DFT computations were also performed with the CAM-B3LYP,[44] PBE0,[45] and LC-PBE[46] functionals. The effects of solvation on the excited state transitions were modeled with PCM TD-DFT calculations.[45] The labels "PCM" and "no-PCM" are adopted to help distinguish whether solvation effects were modeled in the geometry optimization and/or TD-DFT computations.[47]

All computations were performed with the Gaussian09 software package and employed an ultrafine pruned numerical integration grid of composed of 99 shells and 590 angular points per shell. Spherical harmonic components of the basis functions (5d and 7f) were utilized rather than their Cartesian counterparts (6d and 10f). All electronic energies (including the excited states) were converged to at least 1.0×10^{-8} Hartree.

*Synthetic Procedures for AH2: Ethyl 2-(hydroxy(pyridin-2'-yl)methyl)acrylate (**1**):*[48] To a 50 mL round bottom flask was added pyridine-2-carboxaldehyde (5.63 g, 52.6 mmol, 1.0 equiv.), DABCO (0.340 g, 3.00 mmol, 0.05 equiv.), ethyl acrylate (5.52 g, 5.89 mL, 55.1 mmol, 1.05 equiv.), and chloroform (4.0 mL, 13.15 M). The mixture was allowed to stir for 3d at room temperature. During this time the solution slowly changes colors from yellow to red. An aliquot was removed and the reaction was judged complete by TLC. The mixture was concentrated and subjected to flash chromatography using 350 mL SiO_2, 10x 160mm collection tubes, and EtOAc as eluent. Collected product fractions concentrated to yield a yellow oil. (9.94g, 48.0 mmol, 91%). ^{1}H NMR (300 MHz, $CDCl_3$) d 8.55 (dt, *J* = 4.4 Hz, 1.0 Hz, 1H), 7.68 (td, *J* = 7.6 Hz, 1.7 Hz, 1H), 7.43 (d, *J* = 8.6 Hz, 1H), 7.23 (ddd, *J* = 7.3 Hz, 5.1 Hz, 1 Hz, 1H), 6.36 (dd, *J* = 2.0 Hz, 0.5 Hz, 1H), 5.95 (t, *J* = 1.1 Hz, 1H), 5.62 (d, *J* = 6.6 Hz, 1H), 4.80 (d, *J* = 2.0 Hz, 1H), 4.18 (q, *J* = 7.1 Hz, 2H), 1.24 (t, *J* = 7.1 Hz, 3H).

*Ethyl 2-(acetoxy(pyridin-2'-yl)methyl)acrylate (**2**):*[26a] To a 25 mL flask was added Ethyl 2-(hydroxy(pyridin-2-yl)methyl)acrylate (7.00 g, 33.8 mmol, 1.0 equiv) and acetic anhydride (20 mL, 1.7 M). The mixture was heated to 100 ^{o}C with stirring. After 1h, cooled to room temperature and diluted with EtOAc (100 mL). Washed sequentially with saturated $NaHCO_3$ (2 x 100 mL), H_2O (1 x 100 mL), and brine (2 x 100 mL). Dried organic solution with $MgSO_4$ and passed through thick pad of SiO_2 using 5% MeOH:EtOAc. Concentrated to yield a dark oil (7.20 g, 28.9 mmol, 86%). ^{1}H NMR (300 MHz, $CDCl_3$) d 8.59 (d, *J* = 4.5 Hz, 1.0 Hz, 1H), 7.69 (td, *J* = 7.5 Hz, 1.7 Hz, 1H), 7.45 (d, *J* = 7.8 Hz, 1H), 7.22 (ddd, *J* = 7.3 Hz, 3.8 Hz, 1.2 Hz, 1H), 6.74

(s, 1H), 6.49 (t, *J* = 0.9 Hz, 1H), 5.94 (t, *J* = 1.3 Hz, 1H), 4.15 (qd, *J* = 7.0 Hz, 1.0 Hz, 2H), 2.16, (s, 3H), 1.21 (t, *J* = 6.8 Hz, 3H).

*Ethyl(indolizine-2-carboxylate) (**3**):*[26a] To a 25 mL flask was added ethyl 2-(acetoxy(pyridin-2-yl)methyl)acrylate (7.0 g, 28 mmol). The acrylate was set to stir at 120 ^{o}C under a nitrogen atmosphere. After 55 min, the reaction was judged complete by TLC. The reaction mixture was diluted in 50 mL 5% MeOH: EtOAc and passed through a thick pad of SiO_2 using 5% MeOH: EtOAc as eluent. Concentrated to give a dark solid (4.02 g, 21.2 mmol, 75%). ^{1}H NMR (300 MHz, $CDCl_3$) d 7.85 (d, *J* = 6.3 Hz, 1.0 Hz, 1H), 7.80 (s, 1H), 7.36 (d, *J* = 9.2 Hz, 1H), 6.83 (s, 1H), 6.68 (dd, *J* = 9.0 Hz, 6.3 Hz1H), 6.53 (td, *J* = 6.9 Hz, 1,2 Hz, 1H), 4.35 (q, *J* = 7.1 Hz, 2H), 1.38 (t, *J* = 7.1 Hz, 3H).

*Ethyl (1-(thiophen-2'-yl-5'-carboxaldehyde)indolizine)-2-carboxylate (**10**):*[26a,49] To a 25 mL flask was added Ethyl(indolizine-2-carboxylate) (0.12 g, 0.64 mmol), $PdCl_2(PPh_3)_2$ (0.037 g, 0.053 mmol), 5-bromo-2-thiophenecarboxaldehyde (0.30 g, 0.19 mL, 1.6 mmol), KOAc (0.21 g, 2.12 mmol), NMP (2.5 mL) under a nitrogen atmosphere. Set to stir at 80ºC. After 20h, subjected material to column chromatography using 10%EtOAc:Hexanes. Concentrated product spot to yield an orange solid (0.15 g, .50 mmol, 47%). ^{1}H NMR (300 MHz, $CDCl_3$) d 9.95 (s, 1H), 7.96 (d, J = 8.1 Hz, 1H), 7.84 (d, J = 4.0 Hz, 1H), 7.42 (d, J = 8.5 Hz, 1H), 7.34 (d, J = 3.7 Hz, 1H), 7.0 (s, 1H), 6.8 (t, J = 7.3 Hz, 1H), 6.59 (t, J = 7.0 Hz, 1H), 4.25 (q, J = 7.2 Hz, 2H), 1.25 (t, J = 7.3 Hz, 3H).

*3-(ethyl(thiophen-2''-yl-5''-3-pentyl-indolizine-2-carboxylate)-2-cyano-2-propenoic acid (**AH2**)*. To a 10 mL flask added Ethyl (1-(thiophen-2'-yl-5'-carboxaldehyde)indolizine)-2-

carboxylate (0.085 g, 0.29 mmol), $CHCl_3$ (4.75 mL). Bubbled with nitrogen for 30 min. Cyanoacetic acid (0.14g, 1.7 mmol), piperidine (0.33g, 0.39 mL, 4.0 mmol) added. Sealed flask using a plastic stopper and electrical tape. Warmed to 90ºC. After 4.5 h, cooled to rt. Diluted with 150 mL CH_2Cl_2, acidified with AcOH, washed with H_2O (3x 100 mL), Concentrated. Passed crude material through thick pad of SiO_2 using first CH_2Cl_2 (500 mL), then 10% MeOH:CH_2Cl_2 (500 mL), and finally 10% MeOH:5%AcOH:CH_2Cl_2 (500 mL). Concentrated to yield a dark range powder (0.084 g, 0.23 mmol, 84%). ^{1}H NMR (500 MHz, $CDCl_3$). d 8.35 (d, J = 6.3 Hz, 1H), 7.90 (d, J = 4 Hz, 1H), 7.84 (s, 1H), 7.4 (d, J = 6.0 Hz, 1H), 7.35 (d, J = 4.0 Hz, 1H), 7.0 (s, 1H), 6.8 (t, J = 6.5 Hz, 1H), 6.6 Hz (t, J = 6.6 Hz), 4.25 (q, J = 7.0 Hz, 2H), 1.37 (t, J = 7.1 Hz, 3H). HRMS (ESI) *m/z* calculated for $C_{19}H_{14}N_2O_4S$ $[M]^+$: 367.0753, found 367.0707. UV-Vis ($CHCl_3$): λ_{max} = 430 nm (ε = 1,250 $M^{-1}cm^{-1}$), λ_{onset} = 530 nm. Cyclic Voltammetry (0.1 M Bu_4NPF_6 in CH_2Cl_2, sweep width 1.1-(-2.0), 0.1 V/s scan rate): $E^{(S+/S)}$ = 1.22 V (vs NHE). $E^{(0-0)}$ = 2.42 V. $E^{(S+/S*)}$ = -1.12 V [vs NHE, calculated from $E^{(S+/S*)} = (E^{(S+/S)} - E_g^{opt})$].

*Synthetic Procedures for AH3: 2-Phenyl-3-methylindolizine (**6**):*[25] To a 100 mL flask was added 2-ethylpyridine (10.0 g, 93.37 mmol), bromoacetophenone (18.58 g, 93.37 mmol), acetone (50 mL). Set to stir open to air at reflux. After 21h, the reaction mixture was cooled to rt and the resulting white precipitate filtered and washed with acetone. The white solid was then added to a 250 mL flask, along with $NaHCO_3$ (31.00 g, 370.0 mmol). Set to stir open to air at reflux. After 1.5h, a biphasic reaction mixture was observed and upon cooling the flask to rt, the top layer crystallized into a dark mass. Filtered the dark crystals and dissolved them in CH_2Cl_2. Passed through a thin pad of SiO_2 and concentrated to yield an off white solid (17.64 g, 85.11 mmol,

92%). ^{1}H NMR (500 MHz, $CDCl_3$) d d 7.85 (dt, J = 7.0 Hz, 0.9 Hz, 1H), 7.54 (d, J = 7.7 Hz, 1H), 7.45 (t, 7.4 Hz, 1H), 7.39 (s, 1H), 7.35-7.29 (m, 2H), 6.61 (ddd, J = 7.1 Hz, 6.4 Hz, 1.0 Hz, 1H), 6.42 (t, 6.8 Hz, 1H), 2.45 Hz (s, 3H). ^{13}C NMR (125 MHz, $CDCl_3$) d 136.3, 131.3, 129.4, 129.0, 128.7, 126.5, 125.1, 117.8, 115.9, 110.5, 110.1, 105.9, 9.9. IR (neat, cm^{-1}): 3067.7, 2919.3, 2862.0, 1602.8, 1457.6, 736.1. HRMS (ESI) *m*/*z* calculated for $C_{15}H_{13}N$ $[M+H]^+$: 208.1126, found 208.1182.

*1-(thiophen-2'-yl-5'-carboxaldehyde)-2-phenyl-3-methylindolizine (**11**):* To a 25 mL flame dried flask was added 2-Phenyl-3-methylindolizine (0.25 g, 1.2 mmol), $PdCl_2(PPh_3)_2$ (0.043 g, 0.061 mmol), 5-bromo-2-thiophenecarboxaldehyde (0.35 g, 0.22 mL, 1.8 mmol), KOAc (0.24 g, 2.4 mmol), NMP (2.5 mL) under a nitrogen atmosphere. Set to stir at 80ºC. After 6.5 h, subjected material to column chromatography using 10%EtOAc:Hexanes. Concentrated product spot to yield an orange oil that crystallized upon standing (0.35 g, 1.1 mmol, 92%). ^{1}H NMR (300 MHz, $CDCl_3$) d 9.72 (s, 1H), 8.34 (d, J = 6.8 Hz, 1H), 7.55 (d, J = 4.0 Hz, 1H), 7.37-7.25 (m, 4H), 7.17 (d, J = 6.0 Hz, 2H), 6.88 (d, J = 4.0 Hz, 1H), 6.72 (ddd, J = 7.8 Hz, 6.8 Hz, 1.0 Hz, 1H), 6.53 (t, J = 6.3 Hz, 1H), 2.20 (s, 3H). ^{13}C NMR (75 MHz, $CDCl_3$)d 182.6, 143.5, 141.7, 136.9, 135.0, 132.7, 131.6, 130.8, 128.6, 127.4, 127.4, 123.0, 118. 3, 118.0, 114.4, 112.1, 109.6, 9.3. IR (neat, cm^{-1}): 3067.5, 2860.9, 1660.2, 1434.8, 1226.6, 734.9. HRMS (ESI) *m*/*z* calculated for $C_{20}H_{15}NOS$ $[M]^+$: 317.0874, found 317.0906.

*3-(thiophen-2'-yl-5'-2-phenyl-3-methylindolizine)-2-cyano-2-propenoic acid (**AH3**).* For procedure see **AH2**. Yield: (0.032 g, 0.079 mmol, 25%). ^{1}H NMR (300 MHz, $CDCl_3$) d 8.26 (d, J = 6.4 Hz, 1H), 8.04 (m, 1H), 7.36 (m, 1H), 7.29 (m, 1H), 7.25 (m, 1H), 7.22 (m, 2H), 7.08 (m,

2H), 6.67 (t, J = 7.9 Hz, 1H), 6.55 (m, 1H), 6.42 (m, 1H), 2.15 (s, 3H). IR (neat, cm^{-1}): 3429.1, 2200, 1645.5, 1394.9, 1199.1. HRMS (ESI) *m*/*z* calculated for $C_{23}H_{16}N_2O_2S$ $[M]^+$: 385.1011, found 385.0549. UV-Vis ($CHCl_3$): λ_{max} = 557 nm (ε = 8,500 $M^{-1}cm^{-1}$), λ_{onset} = 627 nm. Cyclic Voltammetry (0.1 M Bu_4NPF_6 in CH_2Cl_2, sweep width 1.1-(-2.0), 0.1 V/s scan rate): $E^{(S+/S)}$ = 0.99 V (vs NHE). $E^{(0-0)}$ = 2.06 V. $E^{(S+/S*)}$ = -0.98 V [vs NHE, calculated from $E^{(S+/S*)} = (E^{(S+/S)} - E_g^{opt})$].

*Synthetic Procedures for AH4: 2-Heptylpyridine (**4**):*[50] To a 100 mL flame-dried flask was added 2-picoline (2.0g, 2.12 mL, 21.44 mmol), and THF (50 mL). This solution was cooled to -78ºC and t-Butyl lithium (15.12 mL, 1.7M) was added dropwise to yield a red-orange solution. Set to stir at -78ºC. After 1h, Hexylbromide (7.5 mL, 55.6 mmol) added dropwise at -78ºC. Allowed reaction to warm to rt slowly with stirring. After 20h, passed reaction mixture through thin pad of SiO_2 and concentrated to give a pale yellow liquid (1.90 g, 10.72 mmol, 50%). ^{1}H NMR (300 MHz, $CDCl_3$) d 8.51 (dq, J = 5.0 Hz, 1.0 Hz, 1H), 7.57 (td, J = 7.9 Hz, 1.8 Hz, 1H), 7.13 (d, J = 7.8 Hz, 1H), 7.08 (dm, J = 7.0 Hz, 1H), 2.77 (t, J = 6.2 Hz, 2H), 1.72 (q, J = 7.2 Hz, 2H), 1.38-1.21 (m, 9H), 0.87 (t, J = 7.5 Hz, 3H).

*2-Phenyl-3-hexylindolizine (**7**):* For procedure, see **7**. Yield: (1.0 g, 3.6 mmol, 74%). ^{1}H NMR (300 MHz, $CDCl_3$) d d 7.85 (d, J = 6.9 Hz, 1H), 7.48 (d, 6.8 Hz, 2H), 7.41 (t, J = 7.0 Hz, 2H), 7.34 (d, J = 7 Hz, 1H), 7.33 (s, 1H), 7.30 (m, 1H), 6.60 (ddd, J = 7.8 Hz, 6.5 Hz, 1.0 Hz, 1H), 6.41 (t, J = 6.6 Hz, 1H), 2.85 (t, 7.9 Hz, 2H), 1.57 (q, 7.3 Hz, 2H), 1.31 (q, J = 6.6 Hz, 2H), 1.24 (m, 6H), 0.85 (t, J = 7.0 Hz, 3H). ^{13}C NMR (125 MHz, $CDCl_3$) d 136.6, 131.0, 129.3, 129.2, 128.7, 126.6, 125.1, 118.0, 116.0, 111.8, 110.4, 110.2, 31.9, 29.7, 24.4, 23.0, 14.4. IR (neat, cm^-

[1]): 3067.9, 2925.8, 2854.4, 1603.2, 1457.6, 734.6. HRMS (ESI) *m/z* calculated for $C_{20}H_{23}N$ $[M+H]^+$: 278.1909, found 278.1988.

*1-(thiophen-2'-yl-5'-carboxaldehyde)-2-phenyl-3-hexylindolizine (**12**):* For procedure, see **11**. Yield: (0.17 g, 0.44 mmol, 49%). ^{1}H NMR (500 MHz, $CDCl_3$) d 9.80 (s, 1H), 8.45 (dt, J = 8.1 Hz, 0.8 Hz, 1H), 7.61 (d, J = 5.4 Hz, 1H), 7.45 (dt, J = 8.0 Hz, 1.2 Hz, 1H), 7.39-7.32 (m, 3H), 7.25, (m, 2H), 6.94 (d, J = 4 Hz, 1H), 6.80 (ddd, J = 9.7 Hz, 6.3 Hz, 1.0 Hz, 1H), 6.61 (td, J = 7.2 Hz, 1.3 Hz, 1H), 2.68 (t, J = 8.0 Hz, 2H), 1.48 (m, 2H), 1.27-1.15 (m, 6H), 0.83 (t, J = 6.7 Hz, 3H). ^{13}C NMR (125 MHz, $CDCl_3$)d 182.6, 143.7, 141.5, 137.0, 135.2, 132.8, 131.7, 130.9, 128.6, 127.5, 127.2, 127.1, 123. 3, 123.2, 118.3, 118.2, 115.5, 114.7, 112.1, 3`.8, 31.6, 29.5, 24.2, 22.9, 14.4. IR (neat, cm^{-1}): 3067.6, 2925.8, 1661.1, 1435.4, 1225.8, 700.7. HRMS (ESI) *m/z* calculated for $C_{25}H_{24}NOS$ $[M]^+$: 387.1657, found 387.1754.

*3-(thiophen-2'-yl-5'-2-phenyl-3-hexylindolizine)-2-cyano-2-propenoic acid (**AH4**).* For procedure, see **AH2**. Yield: (0.022 g, 0.048 mmol, 14%). ^{1}H NMR (300 MHz, $CDCl_3$)). d 8.58 (d, J = 7.3 Hz, 1H), 8.2 (s, 1H), 7.71 (m, 1H), 7.5 (m, 1H), 7.4 (m, 4H), 6.9 (m, 2H), 6.73 (m, 2H), 2.68 (m, 2H), 1.49 (m, 2H), 1.25 (m, 6H), 0.85 (t, J = 6.9 Hz, 3H). HRMS (ESI) *m/z* calculated for $C_{28}H_{26}N_2O_2S$ $[M]^+$: 455.1793, found 415.1274. UV-Vis ($CHCl_3$): λ_{max} = 563 nm (ε = 11,300 $M^{-1}cm^{-1}$), λ_{onset} = 627 nm. Cyclic Voltammetry (0.1 M Bu_4NPF_6 in CH_2Cl_2, sweep width 1.1-(-2.0), 0.1 V/s scan rate): $E^{(S+/S)}$ = 0.99 V (vs NHE). $E^{(0-0)}$ = 2.06 V. $E^{(S+/S*)}$ = -0.98 V [vs NHE, calculated from $E^{(S+/S*)} = (E^{(S+/S)} - E_g^{opt})$].

*Synthetic Procedures for AH5: 2-(4'-Methoxyphenyl)-3-methylindolizine (**8**):* for procedure, see **7**. Yield: (2.0 g, 8.4 mmol, 78%). ^{1}H NMR (500 MHz, $CDCl_3$) d 7.84 (d, J = 7.4 Hz, 1H), 7.46 (d, J = 6.8 Hz, 2H), 7.34 (s, 1H), 7.32 (dd, J = 8.4 Hz, 1.2 Hz, 1H), 6.99 (d, J = 7.8 Hz, 2H), 6.60 (ddd, J = 6.2 Hz, 6.4 Hz, 1.0 Hz, 1H), 6.40 (t, J = 6.6 Hz), 3.85 (s, 3H), 2.42 (s, 3H). ^{13}C NMR (125 MHz, $CDCl_3$) d 158.6, 131.2, 130.0, 129.1, 128.8, 125.0, 117.7, 115.9, 114.3, 114.2, 110.2, 110.0, 105.7, 55.6, 9.9. IR (neat, cm^{-1}): 3069.4, 2997.9, 2833.6, 1610.6, 1246.6, 741.4. HRMS (ESI) *m/z* calculated for $C_{16}H_{15}NO$ $[M+H]^+$: 238.1232, found 238.1251.

1-(thiophen-2'-yl-5'-carboxaldehyde)-2-(4''-methoxyphenyl)-3-methylndolizine (13): For procedure, see **11**. Yield: (0.16 g, 0.46 mmol, 44%). ^{1}H NMR (500 MHz, $CDCl_3$) d 9.82 (s, 1H), 8.42 (dt, J = 7.2 Hz, 1.3 Hz, 1H), 7.63 (d, J = 4.2 Hz, 1H), 7.41 (dt, J = 8.9 Hz, 0.5 Hz), 7.17 (dm, J = 8.2 Hz, 2H, 6.99 (d, J = 3.9 Hz, 1H), 6.91 (dm, J = 8.6 Hz, 2H), 6.79 (ddd, J = 8.9 Hz, 6.6Hz, 1.0 Hz, 1H), 6.60 (td, J = 6.7 Hz, 1.4 Hz, 1H), 3.85 (s, 3H), 2.26 (s, 3H). ^{13}C NMR (125 MHz,$CDCl_3$)d 182.7, 159.2, 143.8, 141.6, 137.0, 132.9, 131.9, 131.4, 127.2, 127.1, 123.1, 118.4, 118.0, 114.5, 114.3, 114.2, 112.0, 109.7, 55.5, 9.4. IR (neat, cm^{-1}): 3032.3, 2934.2, 1659.0, 1431.1, 1247.1, 737.0.

*3-(thiophen-2'-yl-5'-2''-(4'''-methoxyphenyl)-3''-methylindolizine)-2-cyano-2-propenoic acid (***AH5**). For procedure see **AH2**. Yield: (0.090 g, 0.22 mmol, 49%). ^{1}H NMR (300 MHz, $CDCl_3$)). d 8.60 (d, J = 6.9 Hz, 1H), 8.25 (s, 1H), 7.75 (d, J = 4.0 Hz, 1H), 7.47 (d, J = 8.8 Hz, 1H), 7.24 (d, J = 6.6 Hz, 2H), 6.9 (d, J = 6.6 Hz, 2H), 6.97 (d, J = 4.0 Hz, 1H), 6.92 (dd, J = 8.2 Hz, 7.0 Hz, 1H), 6.74 (td, J = 7.0 Hz, 1.3 Hz, 1H), 3.90 (s, 3H), 2.28 (s, 3H). IR (neat, cm^{-1}): 3422.3, 2964.1, 2206, 1648.6, 1402.1, 1207.2. HRMS (ESI) *m/z* calculated for $C_{24}H_{18}N_2O_3S$

$[M]^+$: 415.1116, found 415.1130. UV-Vis ($CHCl_3$): λ_{max} = 554 nm (ε = 5,800 $M^{-1}cm^{-1}$), λ_{onset} = 634 nm. Cyclic Voltammetry (0.1 M Bu_4NPF_6 in CH_2Cl_2, sweep width 1.1-(-2.0), 0.1 V/s scan rate): $E^{(S+/S)}$ = 0.97 V (vs NHE). $E^{(0-0)}$ = 2.06 V. $E^{(S+/S*)}$ = -0.96 V [vs NHE, calculated from $E^{(S+/S*)} = (E^{(S+/S)} - E_g^{opt})$].

*Synthetic Procedures for AH6: 2-Hexyl-4-methoxypyridine (**5**):*[51] To a 50 mL flame dried flask was added Mg (0.54 g, 22.16 mmol), THF (25 mL) and one crystal of I_2 under a nitrogen atmosphere. A drop of Hexyl bromide was added and once the reaction started the remaining was added via addition funnel (2.48 mL, 2.92 g, 17.7 mmol). Set to stir at reflux. After 20 min, the reaction was allowed to cool to rt. In a separate flame dried flask was added Ni(dppp)Cl_2 (0.29 g, 0.53 mmol), 2-bromo-4-methoxypyridine (1.0 g, 5.3 mmol), THF (25 mL) and the falsk was cooled to 0ºC. The Grignard solution was added to the pyridine solution via cannula at 0ºC and the reaction allowed to warm to rt with stirring. After 30 min, the reaction mixture was set to stir at reflux. After 2h, the reaction mixture was diluted with 50 mL EtOAc, washed sequentially with sat'd $NaHCO_3$ (50 mL), brine (50 mL), and dried with $MgSO_4$. Filtered the solution and concentrated. Subjected crude product to flash chromatography using a gradient of Hexanes (500 mL) and EtOAc to yield an orange red oil (0.934 g, 4.85 mmol, 92%). ^{1}H NMR (500 MHz, $CDCl_3$) d d 8.31 (dd, J = 6.3 Hz, 0.7 Hz, 1H), 6.63 (t, J = 2.5 Hz, 1H), 6.61 (t, J = 3.1 Hz, 1H), 2.70 (t, 7.9 Hz, 2H), 1.69 (q, J = 7.8 Hz, 2H), 1.34-1.22 (m, 6 H), 0.88 (t, J = 7.0 Hz, 3H).

*2-Phenyl-3-pentyl-5-methoxyindolizine (**9**):* For procedure, see **7**. Yield: (0.10 g, 0.32 mmol, 16%). ^{1}H NMR (300 MHz, C_6D_6) d 7.63 (dm, J = 7.0 Hz, 2H), 7.33 (tm, J = 8.1 Hz, 2H), 7.18 (dt, J = 7.4 Hz, 1.3 Hz, 1H), 6.94 (dd, J = 7.3 Hz, 0.7 Hz, 1H), 6.73 (s, 1H), 6.08 (d, J = 2.5

Hz, 1H), 6.05 (dd, J = 8.4 Hz, 2.6 Hz, 1H), 3.30 (s, 3H), 2.94 (t, J = 7.6 Hz, 2H), 1.68 (m, 2H), 1.32-1.18 (m, 4H), 0.79 (t, J = 7.0 Hz, 3H). ^{13}C NMR (125 MHz, C_6D_6) d 151.9, 137.4, 131.2, 130.3, 129.3, 128.8, 128.4, 126.6, 126.5, 109.7, 109.2, 105.6, 94.0, 54.6, 32.2, 31.5, 24.7, 22.9, 14.3. IR (neat, cm^{-1}): 3063.9, 2953.8, 2927.8, 1646.6, 1222.1, 769.7. HRMS (ESI) *m*/*z* calculated for $C_{20}H_{23}NO$ $[M+H]^+$: 294.1858, found 294.1957.

1-(thiophen-2'-yl-5'-carboxaldehyde)-2-phenyl-3-pentyl-5-methoxyindolizine ***(14)****:* For procedure, see **11**. Yield: (0.16 g, 0.46 mmol, 44%). ^{1}H NMR (300 MHz, $CDCl_3$) d 9.76 (s, 1H), 8.38 (dd, J = 7.5 Hz, 0.7 Hz, 1H), 7.57 (d, J = 4.0 Hz, 1H), 7.38-7.32 (m, 3H), 7.25-7.22 (m, 2H), 6.85 (d, J = 4.0 Hz, 1H), 6.62 (d, J = 2.7 Hz, 1H), 6.38 (dd, J = 7.1 Hz, 2.7 Hz, 1H), 3.87 (s, 3H), 2.6 (t, J = 7.6 Hz, 2H), 1.45 (m, 2H), 1.3-1.2 (m, 4H), 0.85 (t, J = 6.4 Hz, 3H).

3-(thiophen-2'-yl-5'-2''-phenyl-3''-pentyl-5''-methoxyindolizine)-2-cyano-2-propenoic acid ***(AH6)****.* For procedure, see **AH2**. Yield: (0.018 g, 0.043 mmol, 60%). ^{1}H NMR (300 MHz, $CDCl_3$) d 8.53 (d, J = 7.3 Hz, 1H), 8.14 (s, 1H), 7.60 (m, 1H), 7.40 (m, 4H), 7.20 (m, 1H), 6.72 (d, J = 4.1 Hz, 1H), 6.65 (m, 1H), 6.51 (m, 1H), 6.48 (m, 1H), 3.91 (s, 3H), 2.57 (t, J = 7.1 Hz, 2H), 1.66 (m, 2H), 1.43 (m, 4H), 0.83 (t, J = 6.7 Hz, 3H). HRMS (ESI) *m*/*z* calculated for $C_{28}H_{26}N_2O_3S$ $[M]^+$: 471.1742, found 471.1260. UV-Vis ($CHCl_3$): λ_{max} = 597 nm (ε = 12,500 $M^{-1}cm^{-1}$), λ_{onset} = 665 nm. Cyclic Voltammetry (0.1 M Bu_4NPF_6 in CH_2Cl_2, sweep width 1.1-(-2.0), 0.1 V/s scan rate): $E^{(S+/S)}$ = 0.83 V (vs NHE). $E^{(0-0)}$ = 1.88 V. $E^{(S+/S*)}$ = -1.03 V [vs NHE, calculated from $E^{(S+/S*)} = (E^{(S+/S)} - E_g^{opt})$].

SECTION 2. FILM MORPHOLOGY CONTROL IN HIGHLY EFFICIENT INDOLIZINE-BASED SENSITIZERS FOR DSC

INTRODUCTION

As described in Part 1, the key challenges in DSC are twofold: 1) The sensitizers need very narrow band gaps in order to absorb light to 920 nm and thus maximize the short circuit current (J_{sc}). 2) The sensitizers need to exhibit a high level of film morphology control so that upon adsorption onto the semiconductor surface, the redox shuttle is effectively blocked from the surface, thus reducing recombination of electrons from the TiO_2 CB and increasing J_{sc}, V_{oc}, and FF.[7,52,53]

In practice, film morphology manifests in two main ways: either the sensitizer has been modified synthetically with non-conjugated substituents as to physically block the surface of the TiO_2[9,33,34] or the surface of the TiO_2 has been physically blocked with non-title molecules, Figure 15.[10,54] The addition of non-conjugated functionalities often adds more synthetic steps to syntheses, which increases sensitizer cost and synthetic complexity. Conversely, in the very successful "multi-capping" approach reported recently for dye **ADEKA-1** requires the use of very strong anchoring groups such as $–P(O)(OH)_2$ or $–Si(OMe)_3$, which greatly increases the synthetic complexity.[10]

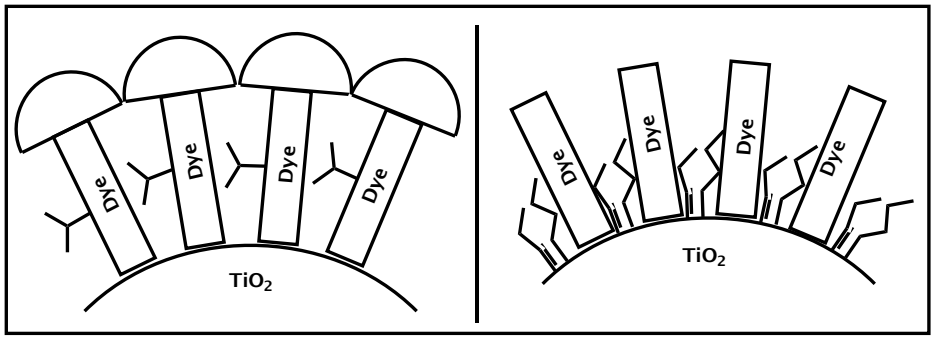

Figure 15. *Left:* Surface blocking via sensitizer non-conjugated substituents. *Right*: Surface blocking via "multi-capping."

DYE SYNTHESIS

We chose to further investigate the potential for indolizine-based DSC sensitizers by incorporating non-conjugated substituents to encourage superior morphology control.[55] We undertook a bottom-up synthesis of the indolizine donor starting with 4-bromo-2-picoline, Scheme 2. After alkylating the picolinic carbon with 2-ethylhexylbromide (an established blocking group),[56] a Suzuki coupling added the first of two bis(hexyloxy)resorcinol morphology control groups to the pyridine ring.[57] The indolizine structure was then formed in a one-pot procedure[55] to generate a Suzuki coupling partner to incorporate the second bis(hexyloxy)resorcinol group.[57] A C-H activation coupling reaction successfully attached the π-bridge functionalities studied to the donor.[26b] The π-bridges we were able to successfully react in this way include thiophene, pyridine (Pyr),[58] 4H-cyclopenta[2,1-b : 3,4-b]dithiophene (CPDT),[59] which are some of the bridges present in the vast majority of state of the art D- π -A dyes (Scheme 2). Once coupled to the donor, the cyano-acrylic acid acceptor group was formed by condensation of an aldehyde group on the bridge.

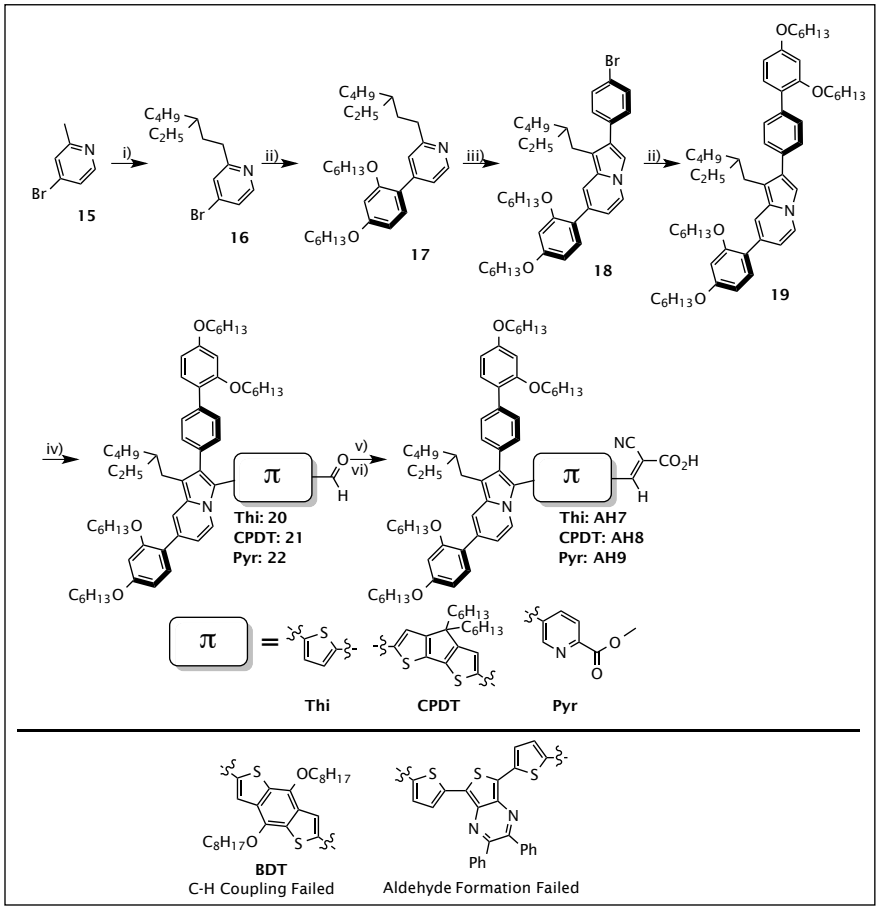

Scheme 2. *Top*: Synthetic avenues to surface-blocking indolzine dyes. *Bottom:* Bridges that did not result in a compete dye. Conditions: i): a): LDA, THF, -78ºC. b): 2-ethylhexylbromide, -78ºC to rt. 1.10 g, 19%. ii): 2,4-bis(hexyloxy)phneylboronic acid, $Pd(PPh_3)_4$, Aliquat 336, Na_2CO_3, H_2O, Tol reflux, **17**:2.28g, 69%, **19**: 3.30g, 88%. . iii): a): 2,4'-dibromoacetophenone, acetone reflux. b): $NaHCO_3$, H_2O reflux, 2.83g, 79%. iv): 5-bromo-2-thiophenecarboxaldehyde, $PdCl_{2(}PPh_3)_2$, KOAc, NMP, 80ºC, **20**:0.086 g, 81%, **21**: 0.017 g, 21% (used without purification), **22**: 0.038 g, 35%. v): cyanoaceticacid, piperidine, $CHCl_3$, 90ºC, **AH7**: 0.030 g, 67%, **AH8**: 0.004g, 25% (impure). vi): **AH9**: a): xs DIBAL, CH_2Cl_2. b): Swern Oxidation c): cyanoacetic acid, piperidine, $CHCl_3$, 0.002g, 4.5% over three steps. *Bottom*: Bridges used that did not result in a completed dye.

Synthesis of dyes with other π-bridges using C-H activation was also attempted but did not lead to completed dyes, including Benzo[1,2-b:4,5-b′]dithiophene (BDT),[60] and their structures including the step that failed are also shown in Scheme 2. Attempts to couple the bridge BDT to inodlizine donor **19** were unsuccessful, even in the presence of very strong donating ligands for the Pd catalyst. A bridge based on 5,6-diphenylpyrazin[2,3]thiophene was succssfully coupled to indolizine donor **19**, however, an aldehyde group could not be installed by deprotonation/quenching with DMF or through a Vilsmeier-Haack reaction.

RESULTS AND DISCUSSION

Formation of the acceptor group generally equates to fully air, water, acid, and chromatography stable molecules, however, the donation strength of the indolizine donor forced the synthesized dyes to be much less stable than should have been expected through great destabilization of the dye ground-state oxidation potential. While **AH7** could be isolated and purified, **AH8** and **AH9** were too unstable to be isolated and/or purified. For **AH8** the extended conjugation of an additional, planarized thiophene resulted in a ground-state oxidation potential substantial above potential stable in O_2. For **AH9**, instability is likely due to the severe twist angle between the indolizine donor and π –bridge, which reduced the ability of the donor to be incorporated into the dye's stabilizing D-π-A conjugated path. The effect of this twist angle can be observed in the very low (10000-20000) extinction coefficient observed in dyes **AH3-AH6**. While full characterization data for these dyes could not be obtained, the optical and electrochemical data collected is compiled in Table 6.

Table 6. Optical and Electronic Properties of Dyes **AH7-9**.

Dye	λ_{max} (nm)[a]	λ_{onset} (nm)[a]	$E_{(0-0)}$ (eV)[b]	$E_{(S+/S^*)}$ (V)[c]	$E_{(S+/S)}$ (V)[d]
AH7	605	685	1.81	−0.93	0.87
AH8[e]	640	750	1.65	−0.95	0.70
AH9[f]	590	690	1.82	−1.12	0.70

[a] Measured in CH_2Cl_2. [b]Estimated from the tangent of the lower-energy tangent of the lambda max transition in the UV-Vis absorption spectrum in CH_2Cl_2. [c]Taken as the difference between the oxidation potentia $E_{(S+/S)}$ and the estimated optical bandgap $E_{(0-0)}$. [d] Measured in a 0.1 M Bu_4NPF_6 in CH_2Cl_2 solution with glassy carbon disk working electrode, Pt reference electrode, and Pt counter electrode with ferrocene as an internal standard. Values are reported versus NHE. [e]: Estimated from impure sample [f]: Estimated from impure sample.

The oxidation potentials for the three dyes are very different, due to the difference in twist angle likely present. Dyes **AH7** and **AH8** are attached from indolizine to a thiophene-type ring group, which is sterically smaller than the six-membered **AH9**. Because the donor-bridge twist angle is much more severe, the oxidation potential observed is not characteristic of a D-π-A dye, but of a strongly donated indolizine subunit. This character change due to twist angle also affected the dye stability (**AH9** was the least stable of the three) and dye $E_{(S+/S^*)}$ (**AH9** had the highest energy (most destabilized excited state, as estimated from absorption onset).

Dyes **AH7**, **AH8**, and **AH9** all survived the reaction conditions and workup and could be characterized to some extent. The only dye stable to purification techniques was **AH7**, which was only stable for 30 min in solution. Our hypothesis for the decreased stability of dyes **AH7-9** was that the combination of poorly paired donor/acceptor strength and severe twist angle between the donor and bridge units greatly decreased dye stability, especially in the presence of acid and oxygen. Likely, the dye could be oxidized by atmospheric oxygen and the sensitivity to acid likely originated from protonation of the indolizine nitrogen. These hypotheses are

supported by the observation that in the knoevenagel condensation's reaction conditions, which include base and inert atmospheric conditions, no decomposition is observed. The UV-Vis absorption spectrum for **AH7** is shown in Figure 16.

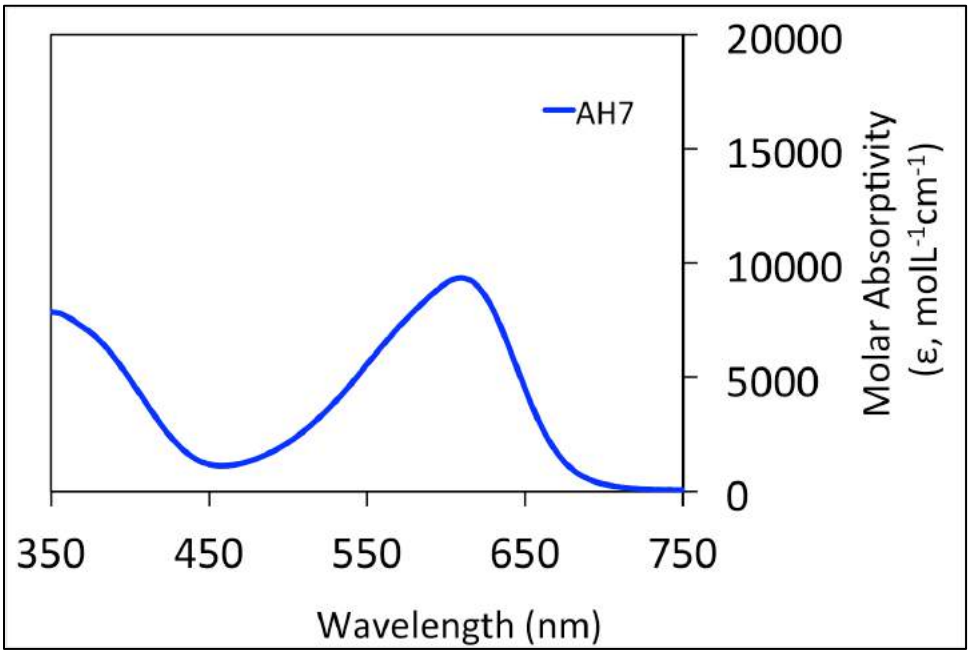

Figure 16. UV-Vis absorption spectrum for **AH7** measured in CH_2Cl_2.

Once it was confirmed that the energy levels for dye **AH7** was suitable for use in DSC, it was tested in devices using a TiO_2 semiconductor. While dye series **AH2-AH6** was tested using only the I^-/I_3^- redox shuttle due to the poor morphology control inherent to the dyes, **AH7** was tested using both the I^-/I_3^- redox shuttle and $Co^{III/II}(bpy)_3$ shuttle (on-going tests). From the equation PCE (η) % = $(J_{sc}V_{oc}FF)/I_{(sun)}$ where J_{sc} = short-circuit current, V_{oc} is the open-circuit voltage, *FF* is the fill factor and $I_{(sun)}$ is the incident light intensity, the device performances under AM 1.5 irradiation were analyzed and the results are compiled in Table 7.

Table 7. Photovoltaic performance of **AH7** compard to **AH3** and **D35**. Measurements taken by Yella, Nazeeruddin, and Grätzel.

Dye	Redox Shuttle	J_{sc} (mA/cm^2)	V_{oc} (mV)	FF	η (%)
AH3	I^-/I_3^-	10.0	680	0.74	5.10
AH7	I^-/I_3^-	14.67	665	0.67	6.67
	$Co^{III/II}$	??	??	??	??
D35	I^-/I_3^-	12.96	750	0.61	6.00
	$Co^{III/II}$	10.7	920	0.68	6.70

When using the I^-/I_3^- redox shuttle, the performance of **AH7** was higher than the simple indolizine dye **AH3** and simple dye with Hagfeldt's triarylamine donor-based dye **D35**.[34b,c] That **AH7** performs better than **D35** is significant in that Hagfeldt's landmark dye is largely regarded as extremely well-performing, both in surface blocking and photon to energy conversion across the dye's absorption spectrum even though it absorbs only ~200 nm of the visible spectrum (530 nm onset). Even though it has a much lower energy CT band, dye **AH7** performs only somewhat better, due to two main factors: first, the extinction coefficient is very low at its largest value (9,350 $Lmol^{-1}cm^{-1}$) and second, the absorption coefficient drops well below 5,000 (the threshold for quantitative photon conversion) between 400-500 nm. The voltage difference between **AH3** and **AH7** can likely be ascribed to the decreased driving force for dye regeneration, while the current difference is due to the red shifted CT band of **AH7**. Dye **AH3** should likely have V_{oc} similar to that of **D35**, however, aggregation contributed to voltage losses by intermolecular energy transfer between aggregated dyes. While **AH7** likely does not aggregate to the same extent, the decreased ΔG_{regen} lowers the voltage well below that of **D35**. Utilizing $Co^{III/II}$ redox shuttles allows for lower ΔG_{regen} requirments (250 mV) and precise matching of redox shuttle to

sensitizer energy level. The more favorable overpotential with Co redox shuttles equates to higher V_{oc} values in most cases, which boosts device performance.

EXPERIMENTAL SECTION

See Chapter 1, Part 1 for General Considerations (Experimental, Photovoltaic Characterization, and Device Fabrication).

Synthetic Procedures to Reach AH7:

*2-(3-ethylheptyl)-4-bromopyridine (***16***):* A flame dried flask was charged with dry, degassed THF (10 mL) and diisopropylamine (3.08 mL, 22.0 mmol) was added and cooled to -78ºC. Once cool, n-butyl lithium (2.5 M, 8.8 mL) added dropwise via syringe. After 40 minutes, the LDA solution was transferred via cannula to a flame dried flask equipped with a stirbar that had previously been charged with THF (10 mL) and 4-bromo-2-picoline (2.4 mL, 20.2 mmol). After 30 minutes, ethylhexylbromide (5.39 mL, 30.4 mmol) added dropwise via syringe, the solution was allowed to warm to rt with stirring, and was monitored by ^{1}H NMR spectroscopy. After 16h, the reaction mixture was diluted with Et_2O (100 mL), quenched with 10% H_3PO_4 (20 mL), and washed with H_2O (3 x 25 mL). material passed through SiO_2 plug using first hexanes, then 10% EA:Hx. Product fractions concentrated to yield a pale yellow oil (1.10 g, 19%). %). ^{1}H NMR (500 MHz, $CDCl_3$) δ 8.33 (d, J = 5.5 Hz, 1H), 7.33 (d, J = 2 Hz, 1H), 7.26 (dd, J = 2 Hz, 5.5 Hz, 1H), 2.73 (t, J = 8 Hz, 2H), 1.65 (m, 2H), 1.37-1.24 (m, 10H), 0.89 (t, J = 7 Hz, 3H), 0.87 (t, J = 7.5 Hz, 3H).). ^{13}C NMR (125 MHz, $CDCl_3$) δ 164.9, 150.3, 133.2, 126.2, 124.5, 39.0, 35.9, 33.6, 33.0, 29.2, 26.1, 23.4, 14.5, 14.4, 11.1.

*2-(3-ethylheptyl)-4-(2,4-bis(hexyloxy)phenyl)pyridine (***17***):* A flask equipped with reflux condenser and stirbar was charged with **16** (1.95 g, 6.86 mmol), 2,4-bis(hexyloxy)bromobenzene (3.05 g, 7.55 mmol) and dissolved in 6:1 Toluene : 2M Na_2CO_3 (aq) (34 mL total). Aliquat 336 (3 drops) was added and the solution bubbled vigorously with N_2. After 30 min, $Pd(PPh_3)_4$ (0.31 g, 0.27 mmol) added in one solid portion from a vial, the reaction mixture was heated to Toluene reflux, allowed to stir, and was monitored by ^{1}H NMR spectroscopy. After 18h, reaction mixture was cooled to rt, the organic layer was separated and the crude reaction mixture loaded directly onto SiO_2 plug. Passed Hexanes (250 mL, then 5%EtOAc:Hexanes (250 mL), then 10%EtOAc:Hexanes (500 mL), then 25%EtOAc:Hexanes (500 mL) through plug. Product fractions concentrated to yield a mixture of product and protodeboronated starting material (2.28g, 69% yield, 3.30 g of a 67% impure mixture). Used without further purification. ^{1}H NMR (300 MHz, $CDCl_3$) δ 8.5 (d, J = 5.4 Hz, 1H), 7.34 (s, 1H), 7.26 (m, 2H), 6.59 (aps, 1H), 6.56 (s, 1H), 3.99 (m, 4H), 2.8 (m, 2H), 1.85-1.74 (m, 6H), 1.5-1.3 (m, 22 H), 0.96-0.87 (m, 12 H).

*2-(4-bromophenyl)-3-(2-ethylhexyl)-5-(2,4-bis(hexyloxy)phenyl)indolizine (***18***):* A flask equipped with a reflux condenser and stirbar was charged with **17** (2.60 g, 5.4 mmol), 2,4'-dibromoacetophenone (1.50 g, 5.4 mmol), dissolved in acetone (25 mL), set to stir, heated to reflux, and monitored by ^{1}H NMR spectroscopy. After 15h, the reaction mixture was cooled to rt, concentrated, and suspended in degassed H_2O (20mL). $NaHCO_3$ added (1.81 g, 21.6 mmol), and the reaction mixture was set to stir, heated to reflux, and monitored by ^{1}H NMR spectroscopy. After 2h, CH_2Cl_2 (50 mL) added, org. layer separated and diluted with Hexanes (200 mL),

passed through a short plug of SiO_2 using first 25% CH_2Cl_2:Hexanes (500 mL), then DCM (1.5L). Concentrated product fractions to yield an off-white solid (2.83 g, 79%). %). ^{1}H NMR (300 MHz, $CDCl_3$) δ 7.80 (d, J = 6.6 Hz, 1H), 7.51 (d, J = 8.4 Hz, 2H), 7.45 (s, 1H), 7.35 (d, J = 8.5 Hz, 2H), 7.27 (s, 2H), 6.71 (dd, J = 1.8 Hz, 4.2 Hz, 1H), 6.55 (m, 2H), 6.46 (apd, J = 8.0 Hz, 1H), 3.95 (m, 4H), 2.77 (m, 2H), 1.83-1.72 (m, 6 H), 1.5-1.24 (m, 22 H), 0.96-0.87 (m, 12 H).

*2-(4-(2,4-bis(hexyloxy)phenyl)-3-(2-ethylhexyl)-5-(2,4-bis(hexyloxy)phenyl)indolizine (***19***):* A flask equipped with reflux condenser and stirbar was charged with **18** (2.83 g, 4.28 mmol), 2,4-bis(hexyloxy)bromobenzene (1.90 g, 4.7 mmol) and dissolved in 6:1 Toluene : 2M Na_2CO_3 (aq) (23 mL total). Aliquat 336 (3 drops) was added and the solution bubbled vigorously with N_2. After 30 min, $Pd(PPh_3)_4$ (0.20 g, 0.17 mmol) added in one solid portion from a vial, the reaction mixture was heated to Toluene reflux, allowed to stir, and was monitored by ^{1}H NMR spectroscopy. After 2h, reaction mixture cooled to rt, the org. layer separated and directly subjected to column chromatography using 350 mL SiO_2, 25% CH_2Cl_2:Hexanes, product spot concentrated to yield a pale yellow solid (3.30 g, 88%). ^{1}H NMR (300 MHz, $CDCl_3$) δ 7.82 (d, J = 7.2 Hz, 1H), 7.59 (d, J = 9 Hz, 2H), 7.49 (d, J = 8.8 Hz, 2H), 7.46 (s, 1H), 7.33 (s, 1H), 7.29 (dd, J = 1.8 Hz, 9 Hz), 6.69 (dd, J = 3 Hz, 7.5 Hz, 1H), 6.56 (m, 4H), 3.98 (m, 8H), 2.84 (apd, J = 7.2 Hz, 2H), 1.89-1.7 (m, 10H), 1.55-1.2 (m, 34 H), 0.96-0.87 (m, 18 H).

*1-(thiophen-2'-yl-5'-carboxaldehyde)-2-(4-(2,4-bis(hexyloxy)phenyl)-3-(2-ethylhexyl)-5-(2,4-bis(hexyloxy)phenyl)indolizine (***20***):* To an amber vial equipped with a stirbar was added 2-

bromo-5-thiophenecarboxaldehyde (0.019 mL, 0.165 mmol), **19** (0.10 g, 0.11 mmol), NMP (1 mL). After degassing with N_2 30 min, $PdCl_2(PPh_3)_2$ (0.0039 g, 0.0055 mmol), KOAc (0.016 g, 0.165 mmol) added in one solid portion. Reaction mixture heated to 80ºC, allowed to stir, and monitored by ^{1}H NMR spectroscopy. After 5 h the reaction mixture was directly subjected to column chromatography using solvent gradient of hexanes to 3%EtOAc:hexanes to 5% acetone:hexanes. Product sport concentrated to yield a red oil (0.086g, 81%). ^{1}H NMR (300 MHz, $CDCl_3$) δ 9.79 (s, 1H), 8.53 (d, J = 7.5 Hz, 1H), 7.58 (apd, J = 4.2 Hz, 2H), 7.54 (d, J = 7.8 Hz, 2H), 7.31 (m, 2H), 7.23 (2, 1H), 6.9 (m, 2H), 6.58 (m, 4H), 3.99 (m, 8H), 2.66 (apd, J = 5.4, 2H), 1.86-1.55 (m, 10H), 1.5-1.05 (m, 34 H), 0.95-0.6 (m, 18 H).

*3-(thiophen-2'-yl-5'-carboxaldehyde)-2-(4-(2,4-bis(hexyloxy)phenyl)-3-(2-ethylhexyl)-5-(2,4-bis(hexyloxy)phenyl)indolizine)-2-cyano-2-propenoic acid (**AH7**).* A flask equipped with a stirbar was charged with **20** (0.043 g, 0.044 mmol), $CHCl_3$ (0.85 mL) and degassed wth N_2. After 30 min, cyanoacetic acid (0.011 g, 0.13 mmol) and piperidine (0.039 mL, 0.31 mmol) added and the flask sealed with a plastic stopper and electrical tape. The reaction mixture was heated to 90ºC with stirring and was monitored by TLC. After 40 min, the reaction mixture was cooled to rt, diluted with CH_2Cl_2 (50 mL), acidified with AcOH (5 mL), washed with H_2O (3 x 100 mL) and passed through a short pad of SiO_2 using CH_2Cl_2 (500 mL), 10% MeOH:CH_2Cl_2 (500 mL), 5% AcOH:10%MeOH:CH_2Cl_2 500 mL. Product fractions concentrated to yield a black solid (0.030 g, 67%). ^{1}H NMR (300 MHz, $CDCl_3$) δ 9.79 (s, 1H), 8.53 (d, J = 7.5 Hz, 1H), 7.58 (apd, J = 4.2 Hz, 2H), 7.54 (d, J = 7.8 Hz, 2H), 7.31 (m, 2H), 7.23 (2, 1H), 6.9 (m, 2H), 6.58 (m, 4H), 3.99 (m, 8H), 2.66 (apd, J = 5.4, 2H), 1.86-1.55 (m, 10H), 1.5-1.05 (m, 34 H), 0.95-0.6 (m, 18 H).

SECTION 3. SYNTHESIS OF INDOLIZINE-BASED SENSITIZERS WITH BIS-RHODANINE ACCEPTOR SUBUNITS FOR DSC

To address both issues raised from dye series **AH7-AH9**, we chose to synthesize dyes that contained stronger acceptors (bis-rhodanine)[61] than the cyanoacrylic acid group. A further advantage of the bis-rhodanine group is that an alkene group is formed between the donor and bis-rhodanine since the bond forming reaction is a C-C bond-forming condensation reaction, which equated to much less severe twist angles. Two types of dyes were synthesized to assess the bis-rhodanine acceptor group. The first type compared the film morphology-controlling donor from **AH7** incorporated into either a D-π-A dye (thiophene bridge) or D-A dye (no bridge). The second type compared the cyanoacrylic acid accepting group with the bis-rhodanine accepting group by incorporating the donor from **AH5** into a D-π-A dye (olefin-thiophene bridge). The dyes resulting from this series and the synthetic route to reach them are shown in Scheme 3.

The bis-rhodanine acceptor was synthesized by first cyclizing octyl isothiocyanate with methyl 2-thiol acetic acid to form rhodanine **20**. The bis-rhodanine **21** was synthesized from condensation with ethyl 2-isocyanatoacetate followed by alkylation with ethyl 2-bromo acetate.[61] Acid hydrolysis of ester **21** yielded acid **22**. To form aldehyde **26** (no π-bridge to help narrow the bandgap), indolizine **19** underwent a Vilsmeier-Haack reaction. Condensation with bis-rhodanine **25** then formed **AH11**. Similarly, condensation of aldehyde **20** with bis-rhodanine **25** yielded **AH10**. Using the hydrolyzed bis-rhodanine proved important, as condensation with bis-

rhodanine ester **25** proceeded smoothly to yield esters **27** and **28**, however, basic hydrolysis with LiOH resulted in decomposition and no product formation.

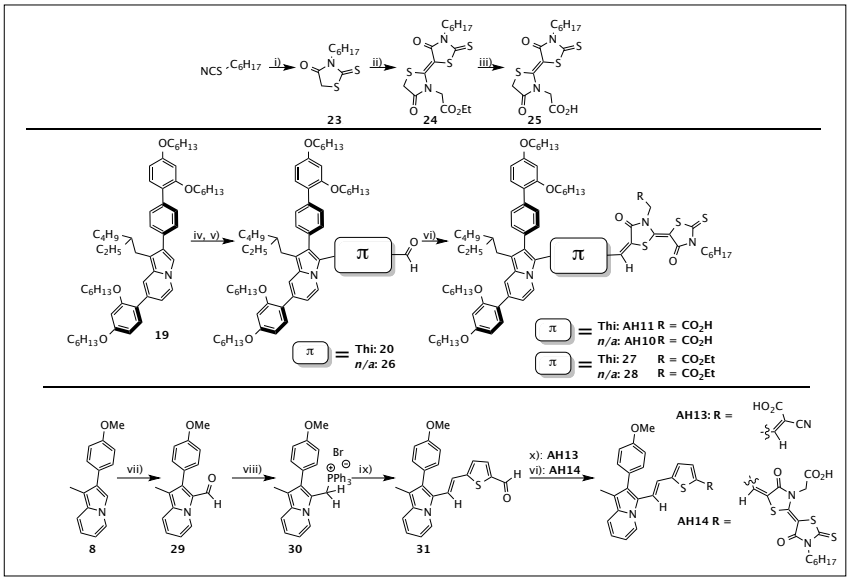

Scheme 3. Top: Synthetic route to bis-rhodanine **25**. Bottom: Synthetic route to D-A dye **AH11** and D-π-A dye **AH10**. Conditions: i): thioglycolic acid, MeOH, H_2O, 100ºC, 1.0 g, 79%. ii): a): $EtCO_2CH_2CNS$, DBU, rt, MeCN. b): bromoethylacetate, 100ºC, 0.56 g, 30%. iii): HCl, AcOH, 90ºC, 0.035 g, 30%. iv): DMF, $POCl_3$, DCE, 0ºC to rt, 0.150 g, 50%. v): 5-bromo-2-thiophenecarboxaldehyde, $PdCl_2(PPh_3)_2$, KOAc, NMP, 80ºC, 0.086 g, 81%. vi): **25** (for acid product) or **24** (for ester product), piperidine, $CHCl_3$, 90ºC, **AH10**: 0.046 g, 45%, **AH11**, 0.006 g, 6% yield, **27**: 0.063 g, quant., **28**: 0.030 g, 41%, vii): DMF, $POCl_3$, DCE, 0ºC to rt, 0.79 g, 87% yield. viii (a): $LiAlH_4$, THF, 0ºC to rt, 0.67 g, 84%. (b): $HPPh_3Br$, $CHCl_3$ reflux, 0.18g, quant. ix): 2,5-thiophenebis(carboxaldehyde), KOtBu, THF, -78ºC to rt. 0.013 g, (85:15 E:Z), 50%. x): cyanoacetic acid, piperidine, $CHCl_3$, 90ºC, 0.005 g, 30%. vi): **25**, piperidine, $CHCl_3$, 90ºC, 0.015 g, 25%.

To synthesize **AH13** & **14** a Wittig reagent was synthesized from indolizine **8** by Vilsmeier-Haack reaction to form aldehyde **29** followed by $LiAlH_4$ reduction to form alcohol **30** and substitution with $HPPh_3Br$ to form Wittig reagent **31**. Olefination with 2,5-thiophenedicarboxaldehyde formed aldehyde **32** and condensation formed cyanoacetic acid-based dye **AH13** as well as bis-rhodanine-based dye **AH14**. All ester products and acid products were stable to purification, with **AH10** being the least stable of the series due to a severe twist angle between the indolizine and thiophene moieties and, as stated in previous section, the potential for decomposition due to heterocycle protonation in acidic media.

Results and Discussion

Dyes **AH10** and **AH11** both exhibit excellent panchromatic (full-spectrum) absorption, as shown in the UV/Vis spectrum in Figure 17. The extinction coefficients for both dyes are much higher than observed for **AH2-9**, due to the elimination of severely twisted aryl-aryl bonds. The extinction coefficient was >10,000 from 350 nm to 700 nm for dye **AH10**. The large red shift observed in **AH10** and **AH11** can be rationalized by the addition of strongly accepting bis-rhodanine and in **AH10**, the presence of the simple π-bridge thiophene. The λ_{onset} for **AH10** is 740 nm and for **AH11** is 650 nm (both in CH_2Cl_2), both of which are more red shifted in comparison with the indoline D-A dye **D205** (λ_{onset} = 570 nm in DMF) that achieved 9.4% PCE.[61] Unfortunately, the energy levels for **D205** are not reported in the literature, however, the energy levels of **D149**, an analogous dye have been reported and will serve as a useful comparison to dye **AH10-11**.[62] Further comparison of the electro-optical properties of the two indolizine dyes with **D149** are listed in Table 8.

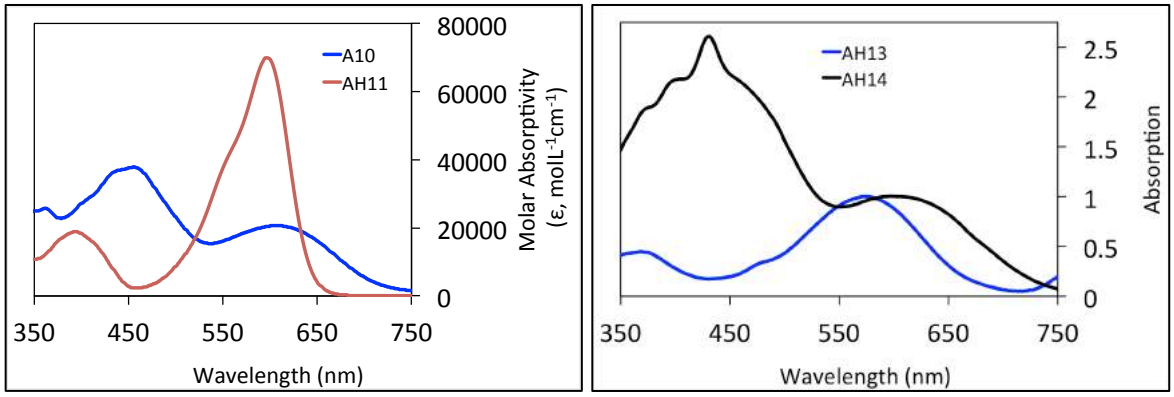

Figure 17. *Left*: UV-Vis absorption spectra of **AH10** and **AH11** in CH_2Cl_2. *Right*: UV-Vis absorption spectra of **AH13** and **AH14** in CH_2Cl_2.

Table 8. Optical and Electronic Properties of dyes **AH10,11,13,14** compared to dye **D149**.

Dye	λ_{max} (nm)[a]	λ_{onset} (nm)[a]	ε ($Lmol^{-1}cm^{-1}$)[a]	E_g^{opt} (eV)[b]	$E_{(S+/S^*)}$ (V)[c]	$E_{(S+/S)}$ (V)[d]
AH10	609	740	20,000	1.67	-0.91	0.76
AH11	596	650	70,000	1.91	-0.91	0.99
AH13	609	720	---	1.71	-1.01	0.71
AH14	616	740	---	1.67	-0.96	0.71
D149	550[e]	610[e]	68,000[e]	2.03[f]	-1.15[g]	0.88[h]

[a] Measured in CH_2Cl_2. [b]:Estimated from the tangent of the lower-energy tangent of the lambda max transition in the UV-Vis absorption spectrum in CH_2Cl_2. [c]Taken as the difference between the oxidation potential $E_{(S+/S)}$ and the estimated optical bandgap $E_{(0-0)}$. [d] Measured in a 0.1 M Bu_4NPF_6 in CH_2Cl_2 solution with glassy carbon disk working electrode, Pt reference electrode, and Pt counter electrode with ferrocene as an internal standard. Values are reported versus NHE. [e] Taken from Ref. 62. [f]: Estimated from the onset of absorption in Ref. 62 to be more comparable to **AH10-11**. [g]: Estimated from the difference between the onset of absorption and the oxidation potential vs. NHE reported in Ref. 62. [h]: Reported in Ref. 62 to have been measured in MeCN.

The energy levels of **AH10-11** are near ideal for use in DSC with the $E_{(S+/S)}$ lying near 0.76 V vs. NHE for **AH10** & **AH13** & **AH14** and was lower (0.99 V vs. NHE) for **AH11**. The $E_{(S+/S^*)}$ lies well above the ideal value of -0.7 V vs NHE energetically. All four have lower

$E_{(S+/S*)}$ values than **D149** due to competing local aromaticity. While the $E_{(S+/S)}$ for **D149** is higher in energy than **AH11**, the former was measured in MeCN while the latter was measured in CH_2Cl_2. Changing solvent can greatly affect the apparent energy levels, so the $E_{(S+/S)}$ are much harder to compare. Besides this difficulty, it appears that dyes **AH11** and **D149** have similar energy levels, with **AH11** absorbing a little more into the NIR region (650 nm λ_{onset} vs. 610 nm λ_{onset}).

Having established the dyes exhibited suitable characteristics for productive photon-to-electric conversion, dyes **AH10**-**AH11** and **AH13-14** were examined in DSC devices with a TiO_2 semiconductor and I^-/I_3^- redox shuttle. From the equation PCE (η) % = $(J_{sc}V_{oc}FF)/I_{(sun)}$ where J_{sc} = short-circuit current, V_{oc} is the open-circuit voltage, *FF* is the fill factor and $I_{(sun)}$ is the incident light intensity, the device performances under AM 1.5 irradiation were analyzed (Table 9).

Table 9. Device performance data for dyes **AH10**-**AH11** and **AH13-14** compared with dye **D149**.[a] Measurements performed by Giordano, Nazeeruddin, and Grätzel.

Dye	J_{sc} (mA/cm^2)	V_{oc} (mV)	FF	η (%)
AH10	4.33	456	0.717	1.46
AH11[b]	7.27	557	0.757	3.15
AH13	7.42	498	0.733	2.78
AH14	0.55	376	0.723	0.15
D149[c]	19.08	638	0.682	8.26

[a]: Electrolyte 960 used as electrolyte, 100 mM LiI additive used in electrolyte, no CDCA additive used. [b]: no LiI added to device. [c]: no LiI added, no CDCA added.

After device optimization with LiI to increase electron injection efficiency into the TiO_2 CB, dye **AH14** had the lowest voltage output at 376 mV with **AH11** being highest at 557 mV.

The voltage was likely highest because it did not require Li^+, which is known to lower voltage output. While indoline dye **D149** has been reported to produce 8.85% PCE, the measured device performance of dyes **AH10-11** an **AH13-14** is much lower, with **AH14** producing the least at 0.14% and **AH11** producing the most at 3.15%. The J_{sc} values for indolizine D-π-A dyes were very low in comparison with indoline dye **D149**. Devices with D-A dye **AH11** and D-π-A dye **AH13**, which had a cyanoacrylic acid acceptor group, had much higher J_{sc} values than **AH10** or **AH14**. While recombination is likely suppressed with **AH11**, it does seem to be completely eliminated, as the J_{sc} value is very low. Furthermore, even though the $E_{(S+/S^*)}$ values for all dyes except **AH11** were well above the TiO_2 CB (Figure 18), LiI additive was needed in to ensure adequate electron injection. The fill factor values were very good, which indicated that performance losses due to resistance were low.

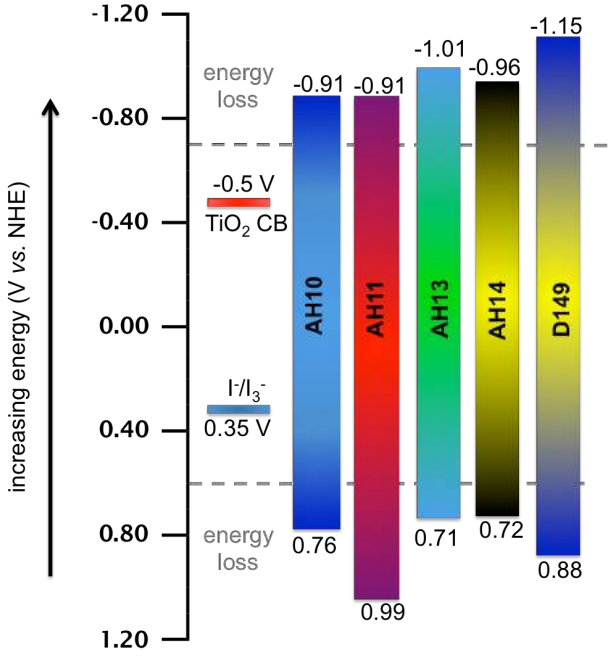

Figure 18. Bandgap diagram of dyes **AH10-14** and dye **D149**.

EXPERIMENTAL SECTION

See Chapter 1, Section 1 for General Considerations (Experimental, Photovoltaic Characterization, and Device Fabrication).

Synthetic Methods to Reach bis-rhodanine acceptor **25**:

*N-hexylrhodanine (***23***)*: A flask equipped with a stirbar and reflux condenser was charged with hexyl isocyanate (0.929 mL, 5.85 mmol), thioglycolic acid (0.67 mL, 8.5 mmol), MeOH (5 mL), and H_2O (58 mL). It was heated to reflux with stirring. After 16h, reactant mixture was extracted with EtOAc (3 x 100 mL), passed through a plug of SiO_2 using CH_2Cl_2, and product spot concentrated. 50% conversion observed, so NEt_3 (0.5 equiv, 0.29 g, 2.9 mmol) and methylthioglycolate (0.5 equiv, 0.36 g, 2.9 mmol) added, allowed to stir at rt, and was monitored by ^{1}H NMR spectroscopy. After 3h, reaction mixture was diluted with Et_2O (50 mL), washed with H_2O (3 x 100 mL), dried with $MgSO_4$ and concentrated to yield a colorless oil (1.0 g, 79%).

*Ethyl 2-(N'-hexylrhodaninyl)-rhodanine N-2-acetate (***24***):* A flask equipped with a stirbar was charged with rhodanine **23** (0.90g, 3.67 mmol), ethyl 2-isocyanato acetate (0.53 g, 3.67 mmol), MeCN (4 mL), DBU (0.55 mL, 0.56 g), and allowed to stir at rt. After 1h, ethyl bromoacetate added and the mixture was warmed to 100ºC with stirring and was monitored by ^{1}H NMR spectroscopy. After two hours, the crude reaction mixture was loaded onto a SiO_2 plug and eluted with CH_2Cl_2. Dissolved in MeOH, left in -4ºC freezer to crystallize overnight. Metallic red crystals obtained (0.56 g, 30% yield).

2-(N'-hexylrhodanin-5-yl)-rhodanine-3-yl)-acetic acid (**25**): A flask equipped with a stirbar was charged with ester **24** (0.37 g, 0.851 mmol), concentrated HCl (5 mL), glacial acetic acid (10 mL), allowed to stir at 90ºC. After four hours, reaction mixture was cooled to rt, extracted with CH_2Cl_2 (3 x 20 mL), dried with $MgSO_4$ and concentrated to yield a yellow/orange powder (0.090 g, 28%). ^{1}H NMR (300 MHz, $CDCl_3$) δ 10.8 (bs, 1H), 4.73 (s, 2H), 4.06 (t, J = 7.5 Hz, 2H), 3.90 (s, 2H), 1.68 (m, 2H), 1.32 (m, 6H), 0.88 (t, J = 6.0 Hz, 3H).

Synthetic Procedures to reach AH10:

2-((thiophen-2'-yl-5'-idine)-2-(4-(2,4-bis(hexyloxy)phenyl)-3-(2-ethylhexyl)-5-(2,4-bis(hexyloxy)phenyl)indolizine))-(N'-hexylrhodanin-5-yl)-rhodanine-3-yl)acetic acid (**AH10**): A flask equipped with a stirbar was charged with aldehyde **20** (0.74 g, 0.075 mmol), bis-rhodanine **25** (0.030 g, 0.075 mmol), $CHCl_3$ (1 mL), and the contents were bubbled with N_2. After 30 min, piperidine (0.031 mL, 0.24 mmol) was added, the solution warmed to 90ºC with stirring, and the reaction was monitored by TLC. After 30 min, the reaction mixture was cooled to rt and diluted with CH_2Cl_2 (250 mL). After acidifying with 5 mL AcOH, the mixture was washed with H_2O (3 x 250 mL) and passed through an SiO_2 plug using first CH_2Cl_2 (500 mL), then 5%MeOH:CH_2Cl_2 (500 mL), then 5% AcOH:5%MeOH:CH_2Cl_2 (500 mL). Washed product fractions with H_2O (3 x 500 mL) and dried organic layer with $MgSO_4$. Concentrated to yield a dark green solid (0.046 g, 45% yield).

Synthetic Prodcedures to reach AH11:

1-Formyl-2-(4-(2,4-bis(hexyloxy)phenyl)-3-(2-ethylhexyl)-5-(2,4-bis(hexyloxy)phenyl)indolizine (**26**)*:* A flame-dried flask equipped with a stirbar was charged with indolizine **19** (0.50 g, 0.55 mmol) and DCE (1.35 mL). After cooling to 0ºC, dry DMF (0.050 mL, 0.65 mmol) and $POCl_3$ (0.060 mL, 0.65 mmol) added, in that order. The solution was then allowed to warm to rt with stirring under N_2 and was monitored by ^1H NMR spectroscopy. After 15h, the reaction mixture was diluted with CH_2Cl_2 (50 mL) and hydrolyzed with KOH (2M, 100 mL). Once hydrolysis was complete by TLC, the organic layer was separated, dried with $MgSO_4$, and concentrated to yield a dark green oil (0.32 g, 62%).

2-(2-(4-(2,4-bis(hexyloxy)phenyl)-3-(2-ethylhexyl)-5-(2,4-bis(hexyloxy)phenyl)indolizin-1-yl)))-(N'-hexylrhodanin-5-yl)-rhodanine-3-yl)acetic acid (**AH11**): A flask equipped with a stirbar was charged with aldehyde **26** (0.071 g, 0.079 mmol), bis-rhodanine **25** (0.035 g, 0.087 mmol), and $CHCl_3$ (1.5 mL), and bubbled with N_2. After 30 min, piperidine (0.022 mL, 0.26 mmol) added, the reaction heated to 90ºC with stirring, and was monitored by ^1H NMR spectroscopy. After 1h, the reaction mixture was cooled to rt and diluted with CH_2Cl_2 (200 mL). After acidifying with 5 mL AcOH, the mixture was washed with H_2O (3 x 250 mL) and passed through an SiO_2 plug using first CH_2Cl_2 (500 mL), then 5%MeOH:CH_2Cl_2 (500 mL), then 5% AcOH:5%MeOH:CH_2Cl_2 (500 mL). Washed product fractions with H_2O (3 x 200 mL) and dried organic layer with $MgSO_4$. Concentrated to yield a dark blue solid (0.006 g, 6% yield).

Synthetic Prodcedures to reach AH13:

1-Formyl-2-(4-methoxyphenyl)-3-methyl-indolizine (**27**): A flame-dried flask equipped with a stirbar was charged with indolizine **8** (0.250 g, 1.05 mmol) and DCE (2 mL). After cooling to 0ºC, dry DMF (0.075 mL, 0.095 mmol) and $POCl_3$ (0.10 mL, 0.095 mmol) added, in that order. The solution was then allowed to warm to rt with stirring under N_2 and was monitored by ^1H NMR spectroscopy. After 18h, the reaction mixture was diluted with CH_2Cl_2 (50 mL) and hydrolyzed with KOH (2M, 50 mL). Once hydrolysis was complete by TLC, the organic layer was separated, passed through a thin pad of SiO_2, dried with $MgSO_4$, and concentrated to yield a pale green solid (0.25 g, 90%).

1-(2-(4-methoxyphenyl)-3-methyl-indolizine)-methanol (**28**): A flame-dried flask equipped with a stirbar was charged with aldehyde **27** (0.79 g, 3 mmol), dried and degassed THF (4.5 mL), and cooled to 0ºC under N_2. Once cooled, $LIAlH_4$ (2.0M in THF, 2.5 mL) added dropwise and the reaction mixture allowed to warm to rt. After 5 min, H_2O added just until bubbling ceased, $MgSO_4$ (25 g) added, the reaction mixture diluted with CH_2Cl_2 (100 mL), filtered, and concentrated to yield a white solid (0.67 g, 87%).

1-(2-(4-methoxyphenyl)-3-methyl-indolizine)-methyltriphenylphosphonium bromide (**29**): A flask equipped with a stirbar and reflux condenser was charged with alcohol **28** (0.082 g, 0.31 mmol), $CHCl_3$ (13 mL), $HPPh_3Br$ (0.11 g, 0.31 mmol), warmed to reflux with stirring under N_2, and

monitored by TLC. After 16h, the reaction mixture was cooled to rt, concentrated, triturated with Et_2O (5 mL), and dried to yield a yellow solid (0.18g, quant.)

5-(2-(2-(4-methoxyphenyl)-1-methylindolizin-3-yl)vinyl)thiophene-2-carbaldehyde (**30**)*:*
A flame dried flask equipped with a stir bar was charged with phosphonium bromide **29** (0.050 g, 0.085 mmol), 2,5-thiophenedicarboxaldehyde (0.012 g, 0.085 mmol), dried and degassed THF (2 mL) under N_2, and the reaction was cooled to -78ºC. Once cool, KOtBu (0.019 g, 0.17 mmol) was dissolved in dried and degassed THF (1 mL) was added dropwise. The reaction mixture was allowed to stir and was monitored by TLC. After 1.5 h, reaction allowed to warm to rt and diluted with CH_2Cl_2 (50 mL), washed with H_2O (2 x 25 mL), passed through a thin pad of SiO_2, and concentrated. Subjected crude product to column chromatography using using 200 mL SiO_2, gradient of 35% CH_2Cl_2:Hexanes to 50% CH_2Cl_2:Hexanes to 60% CH_2Cl_2:Hexanes to 75% CH_2Cl_2:Hexanes to CH_2Cl_2. Product fractions concentrated to yield a red solid (0.020 g, 63%, 85:15 E:Z isomer ratio).

3-(5-(2-(2-(4-methoxyphenyl)-1-methylindolizin-3-yl)vinyl)thiophene)-2-cyano-2-propenoic acid (**AH13**)*:* A flask equipped with a stirbar was charged with aldehyde **30** (0.013 g, 0.035 mmol), $CHCl_3$ (0.85 mL) and degassed wth N_2. After 30 min, cyanoacetic acid (0.009 g, 0.10 mmol) and piperidine (0.031 mL, 0.24 mmol) added and the flask sealed with a plastic stopper and electrical tape. The reaction mixture was heated to 90ºC with stirring and was monitored by TLC. After 30 min, the reaction mixture was cooled to rt, diluted with CH_2Cl_2 (50 mL), acidified with AcOH (5

mL), washed with H_2O (3 x 100 mL) and passed through a short pad of SiO_2 using CH_2Cl_2 (500 mL), 10% MeOH:CH_2Cl_2 (500 mL), 5% AcOH:10%MeOH:CH_2Cl_2 500 mL. Product fractions concentrated to yield a dark blue solid (0.005 g, 30%).

Synthetic Procedures to reach AH14:

2-(5-(2-(2-(4-methoxyphenyl)-3-methyl-indolizine)vinyl)thiophene))-(N'-hexylrhodanin-5-yl)-rhodanine-3-yl)acetic acid (**AH14**): A flask equipped with a stirbar was charged with aldehyde **30** (0.030 g, 0.080 mmol), bis-rhodanine **25** (0.032 g, 0.080 mmol), and $CHCl_3$ (1.3 mL), and bubbled with N_2. After 30 min, piperidine (0.031 mL, 0.24 mmol) added, the reaction heated to 90ºC with stirring, and was monitored by TLC. After 15 min, the reaction mixture was cooled to rt and diluted with CH_2Cl_2 (100 mL). After acidifying with 2 mL AcOH, the mixture was washed with H_2O (3 x 150 mL) and passed through an SiO_2 plug using first CH_2Cl_2 (500 mL), then 5%MeOH:CH_2Cl_2 (500 mL), then 5% AcOH:5%MeOH:CH_2Cl_2 (500 mL). Washed product fractions with H_2O (3 x 200 mL) and dried organic layer with $MgSO_4$. Concentrated to yield a dark blue solid (0.01 g, 10% yield).

SECTION 4. SYNTHESIS OF D-A-π-A INDOLIZINE SENSITIZERS FOR USE IN DSCS

In an attempt to increase the overall conjugation length and lower the $E_{(S+/S*)}$ of indolizine dyes, efforts were made to synthesize sensitizers with a D-A-π-A structure, which has been shown to improve device performance in porphyrin (to world record values with **SM315**), indoline (to 10.7% with **YA422**), and TPA (to TPA-best 10.2% efficiency with **RK1**) dyes, Scheme 4.[9,33,63-65] Towards this aim, we were able to synthesize **AH15** and characterize its absorbance and measure the $E_{(S+/S)}$ and $E_{(S+/S*)}$ energy levels, Figure 19.

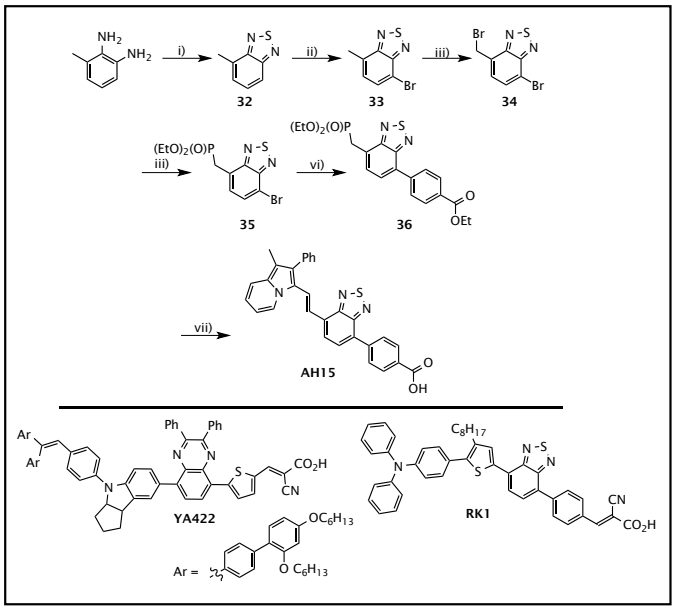

Scheme 4. *Top*: Synthetic route to reach D-A-π-A dye **AH15**. *Bottom*: Structures of dyes **YA422** and **RK1**. Conditions: i): TEA, $SOCl_2$, $CHCl_3$, 1.23 g, quant. ii): Br_2, HBr, (47% in H_2O), reflux, 1.11 g of a 90% pure product, 45%. iii): NBS, $(PhCO)_2$, $CHCl_3$, 75ºC, 1.35g, 95%. iv): $P(OEt)_3$, 120ºC, 0.71 g, 40%. vi): ethyl 4-carboxylphenylboronic acid, $Pd(PPh_3)_4$, Na_2CO_3 (2M in H_2O), Tol, THF reflux, 0.17 g, 96%. vii): 1. **29**, 4-aminophenol, AcOH, Tol, 130ºC. 2 LiHMDS, 90ºC, 0.009g, 25%.

To reach dye **AH15**, the benzothiadiazole bridge portion was constructed first. Benzothiadiazole **32** was formed by reacting 2,3-diaminotoluene with $SOCl_2$ in the presence of a base.[66] Bromination with Br_2 led to formation of **33** and subsequent radical bromination using NBS with benzoyl peroxide as initiator smoothly formed **34**.[67] Substitution with $P(OEt)_3$ gave phosphonate **35** and Suzuki coupling gave ester phosphonate **36**.[68] Reacting **36** with aldehyde **29** in the presence of water and strong base led directly to the formation of **AH15**.

The UV/Vis absorption spectrum of **AH15** is shown in Figure 19. Because it lacks the strongly accepting cyanoacrylic acid unit present on dyes **AH2-7**, the CT band of **AH15** is very blue-shifted (100 nm) in comparison to the analogous **AH13** dye. It is likely that upon installation of a stronger acceptor, the CT band will be at least comparable to **AH13** if not more red shifted. Both dyes exhibit poor absorption in the 450-500 nm range of the visible spectrum, due to the poor high-energy charge transfers, which are observed in dyes **AH10** and **AH14**.

The measurement of the $E_{(S+/S)}$ and $E_{(S+/S*)}$ energy levels of **AH15** gave firm support to the logic that the acid acceptor was not strong enough to balance the exceptional donating strength of the indolizine donor, Figure 19. This is evidenced by the similar $E_{(S/S)}$ values for **AH13** (0.72 V) and **AH15** (0.71 V) but grossly different $E_{(S/S*)}$ values (-1.01 V for **AH13** and -1.19 V for **AH15**, Table 10). The supposition that adding a stronger acceptor is supported by reports of bandgap modification in other series of dyes, but also in the observation that in **AH13** and **AH14** (*Part 1.3*), the addition of the strongly accepting bis-rhodanine only lowered the $E_{(S+/S*)}$ energy level.

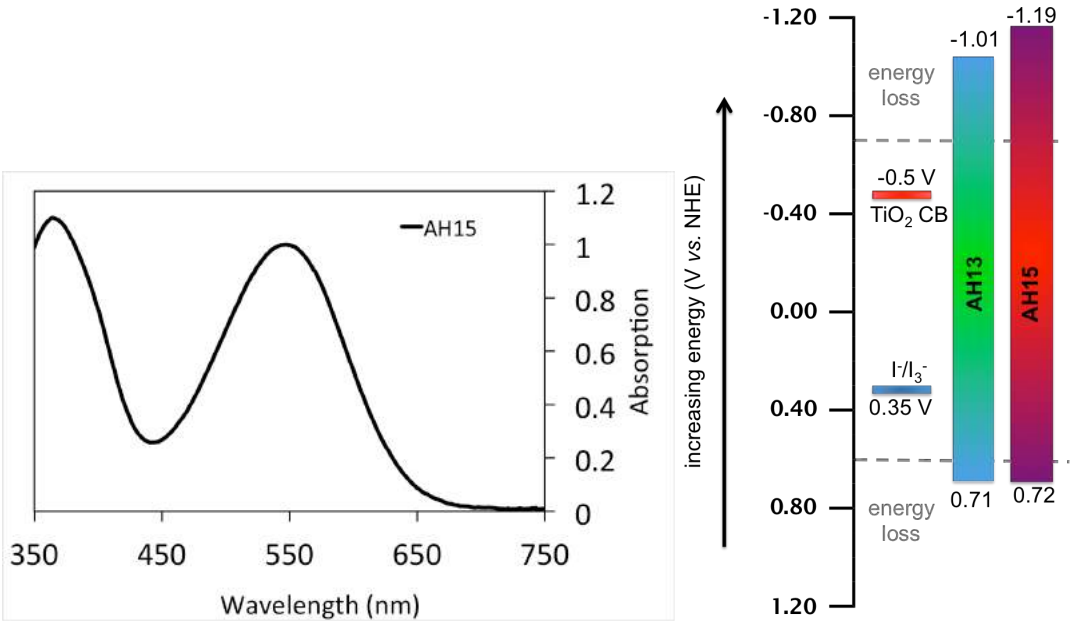

Figure 19. *Left*: UV/Vis absorption spectrum of **AH15** measured in CH_2Cl_2. *Right*: Bandgap diagram of **AH15** and **AH13**.

Table 10. Optical and electronic properties of dyes **AH13** and **AH15**.

Dye	λ_{max} (nm)[a]	λ_{onset} (nm)[a]	$E_{(0-0)}$ (eV)[b]	$E_{(S+/S^*)}$ (V)[c]	$E_{(S+/S)}$ (V)[d]
AH13	609	722	1.72	−1.01	0.71
AH15	550	650	1.91	−1.19	0.72

[a] Measured in CH_2Cl_2. [b]:Estimated from the tangent of the lower-energy tangent of the lambda max transition in the UV-Vis absorption spectrum in CH_2Cl_2. [c]:Taken as the difference between the oxidation potential $E_{(S+/S)}$ and the estimated optical bandgap $E_{(0-0)}$. [d]: Measured in a 0.1 M Bu_4NPF_6 in CH_2Cl_2 solution with glassy carbon disk working electrode, Pt reference electrode, and Pt counter electrode with ferrocene as an internal standard. Values are reported versus NHE.

Before the device performance data for **AH10-14** was obtained by our collaborators in Switzerland, which indicated that olefins were detrimental to sensitizer performance, many attempts at synthesizing olefin dyes with more advanced bridges like BDT or CPDT were undertaken, however, they did not result in final dyes due to poor stability. The attempts will be briefly mentioned here along with the reason for synthetic route failure, Figure 20.

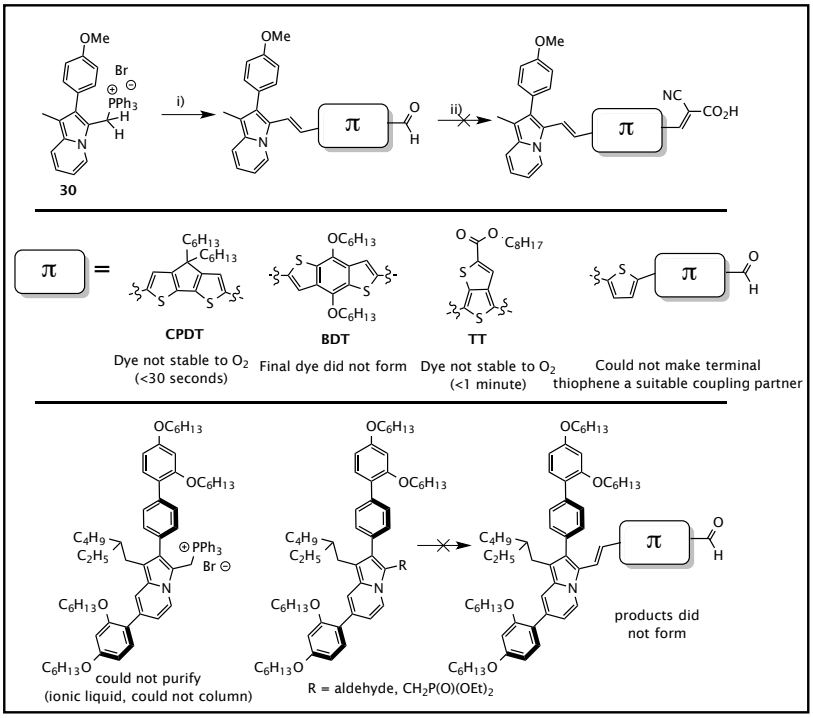

Figure 20. Unsuccessful attempts at synthesizing advanced olefin-containing sensitizers and the reasons for the failure of each. Conditions: i): THF, tBuOK, -78ºC to rt. ii): cyanoacetic acid, $CHCl_3$, piperidine, 90ºC.

The Wittig reaction of **30** proceeded to form the bridge aldehyde for CPDT, BDT, and TT, however, upon knoevenagel condensation with cyanoacetic acid, the final dyes were either too unstable to be characterized or did not appear to form. Many attempts were made at attaching an unfunctionalized thiophene to an indolizine donor and utilizing it for further coupling reactions afterwards, however, none were successful. Some examples of these efforts included: Lithitation of indolizine-bridge and indolizine-olefin-bridge species followed by quenching with halogen, DMF, or SnR_3 electrophiles, all of which yielded a mixture of products due to competing acidities of the benzylic carbon at the 3- position, the 1-proton and the 7-proton.[69]

Also attempted was bromination of unfunctionalized indolizine-bridge compounds, the products of which decomposed very quickly. Vilsmeier-Haack reactions of indolizine-olefin-bridge species also failed due to large amounts of side-product generation during the reaction.

Future attempts at synthesizing D-A-π-A sensitizers utilizing indolizine will focus on the removal of the olefin bridge group, as well as the inclusion of cyanoacrylic acid accepting groups to increase the dye absorption window. The removal of the olefin group is important, as the dyes **AH13-14** both exhibited very poor performance in devices due to the reactive alkene group. The higher planarity observed with olefins imparted larger absorption coefficients for dyes **AH10-AH15**, however, the reactivity of the alkene lowered performance in **AH10-14** to such a degree that further investigation of olefin-including dyes would be a very poor use of time and resources.

The exclusion of olefins from future dyes will not only enhance performance of future indolzine dyes, but make incorporation of cyanoacrylic acid acceptors easier from a synthetic standpoint, as well. To incorporate olefin bridge groups, Wittig or Horner-Wadsowrth-Emmonds (HWE) type olefinations are often utilized, which has two important drawbacks: First, extra synthetic steps must be implemented to install the aldehyde electrophile and phosphonate or phosphonium nucleophile. Second, if using a symmetrical bridge like in **AH13**, a di-aldehyde must be utilized. Conversely, if using an unsymmetrical bridge, an ester like **36** must be utilized on the bridge group instead of an aldehyde in order to prevent non-productive side reactions. In both cases, when using a Wittig nucleophile the desired E olefin product must be separated form the undesired Z product. From an ester group, it takes three synthetic steps to reach the cyanoacrylic acid acceptor, whereas starting from an aldehyde it takes only one step.

EXPERIMENTAL SECTION

See Chapter 1, Section 1 for General Considerations (Experimental)

Synthetic Procedures to reach AH15:

4-Methyl-2,1,3-benzothiadiazole **(32)**: A flask equipped with a stirbar and reflux condenser was charged with 2,3-diaminotoluene (1.0 g, 8.19 mmol), triethylamine (4.6 mL, 32.96 mmol), CH_2Cl_2 (25 mL) and cooled to -78ºC with stirring. Once cool, $SOCl_2$ added dropwise until vigorous bubbling with addition stopped. The reaction mixture was then heated to reflux with stirring and was monitored with TLC. After 22h, the reaction mixture was cooled to rt and poured into 10% HCl (100 mL) and extracted with 100 mL CH_2Cl_2. The organic layer was washed with H_2O (2 x 50 mL), dried with $MgSO_4$, passed through a thin pad of SiO_2 using CH_2Cl_2 as eluent and concentrated to give an off-white solid (1.2 g, quant.).

7-Bromo-4-methyl-2,1,3-benzothiadiazole **(33)**: A flask equipped with a stirbar and reflux condenser was charged with thiadiazole **32** (1.23 g, 9.49 mmol), HBr (10 mL) and heated to 70ºC with stirring. Once warm, Br_2 (0.49 mL, 9.49 mmol) added dropwise, the solution was heated to reflux with stirring, and monitored by TLC. After 24h, the reaction mixture was cooled to rt, extracted with CH_2Cl_2 (3 x 100 mL), and passed through a thin pad of SiO_2 using 50% CH_2Cl_2:Hexanes. Concentrated to give an off-white solid (1.11 g, (10:1 product:doubly brominated product), 54%). Used without further purification.

7-Bromo-4-bromomethyl-2,1,3-benzothiadiazole **(34)**: A flask equipped with a stirbar and reflux condenser was charged with bromothiadiazole **33** (1.1 g, 4.6 mmol), NBS (0.82 g, 4.6 mmol), benzoyl peroxide (0.020 g), $CHCl_3$ (7 mL), heated to 70ºC with stirring, and monitored by ^1H NMR spectroscopy. After 16h, reaction mixture was cooled to rt, concentrated, and directly subjected to column chromatography using 50% CH_2Cl_2:Hexanes. Concentrated product fractions to give an off-white solid (1.35 g, 95%).

7-Bromo-4-(diethylphosphonato)methyl-2,1,3-benzothiadiazole **(35)**: A flask equipped with a stirbar was charged with bromomethylthiadiazole **34** (1.35 g, 4.4 mmol), diethylphosphite (2 mL), heated to 120ºC with stirring, and monitored by TLC. After 2h, reaction mixture cooled to rt and subjected to column chromatography using gradient 30% EtOAc:Hexanes to 50% EtOAc:Hexanes to 60% EtOAc:Hexanes to EtOAc. Product spots concentrated to yield a yellow oil (0.71g, 40%).

Ethyl (7-(4-carboxyphenyl)-4-(diethylphosphonato)methyl-2,1,3-benzothiadiazole **(36)**:

A flask equipped with reflux condenser and stirbar was charged with phosphonate **35** (0.150 g, 0.41 mmol), ethyl (4-carboxyphenylboronic acid) (0.12 g, 0.62 mmol), dissolved in 1:1.5:1 Toluene:THF:2M Na_2CO_3 (aq) (4 mL total), and the solution was bubbled vigorously with N_2. After 30 min, $Pd(PPh_3)_4$ (0.018 g, 0.016 mmol) added in one solid portion from a vial, the reaction mixture was heated to Toluene reflux, allowed to stir, and was monitored by ^1H NMR spectroscopy. After 18h, the reaction mixture was cooled to rt, extracted with EtOAc (3 x 25

mL), washed with H_2O (2 x 25 mL), dried with $MgSO_4$ and concentrated. The crude product was submitted to column chromatography using 200 mL SiO_2, gradient 60% EtOAc:Hexanes to EtOAc to 15%MeOH:EtOAc. Product fractions concentrated to yield a viscous yellow oil (0.17g, 96%).

4-((2-(2-(4-methoxyphenyl)-1-methylindolizin-3-yl)vinyl)-7-(4-benzoic acid) -2,1,3-benzothiadiazole (**AH15**). A flame dried flask equipped with a stir bar was charged with phosphonate **36** (0.047 g, 0.11 mmol), aldehyde **27** (0.026 g, 0.1 mmol), dried and degassed Toluene (1 mL) under N_2, 4-aminophenol (0.004 g, 0.04 mmol), AcOH (1 drop) and the reaction heated to 150ºC under ambient atmosphere to dryness. After 20h, reaction mixture cooled to rt, suspended in dried, degassed toluene (1 mL), LiHMDS (2.0 M in THF, 1.5 mL) added via syringe, the reaction heated to 90ºC with stirring and was monitored by TLC. After 3h, reaction mixture cooled to rt, subjected directly to column chromatography using 100 mL SiO_2, gradient hexanes to 20% EtOAc:hexanes to EtOAc to 1%AcOH:EtOAc. Product spots concentrated to yield a deep purple solid (0.009 g, 12%).

SECTION 5. THE SYNTHESIS OF DOUBLE DONOR OR DOUBLE ANCHOR SENSITIZERS FOR DSC.

While previous parts of this chapter have dealt with indolizine-based sensitizers as a means to efficiently narrow sensitizer bandgaps and thus improve DSC performance, this part will outline the attempts to utilize multiple donors or accepting anchors to achieve the same end. In the rational design of dyes with two acceptors/anchors or two donor groups, the distinction of 'in-parallel' and 'in-series' inclusion is an important distinction to make.

The connection of more than one donor or acceptor 'in-series' would theoretically mean that from the number of donors connected in conjugation effectively 'sum' their donation strength, while the number of acceptors in conjugation effectively 'sum' their accepting strength. While this seems a good strategy to use, as in a series circuit, the bandgap energy is actually a product of overcoming the resonance stabilization energy and absorption-lowering twist angle problems of all the subunits combined. The idea of acceptors in series has been described above in D-A-π-A (current world-record holders in all-organic and metal containing sensitizers, *vide supra*) and D-π-A-A dyes.[64] Positioning anchors in series would not benefit the performance of a sensitizer, as the anchor groups must adsorb to the TiO_2 surface and thus should be on the terminal end of the dyes. Efforts have been made to use dyes of this type, but they will not be described here.

PART 5.1 DOUBLE DONOR DYES

Donors and acceptors/anchors 'in parallel' means that as in a parallel circuit, two or more donors or two or more acceptors are connected to the same bridge unit. Placing acceptors in

parallel is not as important as placing donors in parallel, as evidenced by the sheer number of world-record dyes with acceptors in series. Triarylamine donors, however, need to be placed in parallel rather than in series, because of the two consecutive nitrogen-aryl single bonds that break conjugation. It should be noted that the Wang group has recently reported an N-annulated perylene that does not rely on nitrogen to propagate conjugation.[70,71,72]

Our efforts in sensitizers with multiple donors or anchors have not been the first by any means, as several groups have attempted to make high performing sensitizers with double donor and/or double anchor subunits. In 2008, three reports of such attempts to use double triarylamine donor groups, with different strategies (and degrees of success) were published by a collaboration of the Grätzel/Hagfeldt/Sun research groups, by a collaboration of the Chou/Ho/Lin groups, and by the Tian group, Figure 21.[73,74,75] These initial efforts for double donor dyes have not been followed up until this work.

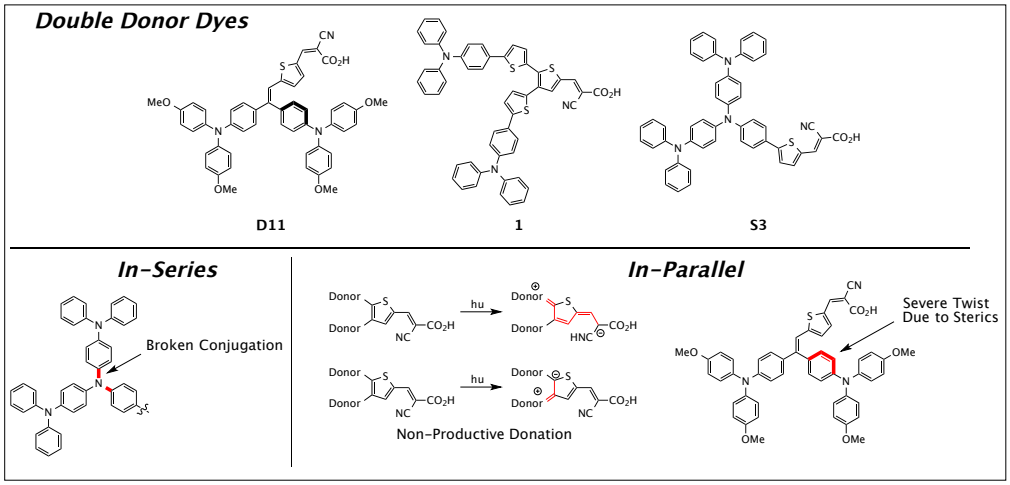

Figure 21. *Top*: Some double donor dyes reported in the literature. *Bottom*: Pictorial description of In-Series and In-Parallel double donor systems and their inherent problems.

In a report by Grätzel et al., the two triarylamine donors were place 'in-parallel' on a double bond, which in theory would allow for both aryl nitrogens to engage the acceptor group equally; however, the dye's ground state energy level was very similar to that of reference dye **C1**.[29] Calculations indicated that one of the triaryl amine donor groups was severely twisted, reducing the donation of this group to very low values. The dye IPCE window extended to just past 700 nm and devices with dye **D11** showed good efficiency (7%).[73]

In a publication by Chou et. al, two triarylamine donors were attached to a thiophene bridge at the 2 and 3 positions, while the acceptor was appended to the thiophene's 5-position. While the two-position of thiophene rings lies in conjugation with the 5-position, the 3-position does not. Therefore, the donor attached to the 3-position only adds 'passive' electron density to the bridge and cannot contribute strongly to the dye's energy levels. An examination of dye **1**'s energy levels shows precisely that. The $E_{(S+/S)}$ value for dye **1** was almost exactly that of reference triarylamine dye **CQ1**. The dye exhibited an IPCE window out to 650 nm and good efficiency (6%).[74]

A report by the Tian group described the use of 'in-series' triarylamine donors appended with either diarylamine groups or carbazole groups. The addition of alkoxy groups to triarylamine marginally increases donor strength, but not strongly due to the two aryl-N bonds in succession that breaks conjugation. Thus, the extra diarylamine or carbazole groups will encourage donation towards the acceptors, but cannot contribute in conjugation. Upon examination of dye **S3**, which has a $(Ar_2N\text{-}Ph)_2NPh$ donor group, the $E_{(S+/S)}$ energy level was also very similar to reference dye **CQ1**, which indicated that as expected, the 'in-series' donor

approach did not help the dye's overall donation. The performance of **S3** was modest, with an IPCE absorption window out to 620 nm and an efficiency of 2.78% efficiency.[75]

With the knowledge of these three approaches in hand, we decided that synthesizing a dye with two donors 'in-parallel' that also were substituted in active positions would be a key target towards advancing double-donor sensitizers. Thus, we sought a donor structure based on doubly substituted fluorene, Scheme 5. In this type of structure, both donors are in conjugation with the acceptor (as in **D11**). The fused fluorene ring allows for both triphenylamine donors to be planar and thus equally donate towards the acceptor, which is what dye **D11** could not accomplish. Our synthetic route to reach dye **AH1** is shown in Scheme 5.

In order to ensure correct bromine atom placement on the fluorene ring, AIBN initiated radical bromination was used, which proceeded smoothly to afford dibromophenanthrenedione **37**. Oxidative hydroxide mediated ring contraction followed by Soxholat extraction afforded dibromofluorenone **38**.[76] HWE reaction proceeded to give fluorenylthiophene **39** and Buchwald-Hartwig coupling with bis(4-hexyloxyaniline) formed bis (hexyloxyaniline) fluorenyl thiophene **40**. Despite low yields, deprotonation with *n*-BuLi followed by electrophilic quenching with DMF gave aldehyde **41**, which was then condensed with cyanoacetic acid to give **AH1**.

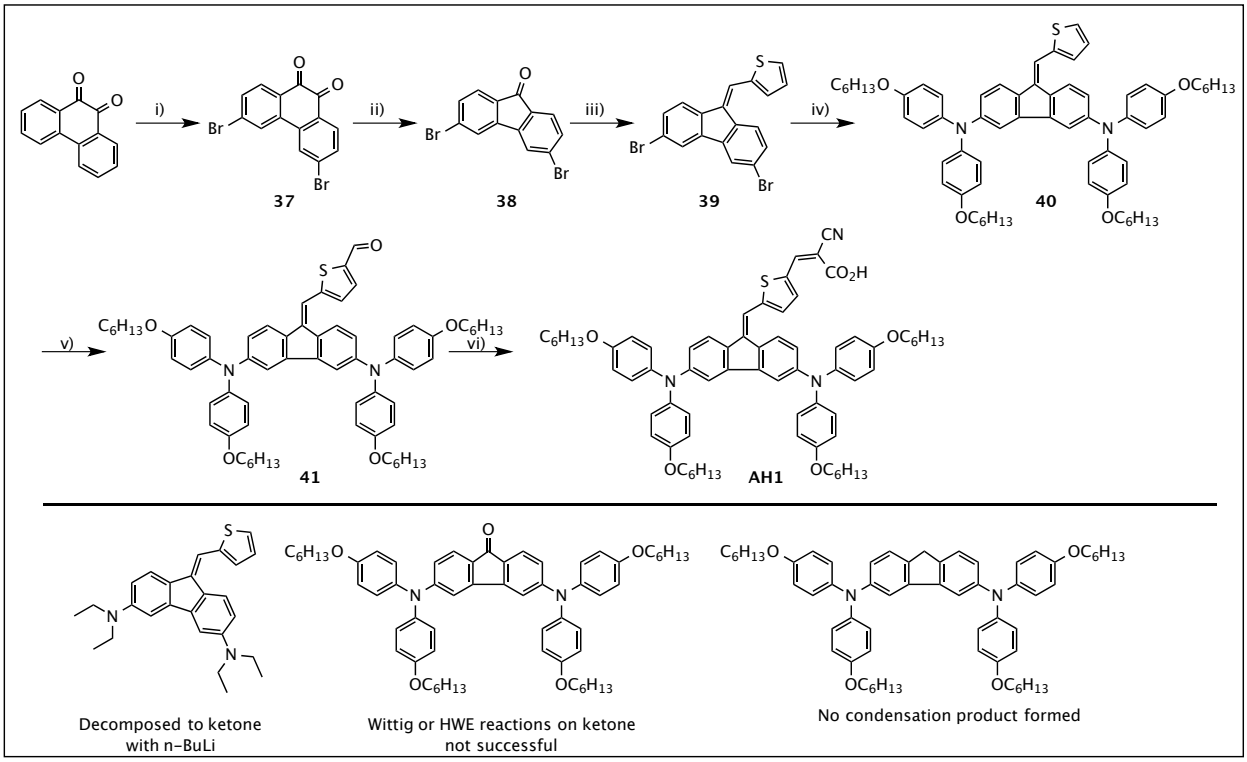

Scheme 5. Top: Synthetic route to reach dye **AH1.** *Bottom*: Structures that did not result in a completed dye. Conditions: i): AIBN, Br_2, $C_6H_5NO_2$, 9.9 g, 50%. ii): a. KOH, H_2O, 140ºC. b. $KMnO_4$, 140ºC, 4.0 g, 70%. iii): NaH, THF, rt, 0.90 g, 97%. iv): bis(4-hexyloxy)aniline, $P(tBu)_3$, $Pd(dbs)_2$, NaOtBu, Tol, rt, 0.390 g, 98%. v): nBuLi, THF, -78ºC, DMF, 0.045 g, 10%. vi): cyanoacetic acid, piperidine, $CHCl_3$, 90ºC.

Once dye **AH1** had been synthesized, its UV/Vis aborption data in both $CHCl_3$ and EtOH were taken, Figure 22. Observing the absorbance in both solvents was important, as the reference dye **D11** had its absorption measured in EtOH, meaning that a good comparison could be made between the two dyes. Performing the measurement in $CHCl_3$ then allowed for a better indication of how the dye's absorption will appear in-device, as the polar environment of $CHCl_3$ has been observed to better mimic the environment found in DSCs. The onset of absorption as well as the

position of the CT band of dye **AH1** is red shifted in comparison to that of reference dye **D11** in EtOH by 60 nm, as compiled in Table 11. In $CHCl_3$, the CT band was significantly broadened and red shifted, leading to a λ_{onset} of 693 nm (Figure 21).

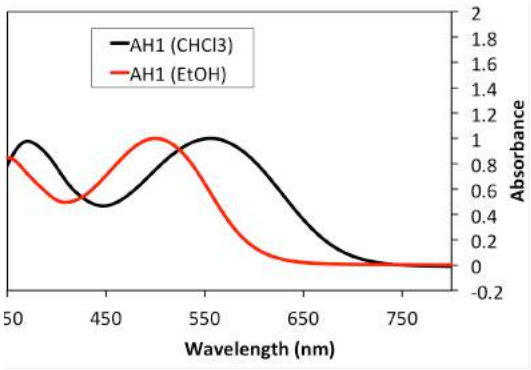

Figure 22. *Left*: UV/Vis Absorption of dye **AH1** in $CHCl_3$ (black) and EtOH (red).

Table 11. Optical and Electronic properties of dyes **AH1**, **D11**, and **C1**.

Dye	λ_{max} (nm)	λ_{onset} (nm)	E_{gopt} (eV)[c]	$E_{(S+/S^*)}$ (V)[d]	$E_{(S+/S)}$ (V)[e]
AH1	500[a]	610[a]		-0.97	0.80
	554[b]	695[b]	1.88		
D11	448[a]	550[a]	2.23[f]	-1.41[f]	0.92[g]
C1	499[b]	590[b]	2.10[h]	-1.06[h]	1.04[h]

[a]: Measured in EtOH. [b]: Measured in $CHCl_3$. [c]:Estimated from the tangent of the lower-energy tangent of the lambda max transition in the UV-Vis absorption spectrum in CH_2Cl_2. [d]Taken as the difference between the oxidation potential $E_{(S+/S)}$ and the estimated optical bandgap E_{gopt}. [e] Measured in a 0.1 M Bu_4NPF_6 in CH_2Cl_2 solution with glassy carbon disk working electrode, Pt reference electrode, and Pt counter electrode with ferrocene as an internal standard. Values are reported versus NHE. [f]: Taken from Ref. 73 [g]: Reported in Ref. 73 to have been measured in MeCN. [h]: Taken from Ref. 29.

The CT band of **AH1** is very red shifted (100 nm) compared to reference dye **C1**, which is one indication that the double donor fluorene unit is much stronger than a simple alkoxytriphenylamine donor. The $E_{(S+/S)}$ energy level was substantially destabilized (0.82 V vs.

NHE) for dye **AH1** in comparison to dye **C1** (1.04 V vs. NHE), while the $E_{(S+/S*)}$ value for each was closer (-0.97 V vs NHE for **AH1** and -1.06 V vs. NHE for **C1**), indicating that not only did dye **AH1** benefit from a much stronger donor, but also excited-state stabilization from competing local aromaticity. In the ground state, two locally aromatic benzene structures are present, while in the excited state one locally aromatic benzene structure and one locally aromatic cyclopentadiene structure, which lowers the energy required to access the excited state, and thus lowers the CT energy. Dye **AH1** has not been tested yet in devices; however, it has been sent to our collaborators in Lausanne, Switzerland.

Several other attempts at synthesizing double donor fluorene dyes were made; however, they were unsuccessful and will be briefly discussed here, Scheme 5. Diethyl amine was coupled to dibromofluorenyl thiophene **40** smoothly; however, upon reaction with *n*-BuLi, the product was quantitatively converted to the undesired fluorenone product. In another attempt, dihexyloxyaniline was coupled to dibromofluorenone **38**; however, the ketone was observed to not undergo Wittig or HWE reaction with carbon nucleophiles. Attempts to utililize a fluorenyl nucleophile condensation reactions did not yield olefin product when reacted with 2-formylthiophene. Future attempts to synthesize fluorene double-donor dyes should likely focus on coupling donor subunits after affixing more bridges or an aldehyde onto structures like fluorenyl thiophene **39**.

PART 5.2 DOUBLE ANCHOR DYES

While efficiency is one key factor in determining how well sensitizers perform, another, more practical aspect of device performance is the stability (or change in performance from the cell's maximum efficiency) over time. It has been noted in other studies that while the cyanoacrylic acid anchor works well for short periods, it does not guarantee that the dye stays adsorbed onto the semiconductor surface.[10,77] In the same way that bidentate chelators have lower dissociation constants than monodentate chelators (stronger binding) in transition metal complexes, dyes with multiple anchor sites should be much less likely to dissociate completely from the TiO_2 surface. While this principle has not been investigated often in all-organic sensitizers, highly performing Ru-based sensitizers **N3**,[78] **N719**,[79] and the so-called "black dye"[80] all utilize double anchors produce very stable devices (with some lasting for 10+ years).[81]

Notable reports of double anchor dyes have recently been published by the Grätzel (2009),[82] Wang (2011),[83] and Chou/Wong (2014)[84] groups, Figure 23. The report by Grätzel et. al in 2009 utilized a single triphenylamine donor/double anchor dye design that was capable of light absorption out to ~700 nm in-device and 5.7% efficiency for **DB-1**. It's worthy to note that **DB-2** utilized rhodanine acceptor groups as the anchor; however, the device performance was poor.[82]

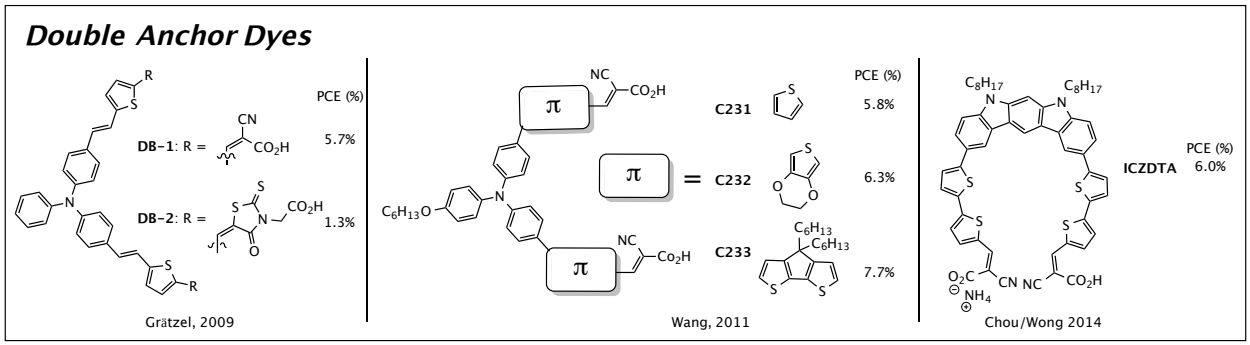

Figure 23. Some recent double anchor structures reported in the literature.

In 2011, the Wang group reported a similar double anchor dye system, in which a single triphenylamine donor was appended twice with three different thiophene bridge groups. In this study, $Co^{III/II}$ electrolytes were used instead of the standard iodide based redo shuttle and the performances increased from thiophene (**C231**) to EDOT (**C232**) to CPDT (**C233**) to range from 5.8% to 7.7% PCE. It is worth noting that the double anchor dyes were compared with their single anchor analogs, and in each case the double anchor dyes performed worse.[83] In 2014, the Chou/Wong groups collaboratively reported a double anchor dye using a fused double-donor system based on carbazole (**ICZDTA**). The double carbazole dye was capable of light absorption out to 650 nm in-device with efficiency of 6.0% PCE.[84] Only the report by Grätzel included stability data over time. Using **DB-1**, the cells were subjected to accelerated ageing tests using full light intensity (100 mW cm^{-2}) at 60ºC for 1000h. After that time period, cells with the double anchor dye were found to retain 67% of their initial efficiency, while the single anchor analog retained only 55% of its original efficiency.

Our approach to the development of double anchor dyes was based on a heterocyclic structure, [2.2.3]cyclazine. Before embarking upon a series of syntheses towards the heterocycle,

we decided it would be an expedient use of time to determine the electronically active positions on the structure (Figure 24). As evident form the calculations, the positions with the most electron density were the 1, 4, and 6 positions on the heterocycle. While it appeared that the bridgehead carbon between the 2 and 3 positions was also active, this position cannot be modified and thus is not important for substitution assessment.

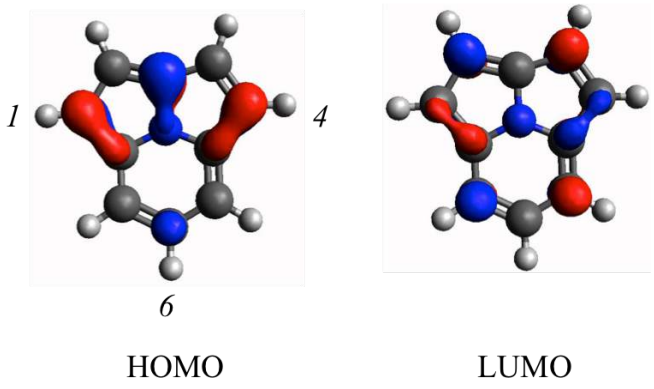

Figure 24. HOMO (*left*) and LUMO (*right*) orbital figures of [2.2.3]cyclazine using TD-DFT calculations.

Once initial substitution leads were established, we then sought to determine precisely which of the three positions held the most promise in full D-π-A dyes. To do this, we next calculated a series of simple D-π-A dyes using dimethylamine as donor and cyanoacrylic acid as acceptor. By comparing the relative shift and the computed oscillator strength (indicative of extinction coefficient) of the vertical transition, a better assessment of important dye architectures can be made. The results of these initial calculations are shown in Figure 25 and the numerical results are tabulated in Table 12.

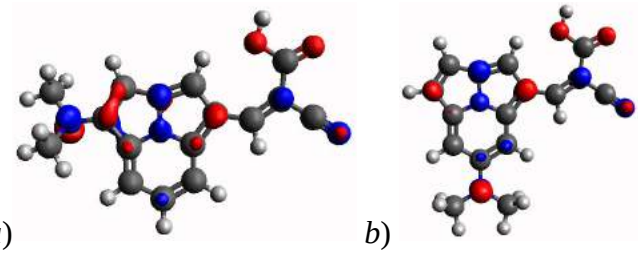

a) *b*)

HOMO

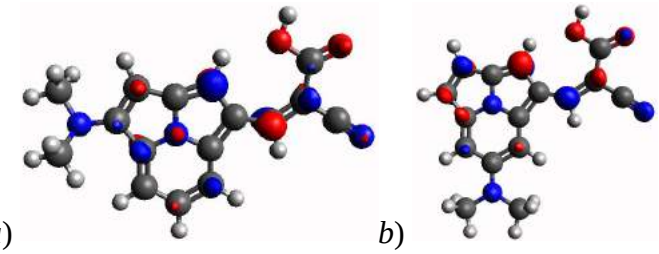

a) *b*)

LUMO

Figure 25. Calculated HOMO and LUMO structures for *a*) 1,4- *b*) 6,4-substituted [2.2.3]cyclazine D-π-A dyes. Contour values set to 0.065.

From the calculated HOMO and LUMO structures, two important points can be made: First, the donor appears to function well in either the 1- or 6-position. Second, the 3-position appears to have significant electron density in the calculated LUMO, which is fortuitous, since another anchor can be easily appended to the 3-position (Scheme 6).

From the calculated results in Table 12, both dyes were calculated to have CT bands that were significantly red-shifted over the parent heterocycle with good oscillator strength values. As expected from the relative orbital electron densities present in Figure 22, the 1,4-substituted cyclazine is red shifted in comparison to the 6,4-substituted cyclazine.

Table 12. Calculated CT band vertical transitions and oscillator strengths.[a]

Dye	Vert. Trans.	Oscillator Strength
1,4	475	0.30
6,4	450	0.37
Parent	360	0.05

[a]: Values calculated using TD-DFT methods (B3LYP/6-311G(d,p) geometry optimization) with calculated states = 10.

Thus, the calculations suggest that while either substitution pattern should lead to a dye with good charge separation and a significant absorption in the visible spectrum, 1,4-substitution would be more favorable than 1,6-substitution.

The synthetic route to a substituted [2.2.3]cyclazine in shown in Scheme 6. Indolizine **6** underwent oxidative dimethylacetylenedicarboxylate (DMAD) cyclization to form cyclazine **42** in good yield and at multi-gram scale (8.5 g yield). Reduction of diester **42** with $LiAlH_4$ gave diol **43**, which was oxidized via Swern oxidation to afford dialdehyde **44**. Future attempts at condensation with cyanoacetic acid have been attempted, but product was not observed.

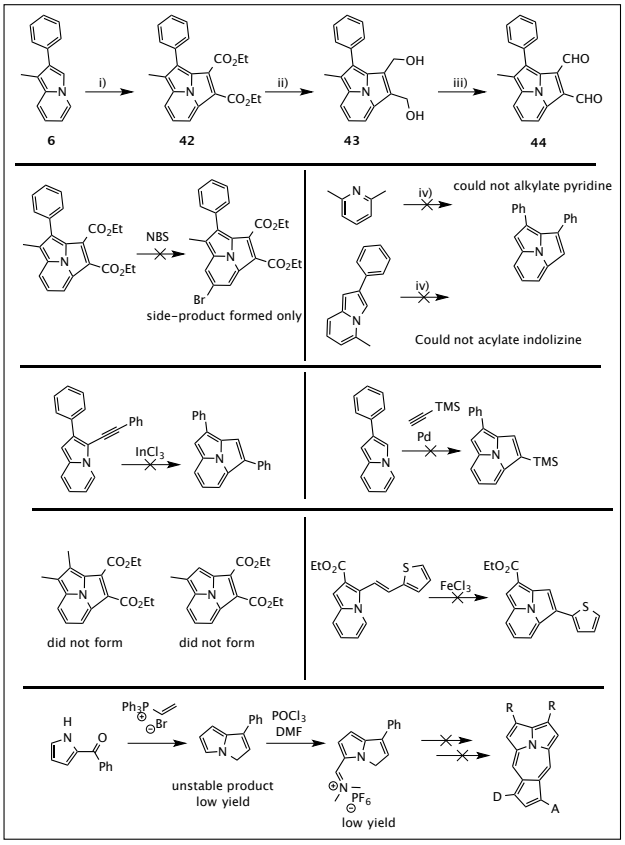

Scheme 6. *Top: Synthetic* route to [2.2.3]cyclazine structures for future development as DSC sensitizers. Conditions: i): a. Tol, DMAD, 90ºC. b. DDQ, rt to 100ºC. 8.5g, 56%. ii): $LiAlH_4$, THF, rt, 0.087 g, quant. yield. iii): Swern oxidation. 0.01 g, ~15%. *Lower Panels*: Unsuccessful attempts towards [2.2.3]cyclazine.

Even though the most successful route in Scheme 6 depicts a cyclazine with 6,4-substitution, we attempted to make several methods for forming the 1,4-substituted heterocycle. Attempts to make a symmetrical 2,3-diphenyl[2.2.3]cyclazine failed due to the steric bulk of 2,6-lutidine. We also made several attempts at transition metal catalyzed ring closures, utilizing $InCl_3$,[23a] $FeCl_3$, and $Pd(OAc)_2$ to no avail. The synthesis of 1,2-dimethyl[2.2.3]cyclazine as well as 1-methyl[2.2.3]cyclazine also failed to form in oxidative cyclization.[85] We also attempted to

form a symmetrical cyclazine by acylation/condensation, however, that also failed.[86] Once it was clear that 6,4-substitution was synthetically most feasible, attempts to brominate diester **42** using NBS also failed due to the selective formation of an unwanted by-product. Before we set out for [2.2.3]cyclazine, we made several attempts to follow procedures towards more complicated heterocycles, as is drawn in the bottom panel. Poor yields and unstable products led us to abandon the route towards these dye architectures in favor of the cyclazines.[87]

EXPERIMENTAL SECTION

See Chapter 1, Section 1 for General Experimental Considerations

Computational Details: All computations were performed with the Gaussian09 software package. The geometry optimization steps were as follows: first the structures were optimized by MM2 in the ChemBio3D (version: 13.0.2.3021) software package and dihedral angles for all relevant groups set to values in-between the global minimum and the next local maximum on the conformational energy diagram as calculated by ChemBio3D (version: 13.0.2.3021) in the dihedral driver toolset. After MM2 optimization, the molecular structures were further optimized by DFT methods: first B3LYP/3-21g, second B3LYP/6-311g(d,p), and finally opt=tight B3LYP/6-311g(d,p) with tight convergence criteria. Lastly, time-dependent density functional theory (TD-DFT) computations were carried out to compute the vertical transition energies and oscillator strengths for the 10 lowest excited states. Symmetry was explicitly turned off for these computations even though all of the optimized structures belonged to the C_1 point group. A representative input file is included for each type of calculation.

Diethyl 3,4-dicarboxylate-1-methyl-2-phenyl[2.2.3]cyclazine (42): A flame-dried flask equipped with a stirbar was charged with indolizine **6** (9.08 g, 43.8 mmol), toluene (80 mL) and the solution was heated to 90ºC. Once hot, DMAD (8.1 g, 56.9 mmol) added dropwise, the solution allowed to stir at 90ºC and monitored by TLC. After 1.5 h, flask cooled to rt and DDQ (9.94 g, 43.8 mmol) added in one solid portion. Solution warmed to 100ºC with stirring and was monitored by TLC. After 30 min, crude material was passed through a pad of SiO_2 using DCM and concentrated. Crude product dissolved in EtOAc (1000 mL), and ascorbic acid added. Washed with H_2O (3 x 500 mL) and concentrated to yield a yellow solid (8.5 g, 56%). ^{1}H NMR (300 MHz, $CDCl_3$) δ 8.39 (d, J = 7.5 Hz, 1H), 7.91 (m 2H), 7.61 (m, 2H), 7.51 (m, 2H), 7.42 (m, 2H), 4.00 (s, 3H), 3.77 (s, 3H), 2.70 (s, 3H).

3,4-bis(hydroxymehyl)-1-methyl-2-phenyl[2.2.3]cyclazine (43): A flame-dried flask equipped with a stirbar was charged with cyclazine **42** (0.10 g, 0.29 mmol) and THF (5 mL). $LiAlH_4$ (2M in THF, 0.288 mL) added dropwise, the reaction mixture allowed to stir at rt and monitored by TLC. After 1.5 h, minimal H_2O added, followed by $MgSO_4$ (xs). Added Et_2O (50 mL), CH_2Cl_2 (20 mL), filtered and concentrated. Passed crude product through SiO_2 plug using CH_2Cl_2 then 5% EtOAc: CH_2Cl_2 to elute the product. Product fractions concentrated to yield a yellow solid (0.087 g, quant.). ^{1}H NMR (500 MHz, $CDCl_3$) δ 7.94 (d, J = 4.8 Hz, 1H), 7.91 (d, J = 4.8 Hz, 2H), 7.59 (m, 2H), 7.52 (m, 2H), 7.40 (m, 2H), 5.20 (s, 2H), 5.08 (s, 2H), 2.69 (s, 3H).

SECTION 6. THE SYNTHESIS OF β-ENOL ETHER π-BRIDGES FOR USE IN DSC

In addition to studying the development and improvement of donors and anchor groups for DSC sensitizers, I also contributed to the development of π-bridge units. While multitudes of these subunits have been reported in the literature (with varying degrees of success), they will not be reviewed here. In general, π-bridges usually fall into two main categories: electron rich or electron poor. Both types of bridges are useful, and both can serve different purposes.

In Figure 26, the two categories of bridge subunits are shown with examples. Bridges that have inductively or resonance donating groups are usually termed as electron rich and generally destabilize the $E_{(S+/S)}$ energy level to a greater degree than the $E_{(S+/S^*)}$ energy level. In contrast, bridges that are termed electron poor generally stabilize the $E_{(S+/S^*)}$ energy level to a greater degree than the $E_{(S+/S)}$ energy level. Expediently utilizing one type of bridge or another can greatly aid in narrowing a sensitizer's bandgap and alter the crystallinity, aggregation, and surface blocking characteristics.

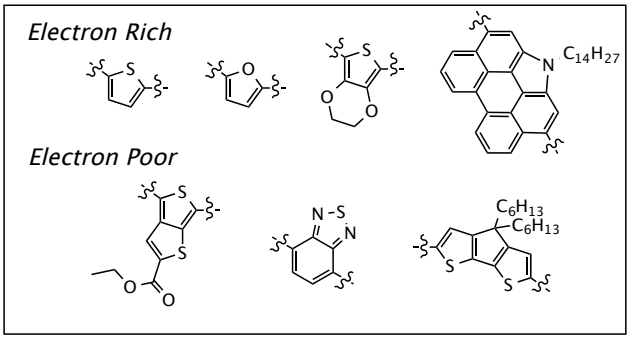

Figure 26. Some examples of electron rich and electron poor π-bridge subunits.

We chose to focus on the synthesis of β-ketoenolether thiophene bridges (Scheme 7) for two reasons: First, we sought a bridge that would allow rapid narrowing of sensitizer bandgap in order to apply low-molecular weight dyes in devices. Choosing dyes with low-molecular weight often equates to less synthetic steps required to make the sensitizer, which also equates to a more practical and economical sensitizer, a key concern for DSC commercialization. Second, we desired a bridge that was morphologically tunable. Morphology control is important for DSC sensitizers, as recombination pathways between semiconductor and redox shuttle or between adsorbed dyes can severely reduce device performance. Thus, judicious bridge selection to tune sensitizer morphology is key in sensitizer design. By altering the non-conjugated substituents on the ester and enol ether groups, the sensitizer's film morphology could be precisely tuned to match device needs.

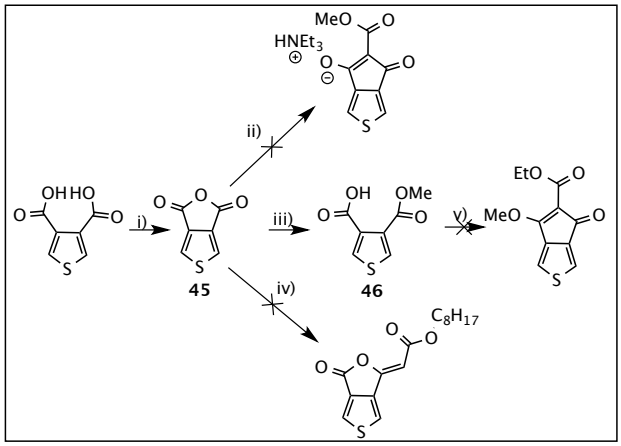

Scheme 7. Synthetic attempts at synthesizing a β-ketoenol ether thiophene bridge. Conditions: i): Ac_2O, reflux, 3.6 g, 80%.

Our approach to synthesizing the β-ketoenolether thiophene bridge (Scheme 7) was started with the cyclization of thiophene-3,4-dicarboxylic acid to form anhydride **45**.[88] We attempted to form a β-ketoenolate directly by methyl acetoacetate condensation; however, this product did not form.[89] We also tried to submit the anhydride directly to a Wittig reaction, but that was also unsuccessful. Our final attempt was the formation of monoester **46** followed by acyl chloride formation and Wittig condensation/cyclization to form the desired β-ketoenolether thiophene.[90] Unfortunately, this did not work either.

EXPERIMENTAL SECTION

See Chapter 1, Section 1 for General Experimental Considerations

1H,3H-thieno[3,4-c]furan-1,3-dione (**45**): A flask equipped with a stirbar and reflux condenser was charged with 3,4-thiophenedicarboxylic acid (5.1 g, 29.5 mmol) and Ac_2O (10 mL). The flask was then warmed to reflux with stirring. Once the reaction was complete, the mixture was cooled to rt and concentrated. The product was dissolved in minimal hot Toluene and allowed to cool. Large, pale brown crystals collected (3.6 g, 80%).

4-(methoxycarbonyl)thiophene-3-carboxylic acid (**46**): A flask equipped with a stirbar was charged with anhydride **45** (1.54 g, 9.9 mmol), methanol (1.69 mL, 41.8 mmol), TEA (1.8 mL, 12.83 mmol), DMAP (0.122 g, 1 mmol), CH_2Cl_2 (30 mL), and allowed to stir at rt. After 24h, reaction mixture was diluted with $CHCl_3$ (20 mL) and washed sequentially with 1 N HCl (20 mL), H_2O (20 mL), Brine (20 mL), and dried with Na_2SO_4. Product concentrated to yield an off-white solid (1.47 g, 79%).

SECTION 7. THE DEVELOPMENT OF MORDANT DYES AS SENSITIZERS FOR DSC.

In the march towards commercialization, DSC will benefit from efforts aimed directly at utilizing very easily constructed architectures for use as sensitizers. While we have explored sophisticated donors, anchors, and π-bridge units, we next aimed to investigate the potential for mordant dyes to be used in DSC. Mordant dyes, or metal-complex fabric dyes have been used as fabric colorants since the middle agents, with textiles to be dyed first being impregnated with metal salt solutions and then soaked in a chelating dye solution to cause a bathochromic color shift in the fabric hue.[91] The "mordant" part of the term is technically the polyvalent metal ion that is chelated by the dye, so the metal dye complexes described here will be termed mordant dyes.

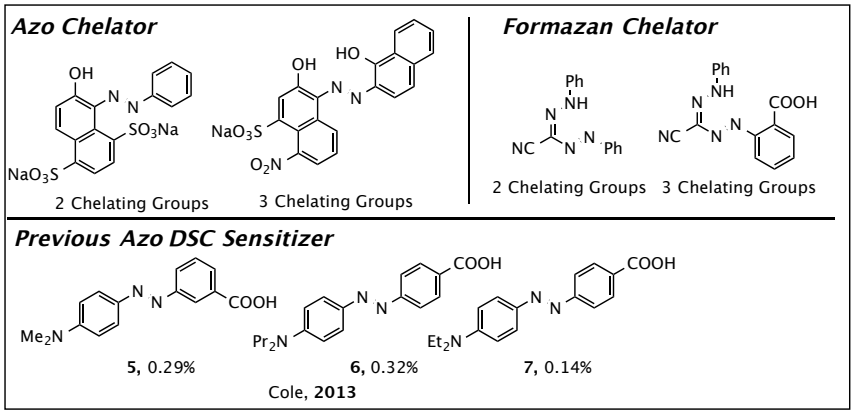

Figure 27. *Top*: Main types of chelating dye groups used in mordant dyes. *Bottom*: Previous azo-based sensitizers reported to be applied in DSC.

The chelating dye groups found in mordant dyes are principally azo/azomethine dyes or formazan type dyes (Figure 27).[92] Both dye types are fully conjugated and have N=N double

bonds. While formazan dyes can chelate metals with both azo groups, azo dyes only have one N=N group. Both can have auxiliary chelators, such as phenols or acid groups to increase the overall chelation number of the ligand. However, only the azo type dyes would allow for the anchoring group to be positioned away from the donor, which is a requirement for reducing recombination of injected electrons into the TiO_2 CB. Our initial assessment was supported by a report by Cole et al. in 2013, in which a series of simple D-π-A dyes with an azo group as π-bridge was tested in DSC.[93] While the dyes did not perform well (0.14-0.32% PCE for the series), they still produced a functional device.

Our strategy was to choose commercially available azo-based chelators and use chelated metal ions to red-shift the absorptions of the chelating dye, as textile dyers from the Middle Ages once did. These dyes do not possess a D-π-A structure as we have investigated in Parts 1-7. Instead, these dyes rely on metal-to-ligand charge transfer (MLCT) events, in which an electron from the metal atom is transferred to the ligand and finally to the anchor adsorbed onto the TiO_2 surface. The structures we chose to focus on are shown in Figure 28.

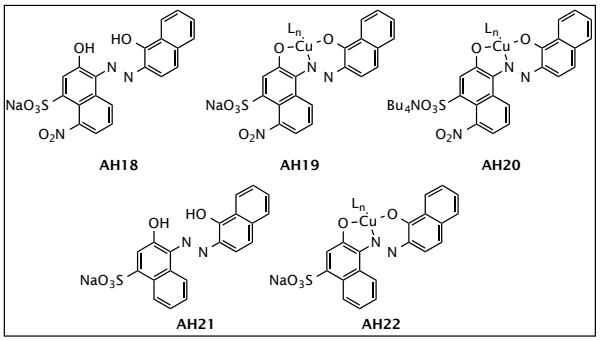

Figure 28. Mordant dyes chosen to be evaluated as DSC sensitizers. *Metallation Conditions:* Ligand (1.0 g, mmol), $CuSO_4$ (mmol), H_2O, reflux, Yield: **AH19**: 0.45 g; **AH22**: 0.48 g.

Even though we have identified over 100 mordant dyes for potential use in DSCs, we chose to work with two commercial dyes (Eriochrome Black T (EBT) and Eriochrome Blue Black B (EBB)) and one metal ion (Cu^{II}). The series we proposed for study was composed of five dyes: **AH18-AH22**. Dyes **AH18** and **AH21** are not metallated, while the others are chelated to one Cu^{II} ion. There is likely another ligand on the Cu^{II} center, however, we did not attempt to determine its identity. To metallate **AH18** and **AH21**, each ligand was heated with $CuSO_4$ in H_2O to 100ºC. Upon cooling to room temperature, a dark solid precipitated and was collected. Dye **AH20** is metallated, however, it contains a tetrabutylammonium cation instead of a sodium cation. This was an important contribution to the study, as the sodium counterion could potentially lower the semiconductor CB energy level and therefore the device maximum V_{oc}. To exchange the counterion, tetrabutylammonium bromide was added to a DMF solution of **AH19** and the solution submitted to size exclusion chromatography.

Once each dye was synthesized, the UV-Vis absorption of each was measured and is shown in Figure 29. The two non-metallated ligands **AH18** and **AH21** both absorbed light out to 620 nm (for **AH18**) and 650 nm (for **AH21**). Upon metallation with Cu, the absorption was red shifted in reference to the non-metallated dye (750 nm for **AH19/20** and 650 nm for **AH22**). Thus, each of the dyes absorbs enough visible light to produce high efficiencies in DSCs (10% theoretical maximum, with 95% IPCE from 400-650 nm, 800 mV V_{oc} and 0.75 FF).

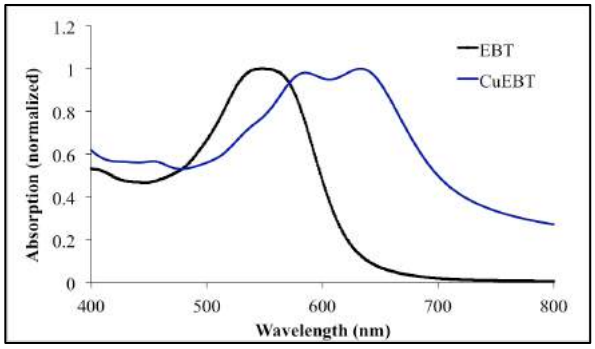

Figure 29. The UV-Vis absorption spectrum of dye **AH18** measured in H_2O.

Next, we sought to verify that the energy levels for each dye were positioned correctly for use in DSC devices. The combined optical and electronic properties of each dye are compiled in Table 13. Metallation of **AH18** greatly stabilized the $E_{(S+/S^*)}$ energy level in dyes **AH19-20** while metallation of **AH21** slightly destabilized the $E_{(S+/S^*)}$ energy level in **AH22**. The metallation of **AH18** resulted in slight destabilization of the $E_{(S+/S)}$ energy level as well, while the metallation of **AH21** led to a slight stabilization of the $E_{(S+/S)}$ energy level.

Table 13. Optical and Electronic Properties of Mordant Dyes **AH18-22**.

Dye Name	$E_{(S+/S)}$	λ_{onset}	E_g^{opt}	$E_{(S+/S^*)}$
AH18	0.88	620 nm	2.0 eV	-1.12
AH19	0.91	750 nm	1.65 eV	-0.74
AH20	0.91	750 nm	1.65 eV	-0.74
AH21	0.79	650 nm	1.91 eV	-1.12
AH22	0.72	690 nm	1.80 eV	-1.18

[a]: Measured in a 0.1 M Bu_4NPF_6 in CH_2Cl_2 solution with glassy carbon disk working electrode, Pt reference electrode, and Pt counter electrode with ferrocene as an internal standard. Values are reported versus NHE. [b]: Measured in H_2O. [c]:Estimated from the tangent of the lower-energy tangent of the lambda max transition in the UV-Vis absorption spectrum in H_2O. [d]Taken as the difference between the oxidation potential $E_{(S+/S)}$ and the estimated optical bandgap $E_{(0\text{-}0)}$.

Thus, the dyes **AH18-22** have the requisite energy levels for use in DSC and they absorb a substantial range of light in the visible region. To examine the kinetics for electron injection, fluorescence lifetime studies were undertaken for each of the dyes in solution and on TiO_2 films to evaluate electron injection efficiencies (η_{eff}, where $\eta_{eff} = 1 - \tau_{TiO2}/\tau_{sol}$).

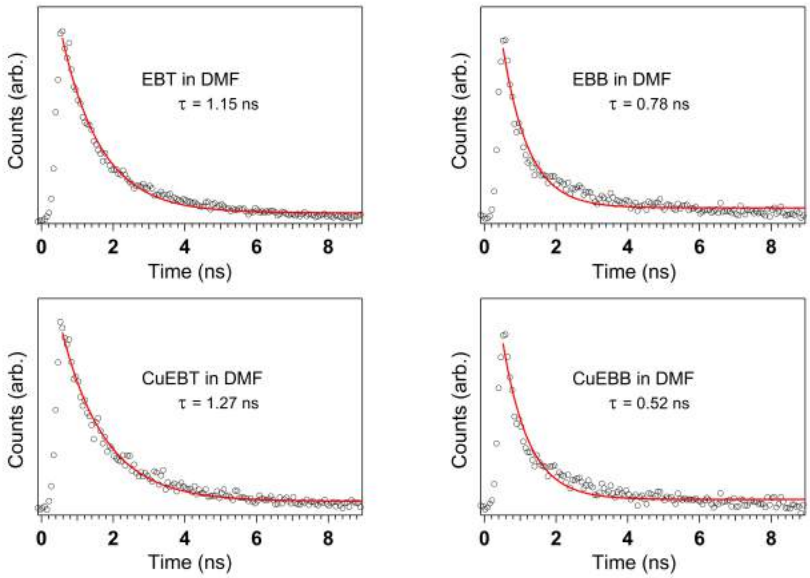

Figure 30. Excited-state fluorescence decay curves for DMF of dyes **AH18-AH22** (EBT = **AH18**, CuEBT = **AH19**/**20**, EBB = **AH21**, CuEBB = **AH22**). Measurements performed by McNamara and Hammer.

Lifetimes of the dyes in dichloromethane solutions (τ_{sol}) were found to be on the order of nanoseconds ranging from 1.27 ns to 0.52 ns (Figure 30, Table 14). Excited-state lifetimes of the dyes on TiO_2 films (τ_{TiO2}) are predicted to be significantly shorter whereas electrons may be injected from the dye into the TiO_2 CB effectively quenching the fluorescence. Without any additives, η_{eff} was found to be >75% for **AH19**. This observation of high injection efficiency is

significant because sulfates are known to be very poor injectors and nitro groups have not been reported to be capable of injection into TiO_2.

Table 14. Excited-state lifetime measurements for dyes **AH18-AH22**.[a] Measurements performed by McNamara and Hammer.

Dye	τ
AH18	1.15
AH19/20	1.27
AH21	0.78
AH22	0.52

[a]:Measurements made in DMF solution.

Having established the mordant dye series exhibits suitable characteristics for productive photon-to-electric conversion, dyes **AH18-AH22** were examined in DSC devices with a TiO_2 semiconductor and I^-/I_3^- redox shuttle. From the equation PCE (η) % = $(J_{sc}V_{oc}FF)/I_{(sun)}$ where J_{sc} = short-circuit current, V_{oc} is the open-circuit voltage, *FF* is the fill factor and $I_{(sun)}$ is the incident light intensity, the device performances under AM 1.5 irradiation were analyzed (Table 15).

Table 15. Device performance data for dyes **AH18-AH22**.[a] Measurements performed by Giordano, Nazeeruddin, and Grätzel.

Dye	J_{sc} (mA/cm^2)	V_{oc} (mV)	FF	*h* (%)
AH18	0.493	306	0.647	0.10
AH19	0.069	343	0.355	0.01
AH21	0.182	394	0.681	0.05
AH22	0.022	301	0.509	0.01

[a]: Electrolyte 960 used as electrolyte, 100 mM LiI additive used in electrolyte,

Unfortunately, Dyes **AH18-22** did not perform well in DSC devices. The J_{sc} values ranged from 0.49 to 0.022 ma/cm^2, the V_{oc} ranged from 394 to 301 mV, and the FF ranged from 0.647 to

0.355. Dye **AH20** was not tested, as **AH19** was not functional. Metallation of ligands **AH18** and **AH21** both resulted in severely reduced FF and J_{sc} values, likely due to facile recombination between the TiO_2 CB and oxidized dye coupled with the absence of a reliable injecting group like -COOH. The V_{oc} was also very low due to the large amount of LiI used in the electrolyte and likely aggregation of dyes on the TiO_2 surface, since no effort was taken to prevent aggregation.

EXPERIMENTAL SECTION

See Chapter 1, Section 1 for General Considerations (Experimental, Photovoltaic Characterization, and Device Fabrication).

Synthetic Procedures to reach AH19:

1:1 Eriochrome Black T : Cu complex (**AH19**): A flask equipped with a stirbar was charged with Eriochrome Black T (1.0 g, 2.17 mmol), $CuSO_4$ (0.35 g, 2.17 mmol), H_2O (10 mL), and heated to 100ºC with stirring. After 4h, the reaction mixture was cooled to rt and NaCl (1 g) added. A precipitate formed, was filtered, and was washed with copious H_2O to yield a black solid (0.48 g).

Synthetic Procedures to reach AH22:

1:1 Eriochrome Blue Black B : Cu complex (**AH21**): A flask equipped with a stirbar was charged with Eriochrome Black T (1.0 g, 2.17 mmol), $CuSO_4$ (0.35 g, 2.17 mmol), H_2O (10 mL), and heated to 100ºC with stirring. After 4h, the reaction mixture was cooled to rt and NaCl (1 g) added. A precipitate formed, was filtered, and was washed with copious H_2O to yield a black solid (0.45 g).

SECTION 8. BENZIMIDAZOLE ACCEPTORS FOR DSC SENSITIZERS

Our last attempt at improving sensitizers for use in DSC was aimed at improving the acceptor group. While many acceptor groups have been developed for use in DSC,[13] such as cyanoacrylic acid, rhodanine and bis-rhodanine, they will not be reviewed here. As a subunit, there are two requirements that acceptors need to meet. First, the acceptor should optimally bare the anchoring group, in order to position the donor group as far from the semiconductor surface as possible. Second, the acceptor group should be sufficiently electron accepting in order to promote a strong CT band in the absorption spectrum.

Our synthetic strategy for improving acceptor groups was based on the benzimidazole group (Scheme 8). Upon oxidative condensation with an aldehyde, the acceptor group can be installed. The benzimidazole acceptor offers a fully conjugated path to the anchor group (important for efficient electron injection) and also offers a donating amine functionality that should serve the dual purpose of helping to destabilize the dye $E_{(S^+/S)}$ energy level and might provide a high energy light absorption band, as was observed in rhodanine dyes. To test our hypothesis, our study included one dye, **AH12**.

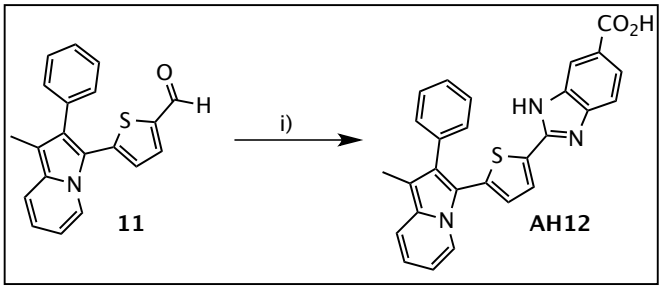

11 **AH12**

Scheme 8. Synthesis of benzimidazole acceptor containing **AH12**. Conditions: i) 3,4-diaminobenzoic acid, piperidine, $CHCl_3$, 90ºC, 0.070 g, 50%.

The UV-Vis absorption spectrum and emission spectrum of **AH12** looked similar to those measured for aldehyde **11** (Figure 31, Table 16), except that the spectrum of dye **AH12** also contained a very weak CT band near 600 nm. The emission spectrum of both in $CHCl_3$ contained an emission near 550 nm. Dye **AH12** did not was not observed to emit from the weak CT band.

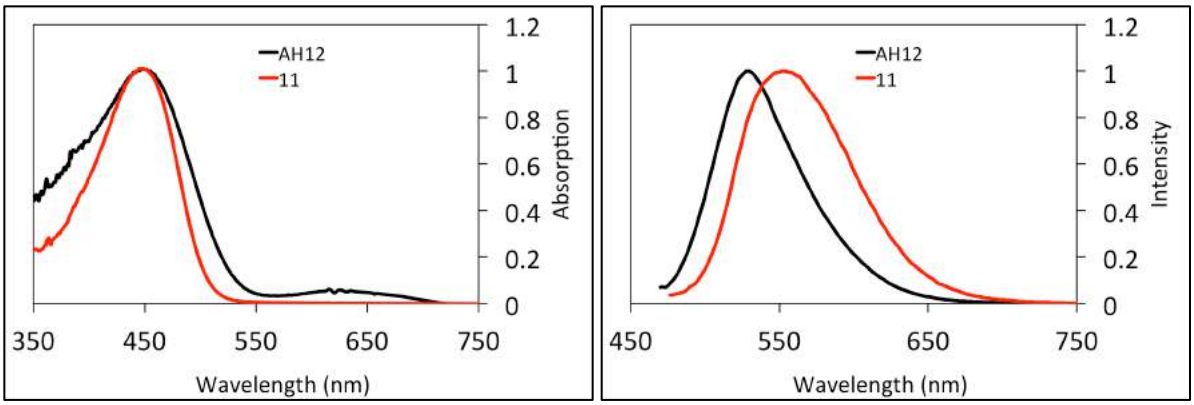

Figure 31. *Left*: UV-Vis absorption spectra of **AH12** and aldehyde **11** measured in $CHCl_3$. *Right*: Emmision spectra of **AH12** and aldehyde **11** measured in $CHCl_3$.

Table 16. Optical and electronic properties of dye **AH12** and aldehyde **11** compared to **AH3**.

Dye	λ_{max} (nm)[a]	λ_{onset} (nm)[a]	(ε $Lmol^{-1}cm^{-1}$)[a]	λ_{em} (nm)[a]	E_g^{opt} (eV)[b]	$E_{(S+/S^*)}$ (V)[c]	$E_{(S+/S)}$ (V)[d]
AH12	455, 620	550, 715	---	530	2.39, 1.73	-1.49, -0.83	0.90
11	455	510	---	560	2.49	-1.49	1.07
AH3	553	633	8,500	625	2.06	-0.98	0.99

[a]: Measured in $CHCl_3$. [b]:Estimated from the intercept of the lower-energy tangent of the lambda max transition in the UV-Vis absorption spectrum and the higher-energy tangent of the emission spectrum in $CHCl_3$. . [c]Taken as the difference between the oxidation potential $E_{(S+/S)}$ and the estimated optical bandgap $E_{(0\text{-}0)}$.
[d]: Measured in a 0.1 M Bu_4NPF_6 in CH_2Cl_2 solution with glassy carbon disk working electrode, Pt reference electrode, and Pt counter electrode with ferrocene as an internal standard. Values are reported versus NHE

The electrochemical properties of dye **AH12** and aldehyde **11** were analyzed with regard to DSC device components to evaluate if the dye is energetically suitable for regeneration from the I^-/I_3^-

redox shuttle and electron injection into a mesoporous TiO_2 semiconductor (Table 16) and determine how the benzimidazole acceptor affected the dye energy levels. In using the weak CT transition towards the calculation of dye energy levels, the benzimidazole acceptor both destabilized the dye $E_{(S+/S)}$ energy level and stabilized the dye $E_{(S+/S*)}$ energy level in relation to **AH3**. This indicates that benzimidazole is a stronger acceptor than cyanoacrylic acid and also contributes to the dye overall donor strength. The high-energy absorption band near 450 nm observed in rhodanine was not observed in **AH12**, however.

While the energetics were suitable for use in DSC, the CT band intensity was too low to adequately generate electricity from photons. Because of this, the "effective" λ_{max} that would actually be observed in-device would be the higher energy absorption at 455 nm and the dye $E_{(S+/S*)}$ energy level would then be -1.49 eV, which would mean that instead of a much stronger acceptor than cyanoacrylic acid, benzimidazole would be much weaker. Thus, in order to make dye **AH12** usable, we decided to investigate the nature of the CT band near 620 nm.

Upon closer examination of the benzimidazole acceptor unit, we realized that the imine nitrogen could be protonated (benzimidazole $pK_a = 5.6$) by the carboxylic acid ($pK_a = \sim 4.5\text{-}5$) in solution (Figure 32). Upon protonation, the neutral imine N bears a positive charge, which greatly increases the heterocycles' accepting ability. However, too much acid causes irreversible decomposition of the dye, while careful titration allows for reversibility. The addition of base to **AH12** caused the already weak CT band to disappear, while the high-energy transition near 450 nm blue shifted. Upon the addition of a small amount of triflic acid to **AH12**, the charge transfer band near 620 nm increased greatly and the high-energy band was somewhat diminished. The

addition of excess acid caused the complete reduction of the CT band and a severe blue shift in the high energy region to near 350 nm.

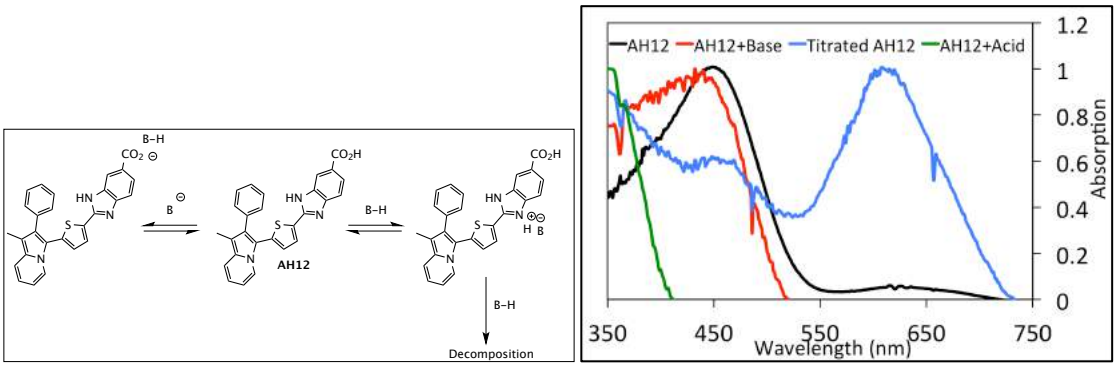

Figure 32. *Left:* Proposed increase of benzimidazole acceptor strength with protonation. *Right*: UV-Vis absorption spectrum of **AH12** in titration studies in $CHCl_3$.

To better understand the absorption spectrum changes we observed in solution, we performed some TD-DFT calculations on **AH12** and some representative charged analogs. We calculated the vertical transitions of the lowest energy absorptions as well as the oscillator strength for each of the structures calculated (Table 17). The results compiled in Table 17 illustrate that the charged nitrogen should indeed make **AH12** a stronger acceptor, with dimethyl alkylated **AH12Me$_2$** having a large red shift (100 nm) in comparison to dye **AH12**. Adding a stronger acceptor to methylated **AH12Me$_2$** to form **AH12Me$_2$CAA** resulted in a further red shift (50 nm). The protonated version of **AH12** to form **AH12+H** as drawn in Figure 30 was calculated to have a transition at 684 nm, nearly 250 nm red shifted from the neutral dye **AH12**. While the exact transition values are likely not accurate, the qualitative conclusions drawn from the relative numbers indicate that protonation of the benzimidazole acceptor greatly increases the heterocycle's accepting power and thus lowers the energy of the lowest energy transition.

Table 17. Calculated vertical transitions and oscillator strengths of dye **AH12** and charged analogs.[a]

Dye	Vert. Trans.	Oscillator Strength
AH12	445	0.52
AH12Me$_2$	557	0.69
AH12Me$_2$CAA	606	0.61
AH12+H	684	0.37

[a]: Values calculated using TD-DFT methods (B3LYP/6-311G(d,p) geometry optimization) with calculated states = 10.

EXPERIMENTAL SECTION

See Chapter 1, Section 1 for General Experimental Considerations

Computational Details: All computations were performed with the Gaussian09 software package. The geometry optimization steps were as follows: first the structures were optimized by MM2 in the ChemBio3D (version: 13.0.2.3021) software package and dihedral angles for all relevant groups set to values in-between the global minimum and the next local maximum on the conformational energy diagram as calculated by ChemBio3D (version: 13.0.2.3021) in the dihedral driver toolset. After MM2 optimization, the molecular structures were further optimized by DFT methods: first B3LYP/3-21g, second B3LYP/6-311g(d,p), and finally opt=tight B3LYP/6-311g(d,p) with tight convergence criteria. Lastly, time-dependent density functional theory (TD-DFT) computations were carried out to compute the vertical transition energies and oscillator strengths for the 10 lowest excited states. Symmetry was explicitly turned off for these computations even though all of the optimized structures belonged to the C_1 point group. A representative input file is included for each type of calculation.

Synthetic procedures to reach AH12:

2-(Thiophen-2'-yl-5'-2''-phenyl-3''-pentyl-5''-methoxyindolizine)-1H-benzmidazole-5-carboxylic acid (**AH12)**: A flask equipped with a stirbar was charged with aldehyde **11** (0.105 g, 0.33 mmol), 3,4-diamino-5-benzoic acid (0.055 g, 0.36 mmol), $CHCl_3$ (3 mL), and was degassed with N_2. After 30 min, piperidine (0.13 mL, 0.99 mmol) added, the reaction warmed to 90ºC with stirring, and the reaction monitored by TLC. After 2h, the reaction was cooled to rt and diluted with CH_2Cl_2 (50 mL), acidified with AcOH (2 mL), washed with H_2O (3 x 50 mL), dried with $MgSO_4$, concentrated, and passed through a plug of SiO_2 using first CH_2Cl_2 (500 mL), then 5%:MeOH:CH_2Cl_2 (500 mL), 5%AcOH:5%MeOH:CH_2Cl_2 (1000 mL). Concentrated product fractions to yield a red solid (0.070 g, 50%).

SECTION 9. THE SYNTHESIS OF HEXACOORDINATE CO-CONTAINING REDOX SHUTTLES FOR DSCS

Another synthetic avenue of research possible with DSC is the development of redox shuttles. The most widely used redox shuttle by far is the I^-/I_3^- redox shuttle. This shuttle is convenient as it is soluble in acetonitrile and negatively charged, which discourages recombination of electrons from the TiO_2 layer and the oxidized redox shuttle.[94] While other similar organic or non-metal redox shuttles (such as $SeCN^-/(SeCN)_3^-$ and Br^-/Br_3^-) have attained some success,[95] the development of negatively charged transition metal redox shuttles has been very slow due to the highly reactive nature of anionic transition metal complexes.

Shuttles such as I^-/I_3^- and Br^-/Br_3^- work through SET reaction directly from the complexation of dye and iodine molecules (as illustrated in the following reactions):[52,94]

$$X^- + Dye^+ \rightarrow [X^-:Dye^+] \qquad (2)$$

$$[X^-:Dye^+] + X^- \rightarrow X_2^- + Dye \qquad (3)$$

Thus, these types of electrolytes are termed two electron shuttles. One disadvantage of using two electron shuttles is that kinetics involved in shuttle regeneration and competing complexation reactions with other species (I_2^-, I_3^-, among others) is very complicated and makes the use of this type of shuttle less than ideal. Even with the complicated kinetics, cells often reach 99% regeneration efficiency with the iodide based redox shuttle. However, the redox shuttle is corrosive to the platinized counter electrode in high concentrations and at low concentrations slow diffusion of I_3^- to the counter electrode can result in voltage losses. Another disadvantage of using this shuttle is that over time the concentration of triiodide in the cell can decrease, which

leads to losses in voltage over time.[94] Yet another disadvantage to using this type of redox shuttle (I^-/I_3^-, $SeCN^-/(SeCN)_3^-$ and Br^-/Br_3^-) is that the overall electronic process involves two electrons and requires a large driving force for efficient dye regeneration.[94] Overpotential of the reaction has been observed to be ~500 mV to ensure the recombination of injected electrons in the conduction band do not recombine with the oxidized dye at a faster rate.[96] Outersphere one electron transition metal complex electrolytes, such as $Co^{2+}(bpy)_3$ allow for much smaller over potentials (150 mV has been observed for the above Co electrolyte) and furthermore they allow for much simpler kinetics through the following equation:

$$M^{n+}(L)_n + Dye^+ \rightarrow M^{(n+1)+}(L)_n + Dye \qquad (4)$$

The energy levels of many neutral or anionic transition metal complexes are not well matched for the energy levels of the TiO_2 layer or the dye HOMO level (Figure 33).[97] As depicted, a typical HOMO energy level of a DSC dye ranges anywhere from 0.8-1.2 V (vs NHE), while the TiO_2 conduction band (CB) is at -0.5 V and the I^-/I_3^- redox shuttle is at 0.35 V. The optimal dye HOMO is at 0.7 V (vs NHE), with the optimal LUMO of the dye residing at -0.70 V, which would mean absorption out to 920 nm. The maximum voltage possible out of the cell is the energy difference between electrons in the TiO_2 CB and the redox potential of the shuttle. Thus, the redox shuttle's oxidation potential should be higher in energy than the dye, but as low as possible in reference to the CB in order to maximize the V_{oc}.

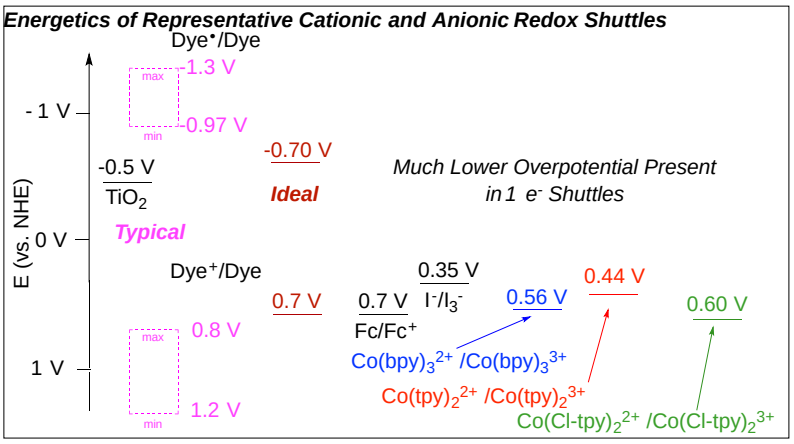

Figure 33. Energy diagram depicting some common redox shuttles and reagents in reference to TiO_2, typical, and ideal dye energy values.

In addition to energetic requirements, sterics also play a key role in determining the value of a particular redox shuttle in DSCs. Firstly, the TiO_2 film used in DSC is 5-20 μm thick, has a porosity of about 50-60% with an average pore size of 15 nm.[8] Thus, the film has a rather cavernous morphology, especially with adsorbed dye molecules on the surface. It follows then, that a redox shuttle with substantial steric bulk would not diffuse into the cavernous spaces of the sensitized TiO_2 very well. Additionally, electrolyte regeneration is also sterically limited, as the oxidized shuttle must diffuse from the sensitized surface to the counter electrode. Thus, poor diffusion (or mass-transport), limits dye regeneration and thus lowers the device J_{sc}. The electron transfer kinetics of electrolyte regeneration at the counter electrode will not be addressed here, but discussion of such is covered elsewhere.[52] Specifically, increasing the oxidized dye diffusion rate while retaining the necessary energy levels and ensuring long-term stability of the electrolyte are important to the advancement of DSC technology.

The diffusion of the oxidized redox shuttle to the counter electrode is a necessary step in charge separation. This diffusion also completes the electrical circuit. The precise amount the diffusion hinders the J_{sc} is known as the diffusion limiting current density (J_{lim}) as illustrated in the equation below:[98]

$$J_{lim} \propto (\varepsilon_p \text{ x } F \text{ x } D_o \text{ x } [R^+]) / l \qquad (5)$$

where ε_p is the porosity, F is a Faraday, D_o is the diffusion coefficient, $[R^+]$ is the concentration of the oxidized shuttle, and l is the electrolyte diffusion distance.

By simply analyzing Equation 5, one logical method of decreasing the diffusion limitation (increasing J_{lim}) common to one-electron shuttles is simply to increase $[R^+]$ in solution. However, not only is $[R^+]$ not very soluble in organic solvents, the concentration increase would merely result in an increase in charge recombination at the photoanode (TiO_2), as illustrated in the equation below:[99]

$$U_{rec} = k_{rec} \text{ x } [R^+] \text{ x } n_s \qquad (6)$$

where U_{rec} is the recombination (specifically in reference to the electron transfer from the semiconductor to the oxidized dye or the oxidized redox shuttle), k_{rec} is the recombination rate, and n_s is the concentration of free electrons at the electrode surface. For these purposes, recombination to the dye is assumed to be negligible. In assembling cells, some amount of oxidized electrolyte is added in order to lower the redox energy and thus boost the V_{oc} of the cell, however, increasing $[R^+]$ also increases the dark current of the cell (which lowers $V_{oc)}$ while enhancing the FF and J_{sc}.

Additionally, while bulky ligands (such as 4,4'-ditert-butyl-2,2'-bipyridine (t-Bu_2bpy) in Co(*t*-Bu_2bpy)$_3$) serve to lower k_{rec} through sterics, D_o is lowered substantially to less than 10 times the value for I_3^- (at low concentration, since the redox shuttle does not follow the Stokes-Einstein equation at high concentration[100]).[101] The effect of diffusion limitation resulting from the use of Co(*t*-Bu_2bpy)$_3$ as shuttle is illustrated in Figure 34.[101]

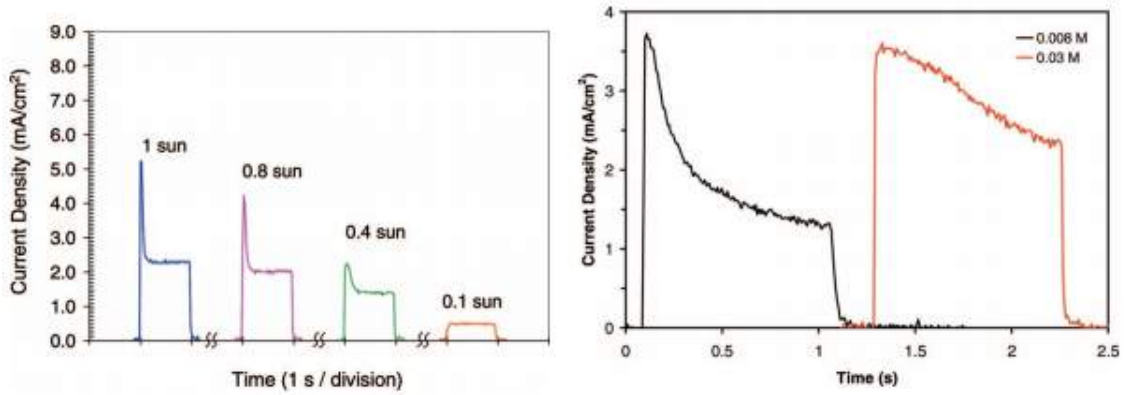

Figure 34. *Left*: The effect of incident light power on diffusion limitation for DSC using Co(*t*-Bu_2bpy)$_3$ as redox shuttle. *Right*: The effect of concentration on diffusion limitation for the same system. Both figures taken from ref. 94. Reprinted with permission from Boschloo, G.; Hagfeldt, A. *Acc. Chem. Res.* **2009**, *42*, 1819. Copyright 2009 American Chemical Society.

As shown above, in all but the lowest intensity case the initial current observed is proportional to light intensity. However, the current drops sharply and levels off at a lower value that is not proportional to the light intensity. Initially, the concentration of electrolyte is sufficient to regenerate the oxidized dye. The number of electrolyte molecules available to regenerate the oxidized dye molecules quickly decreases as each oxidized electrolyte takes much longer to diffuse to the counter electrode and back than the dye takes to absorb a photon and inject the

resulting high-energy electron, which lowers the observed current. This conclusion of small D_o is strengthened by the neighboring figure (Figure 34), which illustrates that increasing the concentration of redox shuttle species mitigates the sharp decline in initial current.

Our synthetic strategy for the synthesis of hexacoordinate Co complexes involved the synthesis of multi-dentate ligands composed of (imidazol-2-ylidene)pyridines used in forming a coordinately saturated Co complex (Scheme 9). After coupling imidazole to 2-bromopyridine, the imine N was alkylated using MeI.[102] The imidazolium was then deprotonated and added to $CoCl_2$. Concentration of the organic solvent revealed only trace amount of product, which we suspected to be the Co^{III} complex, which is NMR detectable. A large amount of white precipitate was formed from the reaction, however, it gave no signals in the ^1H NMR spectrum, therefore, we discarded the precipitate. Unfortunately, Co^{II} is a paramagnetic metal ion, meaning that it (and complexes including it) is not detectable by ^1H NMR.

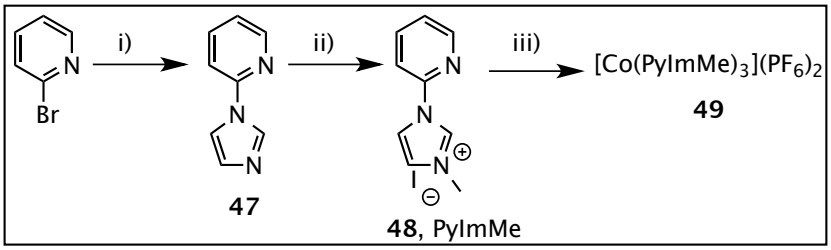

Scheme 9. The attempted synthesis of pyridine NHC Co complex **49**.

Future attempts at synthesizing these types of redox shuttles should focus on the collection of the white precipitate that forms and then one electron oxidation to a diamagnetic Co^{III} complex, which is detectable by ^1H NMR. Once formed, the energy levels of these redox shuttles can then be measured and their potential for use in DSC assessed.

The pyridine-NHC complexes should exhibit all the requirements for DSC redox shuttles: First, they should not absorb visible light, as Co polypyridine complexes are known to not absorb light past 450 nm.[103] Second, the pyridine-NHC complexes will be very tunable, with possible destabilization and stabilization of $E_{(S+/S)}$ energy levels by withdrawing or donating group substitution.[104,105] Third, the complexes are sterically small enough to allow for adequate diffusion and oxidized dye regeneration, as polypyridine ligands allow for good diffusion.[52] Furthermore, the five membered NHC rings are smaller than pyridine rings. Fourth and perhaps most importantly, pyridine NHC ligands should be stronger chelators and thus produce more stable metal complexes in solution.[106] This is extremely important in consideration of the fact that without one-electron redox shuttles that are stable in-device for >10 years (as is I^-/I_3^-), they are not practical choices for commercial DSC application.[107]

CHAPTER 2

SECTION 1. PHOTOCATALYTIC REDUCTION OF CO2 USING RE BIPYRIDYL AND PYRIDYL-NHC COMPLEXES WITH A SIMULATED SOLAR SPECTRUM.

Carbon dioxide is available in tremendous quantities and the problems of scale were discussed in the introduction. Specifically, conversion of CO_2 to fuel could close the 'carbon cycle' and provide power from an non-utilized waste.[108] Simply reducing CO_2 electrochemically is not energetically efficient as the single electron reduction of CO_2 to CO_2●- is very energetically demanding (-1.97 V *vs* NHE in DMF). Multiple electron reduction products may be formed at less negative potentials (i.e. CO at -0.53 V *vs*. NHE or CH_3OH at -0.38 *V* vs. NHE); however the substantial kinetic barriers require a catalyst to drive the reaction. Selectivity between possible products is then dependent on the chosen catalyst.

As discussed in the introduction, the energy to drive these catalytic reductions should be derived directly (photocatalysis) or indirectly (solar cell driven electrocatalysis) from the sun. Numerous reports on electrocatalysis[109] since the 1970's have emerged using a host of transition metals including Re,[110] Ru,[111] Co,[112] Fe,[113] Ni,[112b,114] and others.[115,109b]

While in electroctalysis the catalyst is able to obtain requisite electrons from the electrode surface, in photocatalysis the electrons come from either absorption of a photon by the catalyst followed by excited state reduction from a sacrificial donor (SD) or a separate photosensitizer (PS) molecule absorbs a photon from the sun, has its excited-state reduced by a sacrificial donor, and then reduces the catalyst molecules through outersphere single electron transfer (SET). In the

first manner of operation, the catalyst is responsible for both light absorption and CO_2 reduction, while in the second, the catalyst is not photoactive and thus the responsibility of light absorption falls to the photosensitizer. While there are only three reported series of catalysts capable of performing both light absorption and CO_2 reduction duties,[18,19] there are many catalysts capable of photosensitized CO_2 reduction.[116]

Herein for the first time we report the photocatalytic reduction of CO_2 to CO with a series of Re(PyNHC)(CO)3Cl catalysts as a mononuclear catalyst and with and without the addition of a photosensitizer using a solar simulated spectrum (AM 1.5). The catalysts studied here and results of photosensitized runs with these catalysts compared to $Re(bpy)(CO)_3Cl$ are shown in Figure 35. The most investigated of the photocatalysts are based on $Re(bpy)(CO)_3X$, which was first reported in 1983[18] and has been shown to exhibit good selectivity for CO with a turnover number (TON) of up to 27 and a quantum yield (Φ_{CO}) of up to 0.38.[109c, 117] However, $Re(bpy)(CO)_3X$ catalysts often require inert atmosphere storage and rigorously anhydrous reaction conditions for high performance.[118] We sought to modify the bidentate bpy ligand to access air and water stable complexes to avoid air-free purification and handling techniques as well as to generate a longer lived catalyst. Importantly, water stability is necessary for a high TON catalyst as H_2O is a byproduct of CO_2 reduction.

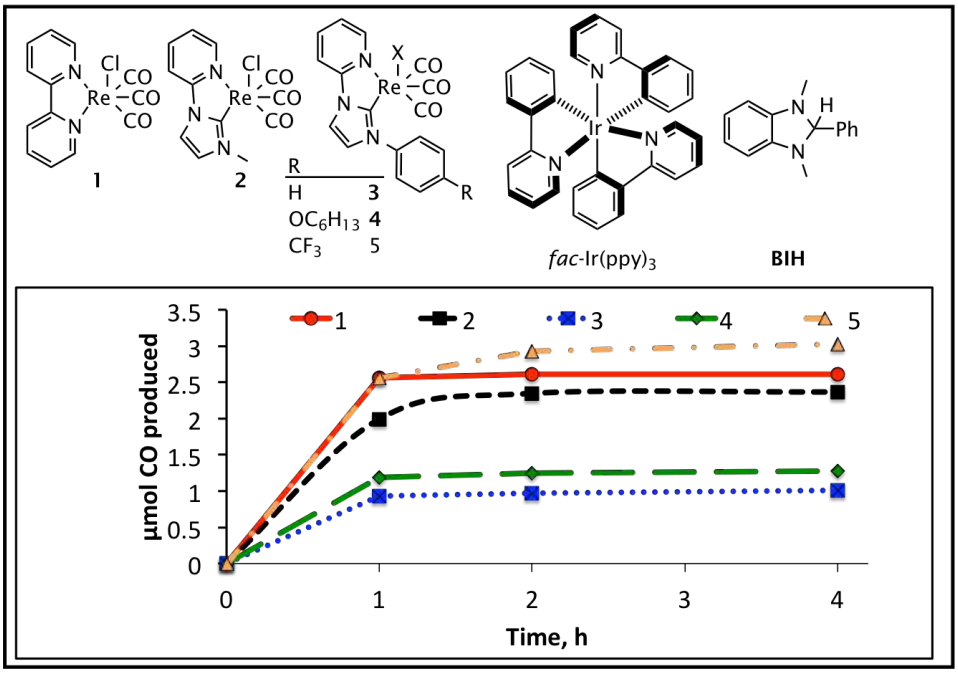

Figure 35. *Top:* Structures of Re(I) pyridyl catalysts used in this study and structures of electron donor **BIH** and **PS** *fac*-Ir(ppy)$_3$. *Bottom:* µmol CO produced versus time for each of the Re(I) catalysts (0.2 µmol catalyst/ 2 mL 10% TEA:MeCN solution with 0.2 µmol *fac*-Ir(ppy)$_3$***** and 0.2 mmol **BIH**). Solutions irradiated with 150W Xe lamp set to 1 sun and equipped with an AM1.5 filter after vigorous bubbling with CO_2 for 15 min. Each data point is the average of two runs.

Several Re(NHC)(CO)$_3$X *complexes* are reported and characterized in literature.[119] To access *catalysts* stable to ambient atmosphere and reaction conditions, we substituted a ring on the bipyridyl ligand for *N*-heterocyclic carbene (NHC) chelating groups with a range of electron donating and withdrawing substituents (Figure 35, Scheme 10).[120] Re-bipyridyl based catalysts are thought to first undergo ligand based reduction on the bipyridyl ligand.[119d,121] NHC ligands

are strongly donating ligands with shortened conjugation lengths. These features raise reduction potentials to higher energies and widen optical band gaps. A photosensitizer (PS) may be used to broaden the absorption window and improve access to the important one-electron reduced (OER) CO_2 reduction catlaysts.[116] *fac*-Ir(ppy)$_3$, has an attractivly positioned reduction potential ($E_{S^-/S}$ of -1.95 V *vs*. NHE) and is suitable for used with sacrificial electron donors such as TEA and 1,3-dimethyl-2-phenyl-2,3-dihydro-1H-benzo[d]imidazole (BIH).[122,123]

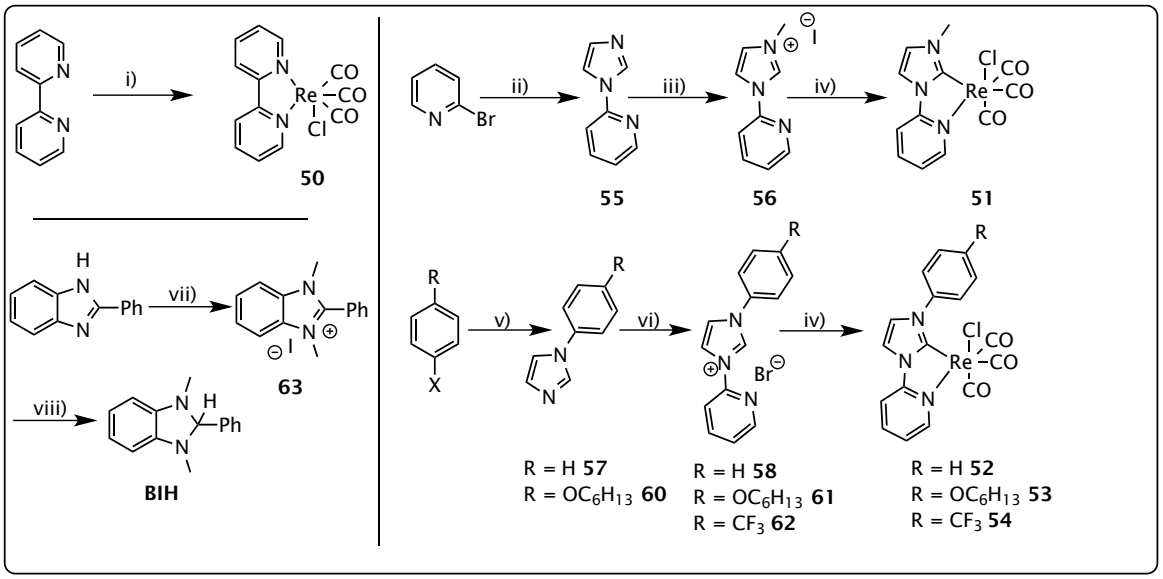

Scheme 10. Synthetic Steps to Reach Re(I) complexes **50**-**54**. Reaction conditions: i): Tol, reflux, 91%. ii): $Cu(OAc)_2 \bullet H_2O$, imidazole, K_2CO_3, TMEDA, DMF, reflux, 68%. iii): MeI, Et_2O, rt, 25%. iv): Tol, TEA, $Re(CO)_5Cl$, reflux, yields: **51**: 39%. **52**: 83%. **53**: 59%. **54**: 33%. v): CuI, imidazole, K_3PO_4, DMF, yields: **57**: 26%, **59**: 64%. vi): 2-bromopyridine, heat, yields: **58**: 53%, **60**: 33%, **61**: 53%. vii): MeI, MeCN, 100ºC, 29%. viii) $NaBH_4$, MeOH, 57%.

Following the rapid (2-3 steps) synthesis of catalystis **51**-**54** (Scheme 10), we wanted to ensure the reduction potentials of complexes **51**-**54** were sufficiently high in energy to reduce CO_2. Each complex was tested with cyclic voltammetry (CV) to determine their oxidation potential,

reduction potential, and the presence of a catalytic current in the presence of CO_2 (Figure 36, Table 18).

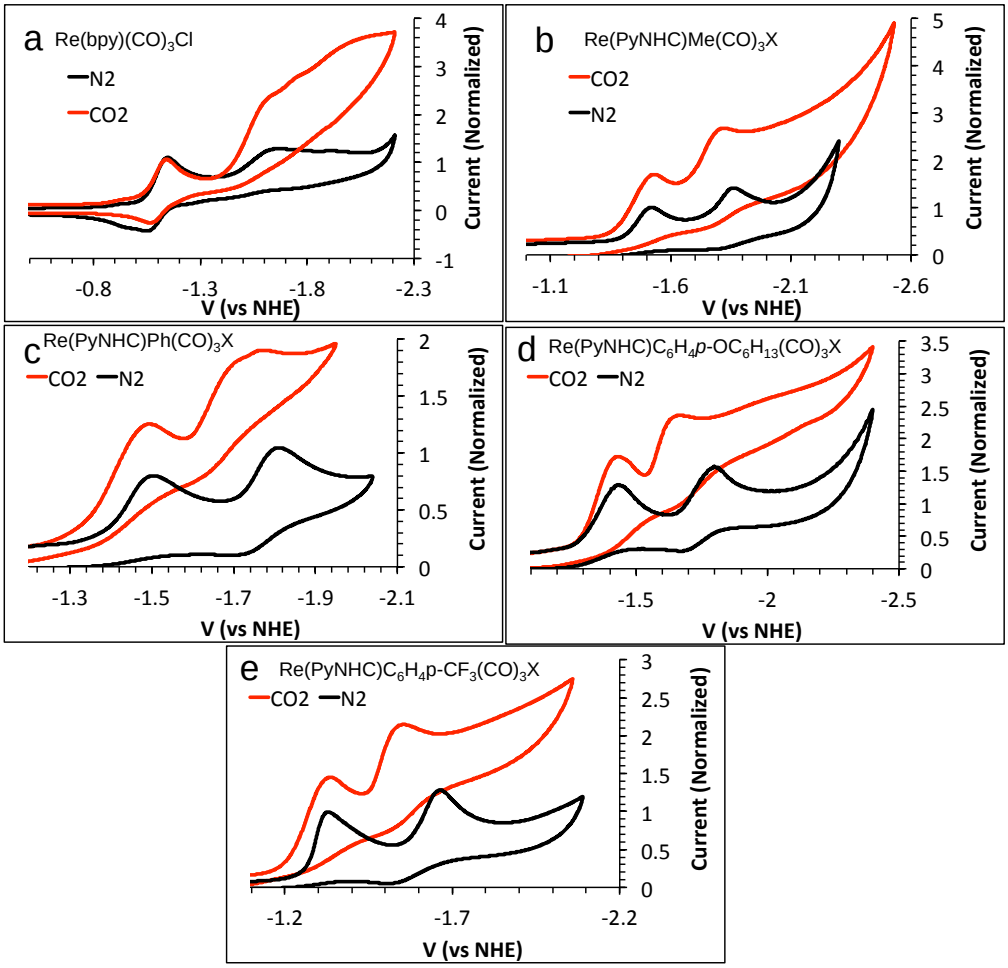

Figure 36. CV data of complexes **50-54** (a-e) in the presence of N_2 (black) and CO_2 (red). Spectrum taken in 0.1 M NBu_4PF_6 in MeCN using Pt reference, Pt counter, and glassy carbon disk working electrodes at a scan rate of 100 mV/s. Spectra were referenced to an internal standard, ferrocence (Fc) using a value of Fc/Fc^+ = 0.4 V *vs*. saturated calomel electrode (SCE) and SCE = 0.24 V *vs*. NHE.[97]

Upon dissolving complex **54** in acetonitrile (MeCN) under an atmosphere of N_2, two irreversible reductions at -1.33 V and -1.76 V *vs*. normal hydrogen electrode (NHE) were observed. The first reduction potentials were 430-250 mV higher in energy for the NHC-Re complexes than **50** under the same conditions (Table 18). The oxidation and reduction potentials observed for **51**-**54** are irreversible and likely metal centered.[119d] Upon exchanging the atmosphere for CO_2 by vigorous bubbling for 15 min, a slight catalytic current increase was observed in the first reduction wave with a larger current increase and anodic shift of the second wave (Figure 36).

Table 18. Electrochemical Properties of Catalysts 1-5.[a]

Catalyst	$E_{(S^+/S)}$ (V)[b]	$E_{(S^-/S)}$ (V)[b]	$E_{(S^-/S^*)}$ (V)[c]
50	1.64	-1.08	1.68
51	1.60	-1.41	1.48
52	1.53	-1.38	1.55
53	1.53	-1.30	1.62
54	1.63	-1.26	1.60
PS[d]	1.01	-1.95	0.43

[a]: Measured in acetonitrile. All values are reported versus NHE. [b]: Values were measured by CV in 0.1M NBu_4PF_6 in MeCN using a Pt reference, Pt counter, and glassy carbon working electrode. Values were measured at the onset of reduction for the irreversible waves. [c]: Taken as the difference in the reduction potential and E_{gopt} via the equation: $E_{S-/S^*} = E_{S-/S} + E_{gopt}$. λ_{onset} was converted to E_{gopt} through the equation $1240/\lambda_{onset} = E_{gopt}$. [d]: PS = *fac*-$Ir(ppy)_3$.

The optical data for complexes **50-54** is compiled in Table 19. The UV/Vis absorption data for the Re complexes indicates that in all cases the Re(PyrNHC) complexes absorb into the visible spectrum and the absorption onset (λ_{onset}) values are blue-shifted relative to Re(bpy) complex **50.** Varying NHC-substituents had minimal effect on λ_{onset} values or on the molar absortivity (ε), the $\lambda_{emission}$ was strongly affected, however (Figure 37). Two emission bands were observed for each complex (505 and 444 nm), and the intensity of the more red-shifted peak increased from complex **51-54** (Figure 37)

Table 19. Optical Properties of Catalysts **50**-**54**.[a]

Catalyst	λ_{max} (nm)	λ_{onset} (nm)[b]	ε ($M^{-1}cm^{-1}$)	λ_{em} (nm)[c]	$E_{0\text{-}0\ (eV)}$[d]
50	370[e]	450[e]	2890[e]	580[e]	2.64[e]
51	358, 402 (sh)	429	4850	444, 505 (sh)	2.98
52	354, 400 (sh)	423	4750	444, 505	2.94
53	351, 402 (sh)	424	4600	444, 505	2.98
54	356, 404 (sh)	433	4800	444, 505	3.05
PS	400, 500 (sh)[f]	520[f]	10,000[f]	540[f]	2.43[f]

[a]: Measured in acetonitrile. sh = shoulder. [b]: Taken from the intercept of the baseline and a tangent line on the absorption spectrum on the low energy side of the longest wavelength transition. [c]: Measured in MeCN using 390 nm excitation wavelength. [d]: Taken as the energy (eV) of the intercept of the absorption and emission curves. [e]: Taken from Ref. 117d. [f]: Taken from Ref. 122b.

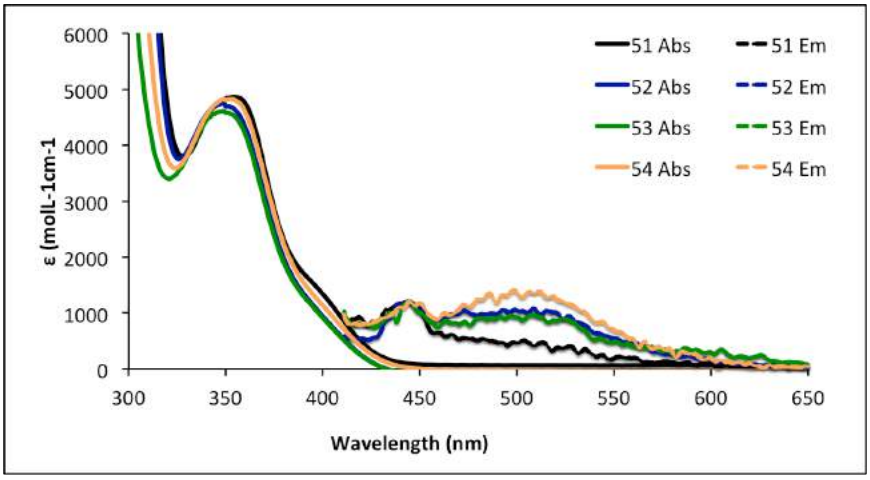

Figure 37. UV-Vis Absorption and emission spectra for complexes **50-54.**

Complexes **51-54** have excited-state reduction potentials ($E_{(S-/S^*)}$, taken as the difference in the reduction potential and the optical band gap) ranging from 1.37 to 1.51 V *vs.* NHE (Figure 38). These are all suitable for the two electron reduction of CO_2 to CO in MeCN by more than 800 mV. BIH is a much stronger electron donor that TEA with an oxidation potential over 500 mV higher in energy. Furthermore, the BIH oxidation potential is considerably closer in energy (ΔG_{red} = -110 mV) than the excited state reduction potential of *fac*-Ir(ppy)$_3$, which allows for much more efficient access to the PS●- state, which accounts for the increase in catalyst performance using the PS with BIH and no reaction with TEA only (ΔG_{red} = -630 mV).

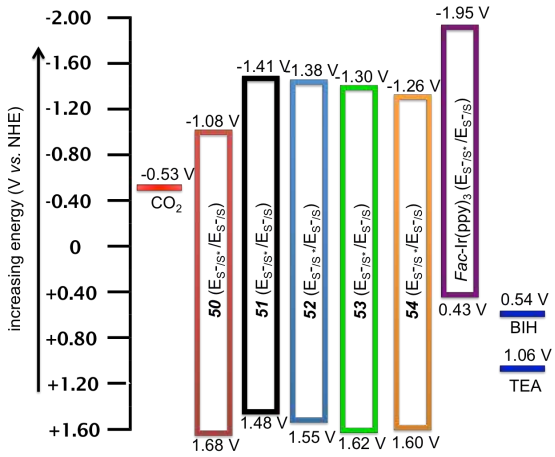

Figure 38. Bandgap diagram depicting the excited state oxidation potential ($E_{S^{-}/S^{*}}$) and OER state ($E_{S/S^{-}}$) of complexes **50-54**, and the PS. Both values were measured by CV in 0.1M NBu_4PF_6 in MeCN using a Pt reference, Pt counter, and glassy carbon disk working electrode. The TEA ($E_{S^{+}/S}$) was taken as the onset of oxidation.

Once the reduction potentials were found to be positioned favorably and the complexes were observed to absorb visible light, for CO_2 reduction, we evaluated complexes **51-54** as catalysts in the photocatalytic reduction of CO_2 with *fac*-Ir(tpy) *using an AM1.5 solar simulated light source* to approximate a practical reduction. Typically photocatalytic reactions operate with cutoff filters to reduce UV and near-IR energy with varying visible light power intensities. As illustrated in Figure 1 (Table 20), the $Re(PyNHC)(CO)_3X$ complexes **51-54** were found to function as CO_2 reduction catalysts, with catalysts **51** (NHC-Me) and **54** (NHC-$PhCF_3$) performing comparably (10 TON) and at higher TONs (15) than standard catalyst **50** (13 TON), respectively.

Table 20. Comparison of Catalyst Performance at One Hour.

entry[a]	catalyst	µmol CO	TON
1	51	2.0	10
2	52	0.93	5
3	53	1.18	6
4	54	2.57	13
5[b]	54	3.03	15
6	50	2.56	13

[a]: 0.2 µmol catalyst/2 mL 10% TEA:MeCN solution with 0.2 µmol *fac*-Ir(ppy)3 and 0.2 mmol BIH. Solutions irradiated for 1 hour after vigorous bubbling with CO2 for 15 minutes with a solar simulator (125 W Xe lamp, AM1.5 filter). Each data point is the average of two runs. [b]: Catalyst was irradiated for 4 hours.

Towards the aim of natural light driven photocatalysis, we utilized AM 1.5 spectrum-simulating filters on a 150 W Xe lamp with our reaction positioned 10 cm from the light source. As illustrated in Figure 35 (Table 20), the Re(PyNHC)$(CO)_3$Cl complexes **51-54** were found to function as CO_2 reduction catalysts, with catalysts **51** (NHC-Me) and **54** (NHC-PhCF_3) performing comparably (10 TON) and at higher TONs (15) than standard catalyst **50** (13 TON), respectively.

All catalysts were found to halt CO production after 1 hour of irradiation except catalysts **51** and **54** which increased CO production for 2 and 4 hours, respectively. Phenyl substituted catalyst **52** and electron donated hexyloxyphenyl substituted catalyst **53** performed at the lowest TONs and turnover frequencies (TOFs). The evaluation of each reaction component on the performance of catalyst **54** is reported in Table 21.

Table 21. Experimental Optimization.

entry[a]	cat	PS[b]	e⁻ donor	µmol CO (TON)
1	54	Yes	TEA, BIH	2.6 (13)
2	54	Yes	TEA	0.04 (0.2)
3	**54**	**No**	**TEA, BIH**	**1.5 (7.5)**
4[c]	54	No	TEA, BIH	0.61 (3.1)
5	54	No	TEA	0.11 (0.6)
6[d]	54	Yes	TEA, BIH	0.04 (0.2)
7	-	Yes	TEA, BIH	0 (0)

[a]: 0.2 µmol catalyst in 2 mL 10% TEA:MeCN solution with 0.2 µmol *fac*-Ir(ppy)3 and 0.2 mmol BIH. Solutions irradiated with a K2 filtered (Newport) 500 W Xe lamp in a water cooled emersion well with a merry-go-round apparatus to approximate the solar spectrum. Reactions were irradiated for 4 hours after vigorous bubbling with CO2 for 15 min. Each data point is the average of two runs. [b]: PS = *fac*-Ir(ppy)3. [c]: Rigorously anhydrous conditions. [d]: Nitrogen atmosphere

The effect of removing the strong electron donor material BIH is remarkable (13 TON with BIH *vs*. 0.2 TON without BIH, Entries 1 & 2).[123] The removal of the PS did not stop catalytic performance of **54** (13 TON *vs*. 11 TON, Entries 1 & 3). *Surprisingly, catalyst **54** is able to efficiently reduce CO_2 without a PS*. Rigorously anhydrous solvents are frequently utilized with complex **50**; however these conditions led to a *decrease* in catalytic performance with **54** (13 *vs*. 3 TON, Entries 1 & 4). Control experiments (Entries 5-7) for removal of PS and BIH, removal of CO_2, and removal of catalyst all led to no appreciable CO formation.

Synthetically turning the monstrously abundant CO_2 into synthetic fuel would prove an immensely useful way to repurpose an underutilized waste from combustion. Because the sun offers far more than enough solar energy to accommodate this goal, photocatalytic reduction of CO_2 could be one way to sustainably reduce atmospheric CO_2 concentration. We aimed to

improve Re(I) pyridyl-based photocatalysts by utilizing a photosensitizer, *fac*-Ir(ppy)$_3$, in order to take the light absorbing burden from the catalyst, and by improving catalyst stability to air and H_2O by substituting a pyridine for an NHC ligand. This led to a decrease in light absorption and destabilization of each complex's reduction potential, however, the potentials of each complex were still positioned correctly. Each of the catalysts performed as CO_2 reduction catalysts in the presence of the PS and the strong electron donor BIH. Catalyst **54** performed comparably to Re(bpy) complex **50** in each set of reaction conditions, and was found to lose less of its initial activity over 4h than complex **50**. Both complexes **54** and **50** reached good TON of (13 for **50** and 15 for **54**) with PS and BIH. Complex **54** attained good TON with no PS, making Re(PyNHC)(CO)$_3$Cl just the fourth series of catalysts capable of unsensitized CO_2 photocatalytic reduction. It is important to note that the TON observed for each catalyst was obtained without rigorous drying of solvents. Rigorously anhydrous solvents lowered the observed TON to 3 in the same time frame. Studies to further catalyst improvement, electron donor optimization, and additive inclusion are currently ongoing.

EXPERIMENTAL SECTION

See Chapter 1, Section 1 for General Experimental Considerations

fac-{2,2'bipyridyl}tricarbonylchlororhenium(I) (**50).**[124] A flame dried flask equipped with a stirbar and reflux condenser was charged with 2,2'-bipyridine (0.108g, 0.69 mmol), chlororhenium (I) pentacarbonyl (0.250 g, 0.69 mmol) and dry, degassed toluene (35 mL). The reaction mixture was then warmed to reflux and allowed to stir. After 2h, the reaction mixture was cooled, concentrated using a rotary evaporator, and the yellow solid triturated with *hot*

hexanes (3 x 19 mL). The solid was dried to yield a fluffy yellow powder (0.290g, 91%). %). ^{1}H NMR (500 MHz, $CDCl_3$) d 9.09 (d, *J* = 5 Hz, 2H), 8.21 (d, J = 7 Hz, 2H), 8.10 (dt, J = 7, 1.5 Hz, 2H), 7.56 (t, J = 7 Hz, 2H).

Synthetic Procedures to Reach Complex **51**

2-(imidazol-1-yl)pyridine (**55**).[125] A flask equipped with a stirbar and reflux condenser was charged with imidazole (1.96 g, 28.8 mmol), K_2CO_3 (7.95 g, 57.5 mmol), 2-bromopyridine (5 g, 3.02 mL, 31.6 mmol), $Cu(OAc)_2$ H $_2$O (1.96 g, 1.44 mmol), TMEDA (0.50 g, 0.65 mL, 4.31 mmol), and DMF (25 mL). The reaction mixture was then warmed to DMF reflux, allowed to stir, and monitored by TLC. After 16h, the reaction mixture was cooled to rt, filtered and diluted with EtOAc (50 mL). The crude product mixture was washed with H_2O (1 x 50 mL), Brine (5 x 50 mL), dried with $MgSO_4$ and concentrated to give a red oil (2.68 g, 68% yield. ^{1}H NMR (300 MHz, $CDCl_3$) d 8.50 (d, *J* = 5.1 Hz, 1H), 7.86 (s, 1H), 7.83 (dt, J = 7.8, 1.8 Hz, 1H), 7.66 (s, 1H), 7.38 (t, J = 7.5 Hz, 1 H), 7.24 (m, 2 H).

2-(3-methylimidazol-1-yl)pyridine iodide (**56**):[126] An Erlenmeyer flask equipped with a stirbar was charged with compound **55** (1.0 g, 6.9 mmol), and Et_2O (15 mL). MeI (0.86 mL, 13.8 mmol) added dropwise, the solution allowed to stir at rt, and monitored by ^{1}H NMR spectroscopy. After 20 h, the reaction mixture was concentrated on a rotary evaporator and the crude product recrystallized from CH_2Cl_2: Et_2O to yield a colorless microcrystalline solid (0.44 g, 25%). ^{1}H

NMR (300 MHz, $CDCl_3$) d 11.9 (s, 1H), 8.51 (m, 2H), 8.26 (d, J = 7.4 Hz, 1H), 8.07 (dt, J = 7.2, 1.5Hz, 1H), 7.49 (t, J = 7.2 Hz, 1H), 7.35 (s, 1H), 4.30 (s, 3H).

fac-{3-methyl-1-(2'-pyridyl)imidazolin-2- ylidene}tricarbonylchlorohenium(I) (**51**):[127] A flame-dried flask equipped with a stirbar and reflux condenser were charged with compound **56** (0.086 g, 0.3 mmol), $Re(CO)_5Cl$ (0.109 g, 0.3 mmol), dry, degassed toluene (5 mL), TEA (0.42 mL, 0.304 g, 3 mmol). The reaction mixture was warmed to reflux, allowed to stir, and monitored by ^1H NMR spectroscopy. After four days, the reaction mixture was concentrated on a rotary evaporator and the crude product subjected to column chromatography using CH_2Cl_2 as eluent. Product fractions were concentrated to yield a pale yellow solid (0.061 g, 39% yield). ^1H NMR (300 MHz, $CDCl_3$) d 8.87 (d, J = 6.3 Hz, 1H), 8.45 (d, J = 2.1 Hz, 1H), 8.27 (m, 2H), 7.70 (d, J = 2.2 Hz, 1H), 7.46 (m, 1H), 3.93 (s, 3H).

Synthetic Procedures to Reach Complex **52**

1-Phenylimidazole (**57**):[128] A flame dried flask equipped with a stir bar was charged with imidazole (1.02 g, 14.96 mmol), bromobenzene (1.12 mL, 1.68 g, 10.68 mmol), dry, degassed DMF (11 mL). Solid CuI (0.41 g, 2.14 mmol) and K_3PO_4 (4.54 g, 21.4 mmol) were added to the flask together in one portion. The reaction mixture was then heated to 100ºC, allowed to stir, and monitored by ^1H NMR spectroscopy. After 40h, the reaction mixture was cooled to rt and diluted with Et_2O (100 mL), washed 3x with H_2O (200 mL), and dried with $MgSO_4$. Once concentrated, the crude product mixture was submitted to column chromatography using 50% Hexanes: 50%

EtOAc eluent. Product fractions were concentrated to give a pale yellow oil (0.24 g, 26%). ^{1}H NMR (500 MHz, $CDCl_3$) d 7.87 (s, 1H), 7.49 (apt, J = 7.5 Hz, 2H), 7.41-7.36 (m, 3H), 7.30 (s, 1H), 7.22 (s, 1H).

2-(3-phenylimidazol-1-yl)pyridine bromide (**58**):[129] A sealable tube was charged with compound **57** (0.24 g, 1.68 mmol), 2-bromopyridine (0.32 mL, 0.53 g, 3.35 mmol), heated to 175ºC *under* N_2 and monitored by ^{1}H NMR spectroscopy. After 14h, the reaction mixture was cooled to rt, at which time a ppt formed. The tube's contents were dissolved in dichloromethane and the product precipitated using Et_2O as a pale brown microcrystalline solid (0.270 g, 53%). ^{1}H NMR (500 MHz, d_6-DMSO) d 10.58 (s, 1H), 8.74 (s, 1H), 8.71 (d, J = 3 Hz, 1H), 8.27 (t, J = 5 Hz, 1H), 8.15 (d, J = 7.4 Hz, 1 H), 7.94 (d, J = 7.5 Hz, 2H), 7.73-7.69 (m, 3H), 7.65 (t, J = 7.4 Hz, 1H).

fac-{3-phenyl-1-(2'-pyridyl)imidazolin-2- ylidene}tricarbonylchlororhenium(I) (**52**):[127] A flame-dried flask equipped with a stirbar and reflux condenser were charged with compound **58** (0.10 g, 0.33 mmol), $Re(CO)_5Cl$ (0.12 g, 0.33 mmol), dry, degassed toluene (5 mL), TEA (0.46 mL, 0.33 g, 3.3 mmol). The reaction mixture was warmed to reflux, allowed to stir, and monitored by ^{1}H NMR spectroscopy. After 20h, the reaction mixture was concentrated on a rotary evaporator and the crude product precipitated from DCM to yield a pale yellow solid (0.144 g, 83% yield). ^{1}H NMR (500 MHz, d_6-DMSO) d 8.81 (s, 1H), 8.69 (s, 1H), 8.37 (s, 2H), 8.0 (s, 1H), 7.71-7.75 (m, 6H).

Synthetic Procedures to Reach Complex **53**

1-bromo-4-hexyloxybenzene (***59***):[130] A flask equipped with a stirbar and reflux condenser was charged with 4-bromophenol (37 g, 214 mmol), K_2CO_3 (45 g, 321 mmol), Hexyl bromide (33 mL, 235 mmol) and DMF (200 mL). The mixture was allowed to stir at 100ºC and monitored by TLC. After 16h, the reaction mixture was cooled to rt and diluted with Et_2O (400 mL), washed sequentially with 10% K_2CO_3 (w/w, 150 mL), H_2O (2 x 100 mL), brine (2 x 150 mL), dried with $MgSO_4$, and concentrated. The crude product was then passed through 400 mL silica plug using hexanes and concentrated to yield a colorless oil (44 g, 80%). ^{1}H NMR (300 MHz $CDCl_3$) d 7.36 (d, J = 6.9 Hz, 2H), 6.77 (d, J = 6.8 Hz, 2H), 3.91 (t, J = 6.6 Hz, 2H), 1.74 (m, 2H), 1.47 (m, 2H), 1.33 (m, 4H), 0.93 (t, J = 6.1 Hz, 3H).

1-(4-hexyloxybenzene)imidazole (**60**):[131] A flame dried flask equipped with a stir bar was charged with imidazole (1.02 g, 14.96 mmol), compound **59** (2.38 g, 10.68 mmol), dry, degassed DMF (11 mL). Solid CuI (0.41 g, 2.14 mmol) and K_3PO_4 (4.54 g, 21.4 mmol) were added to the flask together in one portion. The reaction mixture was then heated to 130ºC, allowed to stir, and monitored by ^{1}H NMR spectroscopy. After 20h, the reaction mixture was cooled to rt and diluted with Et_2O (100 mL), washed 3x with H_2O (200 mL), and dried with $MgSO_4$. Once concentrated, the crude product mixture was passed through a short plug of silica using first 50% Hexanes: 50% Et_2O eluent, then EtOAc to elute pdt. Product fractions were concentrated to give a pale yellow oil (1.44 g, 64%). ^{1}H NMR (500 MHz, $CDCl_3$) d 7.75 (s, 1H), 7.28 (d, J = 8.5 Hz, 2H),

7.20 (s, 1H), 7.19 (s, 1H), 6.97 (d, J = 8.6 Hz, 2H), 3.90 (t, J = 7 Hz, 2H), 1.79 (m, 2H), 1.48 (m, 2H), 1.36 (m, 4H), 0.92 (t, J = 6.8 Hz, 3H).

2-(3-(4-hexyloxyphenyl)imidazol-1-yl)pyridine bromide(**61**):[130] A sealable tube was charged with compound **60** (0.5 g, 2.38 mmol), 2-bromopyridine (0.45 mL, 0.75 g, 4.76 mmol), heated to 175ºC *under* N_2, and monitored by ^{1}H NMR spectroscopy. After 6 h, the reaction mixture was cooled to rt, at which time a ppt formed. The tube's contents were dissolved in dichloromethane and the product precipitated using Et_2O as a pale brown microcrystalline solid (0.293 g, 33%). IR (neat, cm^{-1}): 3134.4, 2930.9, 2857.3, 1598.2, 1542.3, 1255.1, 1186.9, 825.3, 778.4. ^{1}H NMR (500 MHz, $CDCl_3$) d 11.8 (s, 1H), 9.2 (d, J = 8 Hz, 1H), 8.51 (s, 2H), 8.09 (t, J = 7.7 Hz, 1H), 8.0 (d, J = 8.5 Hz, 2 H), 7.79 (s, 1H), 7.47 (t, J = 10 Hz, 1H), 7.05 (d, J = 8 Hz, 2H), 3.96 (t, J = 6 Hz, 2H), 1.77 (m, 2H), 1.44 (m, 2H), 1.34 (m, 4H), 0.91 (t, J = 6.4 Hz, 3H).

fac-{3-(4-hexyloxyphenyl)-1-(2'-pyridyl)imidazolin-2-ylidene}tricarbonylchlororhenium(I) (**53**):[127] A flame-dried flask equipped with a stirbar and reflux condenser were charged with compound **61** (0.10 g, 0.27 mmol), $Re(CO)_5Cl$ (0.097 g, 0.27 mmol), dry, degassed toluene (5 mL), TEA (0.38 mL, 0.27 g, 2.7 mmol). The reaction mixture was warmed to reflux, allowed to stir, and monitored by ^{1}H NMR spectroscopy. After 20h, the reaction mixture was concentrated on a rotary evaporator and the crude product precipitated from DCM to yield a pale yellow solid (0.10 g, 59% yield). IR (neat, cm^{-1}): 3133.4, 29321, 2015.7, 1918.0, 1888.2, 1543.8, 1488.1, 1248.2, 772.9. ^{1}H NMR (500 MHz, $CDCl_3$) d 8.81 (s, 1H), 8.95 (d, J = 4.5 Hz, 1H), 8.06 (apq, J

= 6.5 Hz, 1H), 7.69 (s, 1H), 7.62 (d, J = 8 Hz, 1H), 7.58-7.56 (m, 2H), 7.33 (apq, J = 8 Hz, 1H), 7.05 (d, J = 8.4 Hz, 2H), 4.02 (t, J = 7.6 Hz, 2H), 1.81 (m, 2H), 1.45 (m, 2H), 1.35 (m, 4H), 0.92 (t, J = 6.8 Hz, 3H).

Synthetic Procedures to Reach Complex **54**

2-(3-(4-trifluoromethylphenyl)imidazol-1-yl)pyridine bromide (**62**):[130] A sealable tube was charged with 1-(4-trifluorophenyl)imidazole (0.5 g, 2.35 mmol), 2-bromopyridine (0.41 mL, 0.72 g, 4.7 mmol), heated to 175ºC *under* N_2, and monitored by ^{1}H NMR spectroscopy. After 3 days, the reaction mixture was cooled to rt, at which time a ppt formed. The tube's contents were dissolved in dichloromethane and the product precipitated using Et_2O as a pale brown microcrystalline solid (0.270 g, 53%). IR (neat, cm^{-1}): 3058.9, 3022.7, 1547.1, 1134.2, 8371, 779.7. ^{1}H NMR (500 MHz, DMSO) d 10.75 (s, 1H), 8.79 (s, 1H), 8.72 (d, J = 4.1 Hz, 1H), 8.68 (s, 1H), 8.3 (t, J = 8.2 Hz, 1H), 8.23-8.20 (m, 3H), 8.14 (d, J = 8.2 Hz, 2H), 7.71 (t, J = 7.6 Hz, 1H). ^{13}C NMR (500 MHz, DMSO) d 149.3, 146.2, 140.7, 137.7, 134.9, 130.1, 127.4, 125.6, 124.7, 123.3, 122.5, 122.3, 120.1, 114.8.

fac-{3-(4-trifluoromethylphenyl)-1-(2'-pyridyl)imidazolin-2-ylidene}tricarbonylchlororhenium(I) (**54**):[127] A flame-dried flask equipped with a stirbar and reflux condenser were charged with compound **62** (0.11 g, 0.3 mmol), $Re(CO)_5Cl$ (0.11 g, 0.3 mmol), dry, degassed toluene (5 mL), TEA (0.42 mL, 0.30 g, 3.0 mmol). The reaction mixture was warmed to reflux, allowed to stir, and monitored by ^{1}H NMR spectroscopy. After 4 days, the

reaction mixture was concentrated on a rotary evaporator and the crude product submitted to column chromatography using CH_2Cl_2/acetone as eluent. Product fractions washed with H_2O (3 x 25 mL), dried with $MgSO_4$, and concentrated to yield a pale yellow solid (0.073 g, 33% yield). IR (neat, cm^{-1}): 2089.1, 2924.1, 2017.8, 1919.2, 1890.2, 1487.4, 1323.1, 774.1. ^{1}H NMR (500 MHz, d_6-DMSO) d 8.89 (d, zj = 5.4 Hz,1H), 8.73 (d, J = 2.3 Hz, 1H), 8.39 (d, J = 3.5 Hz, 2H), 8.06 (m, 3H), 7.94 (d, J = 8.3 Hz, 2H), 7.58 (apq, J = 5.3 Hz, 1H).

Synthetic Route to Donor Compound **BIH**

*1,3-dimethyl-2-phenylbenzimidazolium iodide (***63***):*[132] A sealable tube equipped with a stirbar was charged with 2-phenylbenzimidazole (2.50 g, 12.97 mmol), MeI (4 mL, 9.14 g, 64.36 mmol), MeCN (15 mL) and allowed to stir at 100ºC, and was monitored by TLC. After 2 days, the reaction mixture was concentrated and the crude product passed through a short silica plug using acetone. Concentrated crude product to ½ volume, then cooled to 0ºC. After 16h, the mixture was filtered to yield a white microscrystalline solid (1.31g, 29%). ^{1}H NMR (500 MHz $CDCl_3$) d 8.07 (d, J = 8.07 Hz, 2h), 7.79-7.71 (m, 7H), 4.03 (s, 6H).

*1,3-dimethyl-2-phenyl-2,3-dihydro-1H-benzo[d]imidazole (***BIH***)*:[132] A flask was charged with compound **14** (1.31 g, 4.78 mmol) and MeOH (50 mL) and cooled to 0ºC. Once cool, $NaBH_4$ (0.27 g, 7.17 mmol) added and the reaction mixture allowed to warm to room temperature and monitored by ^{1}H NMR spectroscopy. After 1h, MeOH (50 mL) and H_2O (100 mL) added, at which time a white precipitate formed. The precipitate was collected, dissolved in CH_2Cl_2,

washed with 1:1 H_2O:MeOH, and concentrated to yield a fluffy white solid (0.40 g, 57%). ^1H NMR (500 MHz, d_6-DMSO) d 7.54 (d, J = 5.5 Hz, 2H), 7.44 (d, J = 5 Hz, 3H), 6.61 (s, 2H), 6.44 (s, 2H), 4.87 (s, 1H), 2.48 (s, 6H).

SECTION 2. SYNTHESIS OF CR-PICOLINATE COMPLEXES FOR THE HOMOGENEOUS CATALYTIC PRODUCTION OF METHANOL FROM CO_2.

The electrocatalytic reduction of CO_2 has been known since the 1970's, and many catalysts have been reported to effect the formation of many products (including CO, CO_2H_2, HO_2CCO2H, CH_4, MeOH) from CO_2.[109, 110-115] In each of these instances, energy comes from electron transfer from the cathode surface to the catalyst (either on the surface or near the surface). While CO_2 can be reduced to CO_2H_2 at -1.97 V (vs NHE in DMF), this energy is very high. Because the kinetic barriers to other reduced products are prohibitively high, a catalyst must be used. The energy gain from lowering the activation energy often comes with the trade-off of an overpotential (the potential difference in the standard reduction potential and the observed reduction potential), which increases the potential needed to effect reduction.

Based upon the recent local proton source work of Savéant and Robert[113b,116b] in conjunction with reports of Group 6 metals coordinating carbonyl compounds, we reasoned that an electron deficient Cr^{III} center with a ligand capable of forming hydrogen bonds near the metal could be promising CO_2 reduction catalysts.[133] We have improved upon the synthesis of the 2,6-pyridinedipicolinate (abbreviated *dipic*) complex $[Cr(dipic)_2]Na$, **64**, and have evaluated the electrocatalytic activity of the complex towards CO_2.

While previous reports of Cr picolinate syntheses were on small scale and relied upon weeks of crystallization,[134] we improved the synthesis to be completed within a matter of hours instead. We were able to obtain the pure dark purple $[Cr(bispic)_2]Na$ complex (0.50 g) **64** in the span of a few hours (workup included). Cyclic voltammagrams of complex **64** in DMF are shown in

Figure 39. Two reversible reduction waves were observed under N_2 at -1.05 V vs. NHE and -1.42 V vs NHE. The first reduction is ligand-centered, while the second is metal-centered, as described previously.[134] Upon bubbling with CO_2 for 15 min, the second reduction wave exhibited a catalytic current, with the reversibility of each wave reduced substantially, as would be expected for CO_2 reduction. Upon addition of H_2O, both waves shift anodically, while the magnitude of the second reduction wave remained larger than under N_2. Each change in the CV spectrum listed here indicates catalytic CO_2 reduction by Cr complex **64**.

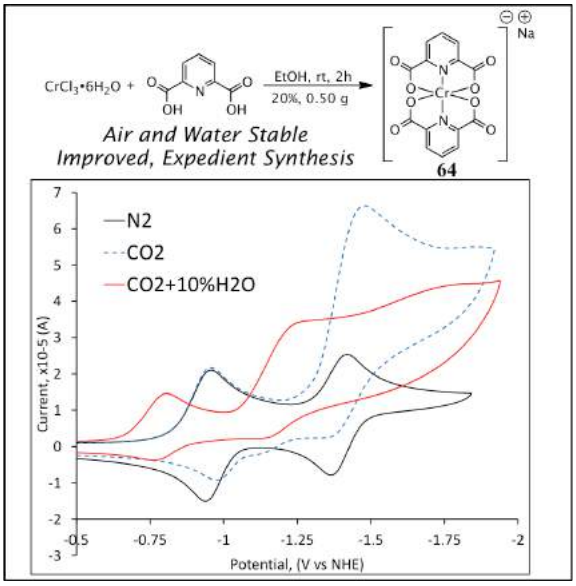

Figure 39. *Left: Top*: Synthesis of Cr complex **64**. *Bottom*: CV of **64** under N_2 (black), CO_2 (blue dash), and CO_2 with 10% H_2O added (red) in DMF with 0.1M NBu_4PF_6 supporting electrolyte and a scan rate of 100 mV/s, starting negative. Ferrocene was used as internal standard and referenced to NHE using the value Fc/Fc^+ = 0.69V vs. NHE as reported by Connelly and Geiger.[97] The saturated Calomel Electrode (SCE) is taken as 0.24 V vs NHE. CV was measured using Pt counter, Pt reference, glassy carbon working electrode.

Because complex **64** exhibited a catalytic current with CO_2 (See Figure 39) controlled-potential electrolyses were performed to assess the catalytic rate and selectivity of complex **64**. Electrolyses were performed at potentials more negative than the observed onset of catalysis in CV and the product selectivity at each potential evaluated. Electrolysis of a 2.5 mM solution of complex **64** dissolved in 0.1M NBu_4PF_6 in anhydrous DMF -1.79 V (vs NHE) (as determined by CV under N_2 and CO_2 directly prior to electrolysis) produced no CO or HCOOH. Upon electrolysis at -1.7 V vs NHE after the addition of 10% H_2O (5.5 M), the section of the purple solution nearest to the RVC working electrode turned brown-orange. After ceasing the electrolysis at 1h, the discolored section regained its original purple appearance, however, the CV of this solution appeared to contain substantially less (~20% of the original) of complex **64**. Longer electrolyses (8h), led to a more persistent yellow color change, however, over time the solution regained its previous purple color. Unfortunately, no reduction products have been observed from any electrolysis and efforts to detect methanol are currently underway.

Regarding the observed color change observed during DMF/H_2O electrolysis, we suspect that the dipicolinate ligand becomes more freely dissociated from the Cr^{III} metal center upon the first reduction. Direct observations of ligand substitution in Cr picolinate and polypyridine complexes has been observed by us in the course of this investigation and by others in the synthesis of mixed picolinate complexes, such as Cr(dipic)(phen)Cl.[134] As $Cr(dipic)_2$ is coordinately saturated, it is likely that the active species is a Cr complex that has undergone a ligand dissociation, with the vacant coordination positions taken by solvent. We attempted to synthesize coordinatively unsaturated Cr dipicolinate complexes, however, upon electrolysis, the complexes

reverted to the $Cr(dipic)_2$ form, which was also observed before (Figure 40).[125] A complex based on imidazole-2-carboxylate did not result in a complex that was stable enough to assess as a CO_2 reduction catalyst. The only other complex we synthesized that did not result in the formation of complex **64** upon dissolution or reduction was complex **65**, which did not include a bis-picolinate ligand.

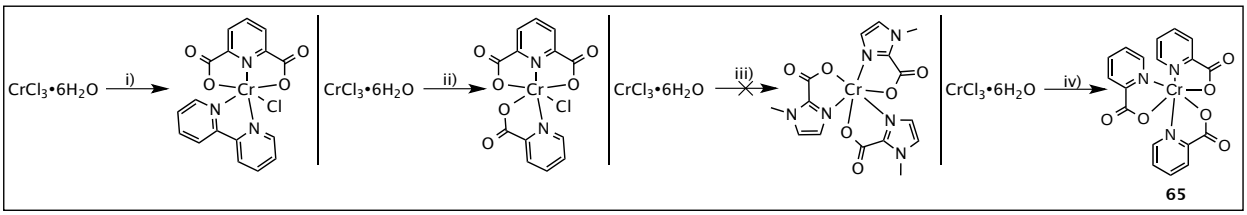

Figure 40. The synthesis of other Cr picolinate complexes.

We next sought to investigate the propensity for complex **64** to function as a photocatalyst for CO_2 reduction. As reported previously,[134] complex **64** absorbs visible light up to 650 nm. Emission at 440, 470, and 500 nm was observed upon excitation at 400 nm, with τ_0 = 3 ns (Figure 41). Upon addition of triethylamine (TEA) to complex **64** in degassed MeCN, the emission was quenched ($k_q = 1.3 \times 10^{10}$ $Lmol^{-1}s^{-1}$, Figure 41), which indicated that **64*** could be reduced by TEA to **64●$^-$**. Unfortunately, exhaustive attempts to apply complex **64** towards CO_2 photoreduction in a veriety of solvents (DMF, DMA, MeCN, H2O) failed to yield CO or CO_2H_2. Attempts to incorporate commonly used transition metal photosensitizers ($Ir(ppy)_3$ or $Ru(bpy)_3$), strong organic photosensitizers (perylene, phenanthrene, pyrene) or strong electron donor material 1,3-dimethyl-2-phenyl-2,3-dihydro-1H-benzo[d]imidazole (BIH) also resulted in no CO or CO_2H_2 formation however, the production of methanol has not been excluded yet.

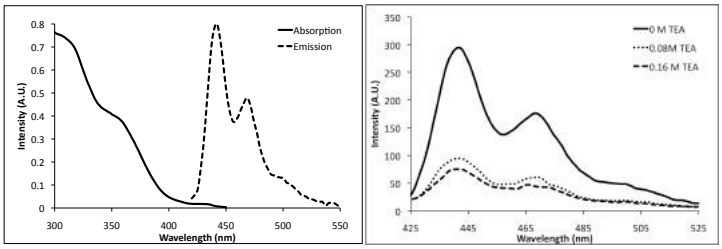

Figure 41. *Left*: Absorption and Emission of complex **64** in MeCN. *Right*: Emission quenching of complex **64** using TEA as quencher.

EXPERIMENTAL SECTION

General Considerations: All commercial reagents were purchased and used as received. Unless otherwise noted, all experiments were carried out under a N_2 atmosphere. Before each measurement involving change of atmosphere, each solution was bubbled with the new gas for at least 15 minutes. After each electrolysis, the electrode was cleaned by electrolysis at +1.0 V vs NHE for 20 min. CV measurements were made using a glassy carbon disk working electrode, a Pt counter and Pt reference, with Ferrocene used as internal reference. For controlled potential electrolyses were performed with 30 ppi RVC working electrode (Duocel), Pt counter and Pt reference. Cyclic voltammograms were measured and controlled potential electrolyses were performed with a C–H Instruments electrochemical analyser. UV–Vis spectra were measured with a Cary 5000 UV–Vis spectrometer. Headspace analysis was performed using a gastight syringe with stopcock and Agilent 7890B Gas Chromatograph (*Column*: Agilent PorapakQ 6 ft, 1/8 O.D.). Quantitation of CO and CH_4 were made using an FID detector, while H_2 was quantified using a TCD detector (all calibrated using standards purchased from BuyCalGas.com). Formic acid analysis was performed by following a previously reported

procedure.14

*Improved Synthesis of [Cr(dipic)$_2$]Na, (**64**):*[134] An Erlenmeyer flask equipped with a stirbar was charged with 2,6-pyridine-dipicolinic acid (1.22g, 1.95 mmol), and $CrCl_3$ hexahydrate (1.0 g, 3.7 mmol). EtOH (150mL, absolute) added and the green solution allowed to stir at room temperature. After 1h, a 0.1M NaOH solution was added dropwise to the dark blue solution until it turned purple. Once the solution had turned purple, Acetone (150 mL) was added and the solution filtered through a 45 μm filter (Airdisk, Target2, Nylon). After filtration, Ethyl ether added until the solution turned just cloudy, after which the suspension was cooled to -78ºC. The resulting purple precipitate was filtered and dried to yield a dark purple powder (20%, 0.50 g). UV-Vis (DMF): λmax = 548 nm (ε = 80 M-1cm-1), λonset = 650 nm. Cyclic Voltammetry (0.1 M Bu4NPF6 in DMF, sweep width 1.0-(-2.0), 0.1 V/s scan rate): Red1 = -0.94 V (vs NHE), Red2 = -1.39 V (vs NHE).

SECTION 3. THE APPLICATION OF AU NANOPARTICLES TOWARDS CO_2 REDUCTION.

Our collaborators in the Dass group are experts in the synthesis and characterization of Au nanoparticles of many sizes and with many different types of ligands.[135] Au nanoparticles have been applied as catalysts in a variety of reactions including oxidations (such as CO to CO_2) and reductions (such as CO_2 to CO).[136] As the nanoparticles have different sizes, shapes, and certainly different electronic and steric environments depending on the chosen ligands, atom distribution, and method of synthesis, each type of nanoparticle is worthy of screening in small molecule catalysis. Specifically in the reaction of gas molecules, each size and particle shape/morphology has unique adsorption characteristics and thus likely different catalytic activities. We were particularly interested in the application of the Dass group's atomically precise Au nanoparticles as catalysts for CO_2 reduction.

Only recently have Au nanoparticles been reported to act as electrocatalysts for CO_2 reduction, starting with a collaborative report led by Kaufman in 2012[137] and followed up by a collaborative effort led by Sun in 2013[138] and a collaboration led by Cuenya in 2014.[139] Kaufman et al. tested different sizes of Au nanoparticles, from Au_{25} to 2 nm and 4 nm particles. The nanoparticles were included as an additive to carbon black inks and painted onto a glassy carbon electrode. The painted electrodes were then used as the working electrode in an electrochemical setup for CO_2 reduction experiments. Kaufman found that the smallest size nanoparticle (which was also protected with thiolate ligands) tested (Au_{25}) gave the most pronounced response to CO_2 and was observed to produce CO and H_2 in a ~100:1 ratio, indicating good selectivity for

CO production (Figure 42). It is worth noting here that all three nanoparticle sizes outperformed bulk Au.[137]

Sun et al. chose to compare 4 nm, 6 nm, 8 nm, and 10 nm Au nanoparticles using a treatment similar to that of Kaufman to prepare the carbon working electrodes. The bare nanoparticles (non-ligated) were suspended in hexane and carbon black added. A paste was made from the mixture and painted onto activated carbon paper support. Instead of increased catalytic activity with smaller sizes, as was observed by Kaufman, Sun et al. noted the 8 nm nanoparticle was the most active due to the high edge-to-surface-area ratio of the nanoparticle, and had moderate selectivity (90:10 CO:H_2) for reduction products (Figure 42).[138]

Cuenya et al. also investigated the correlation between nanoparticle size, CO_2 reduction activity, and selectivity for CO_2 reduction. Bare nanoparticles of five different sizes (1.1, 1.8, 3.2, 4.3, 7.7 nm) were deposited onto glassy carbon support and used as electrocatalysts in CO_2 reduction. While Cuenya et al. also noted a more pronounced activity towards CO_2 reduction for 8 nm particles, they also noted a strong dependence on size and selectivity (Figure 42). With decreasing size, it was observed that H_2 production increased to that even above the selectivity observed when bulk Au foil was used as electrode.[139]

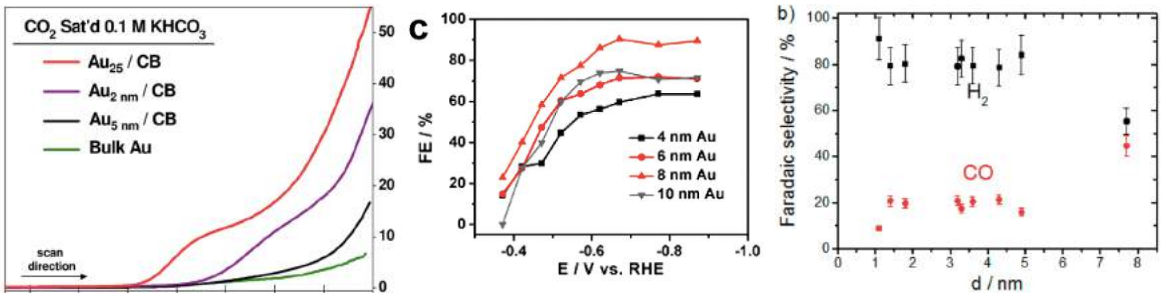

Figure 42. Past reports of Au nanoparticle CO_2 catalysts. *Left:* Illustration of size dependence in "bare" Au nanoparticles and in ligated Au_{25} in the magnitude of catalytic current. X-axis = potential, from 0 to -1.4 V vs RHE, Y-axis = current (mA cm^{-2}). Figure taken from Ref. 137. *Middle*: Illustration of size dependence in "bare" Au nanoparticles in the faradaic efficiency for CO formation. Figure taken from Ref. 138. *Right*: Illustration of size dependence in "bare" Au nanoparticles in the faradaic selectivity for CO and H_2 formation. Figure taken from Ref. 139. Reprinted with permission from Kauffman, D. R.; Alfonso, D.; Matranga, C.; Qian, H.; Jin, R. *J. Am. Chem. Soc.* **2012**, *134*, 10237. Zhu, W.; Michalsky, R.; Metin, Ö.; Lv, H.; Guo, S.; Wright, C. J.; Sun, X.; Peterson, A. A.; Sun, S. *J. Am. Chem. Soc*. **2013**, *135*, 16833.Mistry, H.; Reske, R.; Zeng, Z.; Zhao, Z.-J.; Greeley, J.; Strasser, P.; Cuenya, B. R. *J. Am. Chem. Soc.* **2014**, *136*, 16473. Copyright 2012,2013,2014 American Chemical Society.

Because Kaufman observed them to be superior catalysts, our approach to applying Au nanoparticles in CO_2 reduction was to start by assessing the catalytic current of atomically precise thiolate-ligated nanoparticles under CO_2 atmosphere with CV measurements. We obtained a sample of $Au_{137}(SEtPh)_{56}$ from the Dass group and collected CV measurements under both N_2 and CO_2 (Figure 43). We observed a massive increase in catalytic current in the presence of CO_2, which indicated that the nanoparticles were indeed active towards CO_2. This observation contributed to a collaborative publication in 2014.[115f] Further research into the catalytic activity of these nanoparticles is currently being undertaken in the group, especially the dependence of

nanoparticle size and number of potential binding sites on catalytic activity. Progress has been inhibited due to produt detection method development, which will be discussed later (Section 6).

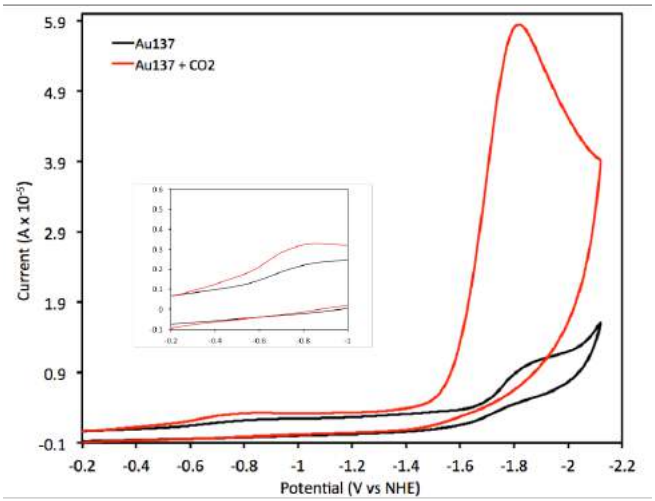

Figure 43. Cyclic voltammograph of $Au_{137}(SEtPh)_{56}$ under N_2 (black) and CO_2 (red) in DMF with 0.1 M Bu_4NPF_6 as electrolyte and a scan rate of 100 mV/s. Ferrocene was used as an internal standard and reference to NHE using the value Fc/Fc^+ = 0.69 vs. NHE reported by Connelly and Geiger.[97] Measured with platinum reference, platinum counter, and glassy carbon working electrode.

SECTION 4. TOWARDS IRON PORYPHYRINS WITH SECONDARY COORDINATION SPHERES TARGETING CO_2.

Transition metal porphyrin complexes are a prinicipal group of chemicals and the group has been applied towards a myriad of applications, including as CO_2 reduction catalysts.[53,109b,140] Iron and Co porphyrins have both been reported to be photo- (UV light) and electrocatalysts for CO_2 reduction;[113a-b,116c] however, the catalytic rate reported in these early papers was low and the TON low as well. Not long before we embarked on this avenue of research and unknown to us, Saveant reported a very efficient porphyrin electrocatalyst for CO_2 reduction that was similar in design to our target porphyrins. The porphyrin was decorated with 2,6-dihydroxybenzene groups at the meso positions (Figure 44) and achieved very high TON, due to the phenol functional groups acting as proton-relays. Upon seeing this result, our synthetic strategy was to synthesize Fe porphyrin complexes that would bear H-bond donor or acceptor groups to achieve the same end (Figure 44). Porphyrins with H-bond donors could potentially act as both proton relays and could help lower the activation energy of CO_2 reduction through precoordinating the gas with H-bonds. H-bond acceptors on the porphyrin ring could hydrogen bond with H_2O to also achieve the same end.

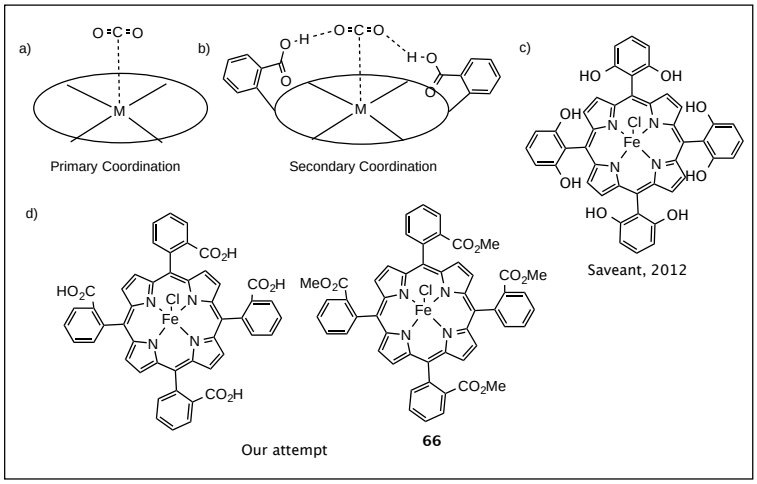

Figure 44. a): Illustrative example of primary CO_2 coordination. b): Illustrative example of secondary coordination of CO_2. c): Porphyrin catalyst reported by Saveant in 2012. d): Our approach to testing the secondary coordination sphere hypothesis.

Our hypothesis was that the inclusion of carboxylic esters to each meso-phenyl group would act as H bond donors and acceptors. Fortuitously, this complex was commercially available. We also planned to test the analogous methyl ester complex **66**, as the ester groups would lack H bond donor capability but retain the H bond accepting capability of the carbonyl. We chose to study the unsubsituted porphyrin as a control. The Fe (III) tetraphenyl and tetra(benzoic acid) porphyrin complexes waere commercially available. Ester **66** was synthesized in two overall steps by first forming the porphyrin ring and then metallating it with Fe (Scheme 11).

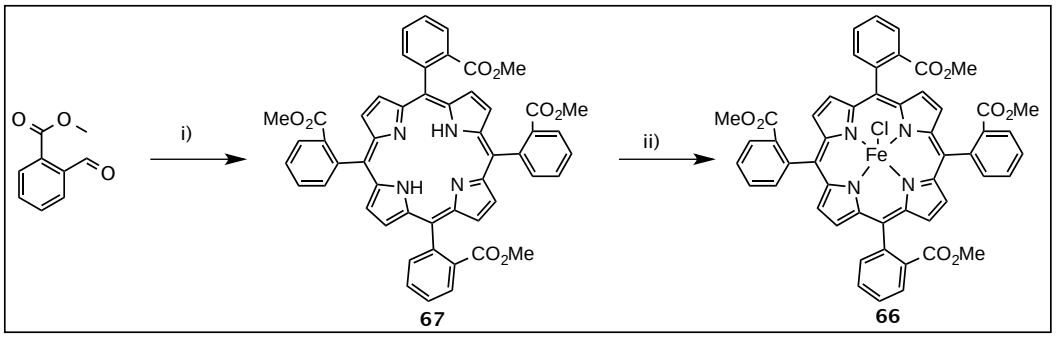

Scheme 11. Synthesis of tetra ester porphyrin **66**. Conditions: i): a: pyrrole, BF_3•OEt_2, $CHCl_3$ b: DDQ, 65ºC, 0.122 g, 14%. ii): $FeCl_2$, THF, reflux, 0.10 g, 90%.

Once all the complexes required were in hand, we set out to the task of determining the energy levels of each reduced state by CV (Table 22). The addition of carboxylic acid groups shifted the reduction potentials more negative for the second and third reductions, while it slightly stabilized the first reduction. Installation of ester groups instead of acid led to less negative second and third reductions but also more positive first reduction values vs NHE.

Table 22. Reduction potentials of the Fe porphyrin complexes tested.[a]

Complex	M^{III}/M^{II}	M^{II}/M^{I}	M^{I}/M^{0}
FeTPPCl	–0.08	–0.83	–1.49
FeTP(CO_2H)PCl	–0.06	–0.90	–1.65
FeTP(CO_2Me)PCl, **66**	–0.02	–0.89	–1.51

[a]:Values were measured by CV in 0.1M NBu_4PF_6 in MeCN using a Pt reference, Pt counter, and glassy carbon working electrode with Fc as internal reference. All values reported vs. NHE.

Thus, the teracarboxylic acid complex and tetra ester were observed to have favorable reduction potentials for CO_2 reduction.

Unfortunately, before we could adequately screen the acid and ester porphyrin catalysts for activity as CO_2 reduction photocatalysts, Robert reported an Fe porphyrin appended with phenol groups at the meso positions that functioned very well as a photocatalyst with a photosensitizer.[116b] The catalyst achieved >100 TON and was photosensitized with inexpensive 9-cyanoanthracene (9-CA). We then chose to forego any further testing with Fe porphyrins, as we wished to spend time developing other catalysts, such as the RePyNHC catalysts described in Part 1 of this chapter.

EXPERIMENTAL SECTION

General Considerations: See Part 1 of this chapter for general considerations.

Synthetic procedures to reach complex 66:

Tetra-meso-(methyl o-carboxyphenyl)porphyrin (67): A flask equipped with a stirbar was charged with methyl-2-carboxylbenzaldehyde (0.49 g, 3 mmol), pyrrole (0.201 g, 3 mmol), $CHCl_3$ (300 mL), and $BF_3{\bullet}OEt_2$ (0.114 mL, 0.6 mmol), all under Ar, and allowed to stir at rt. After 2h, DDQ (0.51 g, 2.25 mmol) added, the reaction heated to 65ºC, allowed to stir, and monitored by TLC. After 1.5 h, TEA (2 mL) added, the reaction mixture concentrated, loaded onto an SiO_2 plug, eluted with 90:10 EtOAc: CH_2Cl_2 and concentrated. Recrystallized from acetone/hexanes to give a dark purple solid (0.122 g, 14%). ^{1}H NMR (300 MHz, $CDCl_3$) δ 8.58 (m, 12 H), 8.36 (m, 4H), 8.17 (m, 4H), 7.86 (m, 8 H), 2.88 (s, 12H), -2.44 (s, 2H).

Chloro-Fe(III) Tetra-*meso*-(methyl o-carboxyphenyl)porphyrin (66): A flame-dried flask equipped with a reflux condenser and stirbar was charged with **67** (0.10 g, 0.12 mmol), $FeCl_2$ (0.15 g, 1.2 mmol), dried and degassed THF (30 mL), heated to reflux, allowed to stir, and

monitored by TLC. Ater 3h, the reaction mixture was cooled to rt and concentrated. The crude product was passed through an SiO_2 plug using 10% MeOH: CH_2Cl_2 to yield a dark purple product (0.10 g, 90%). *Paramagnetic*

SECTION 5. THE DEVELOPMENT OF MORDANT DYES AS CO_2 REDUCTION CATALYSTS.

In Section 7 of Chapter 1, so-called mordant dyes were discussed, as well as their potential application as DSC sensitizers. Because they are strong light absorbers, we chose to also investigate them as possible photocatalysts for CO_2 reduction. Based on our previous studies with Cu mordant dyes (Table 13), the reduction potential of mordant dyes can be favorable for CO_2 reduction. Our strategy, therefore, was to test a single mordant dye complex first, before launching into a large amount of screening and mordant dye synthesis. The dye we chose to synthesize was based on Eriochrome Black T (EBT) because of its three chelating functionalities (Figure 45).

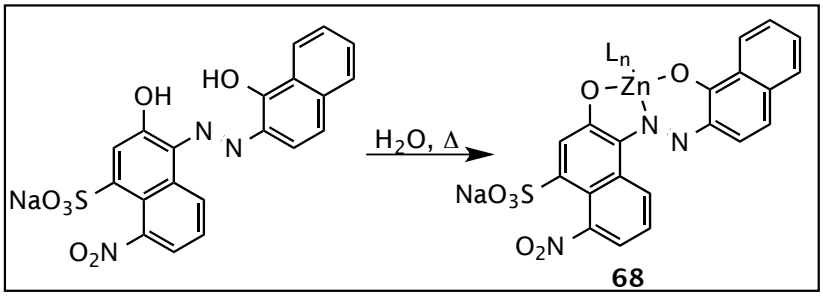

Figure 45. Synthesis of Zn mordant dye **68**.

Upon the synthesis of mordant dye **68**, its energy levels and activity for CO_2 reduction were checked with CV. Zn is a non-redox active metal, therefore, the only reductions which should arise stem from the ligand (Figure 46). We chose ths dye first as a suitable test to ensure any included metal was the important and catalytically active portion of the molecule. As expected, multiple reduction waves are observed at -0.43 V, -1.27 V, and -2.03 V vs NHE for complex **68** under N_2, but unexpectedly, one of the waves increased substantially under CO_2.

Upon collection of this data; however, it became clear that significantly more time would need to be devoted to determining the nature of the current increase. We were embroiled in multiple other (more promising) catalyst screening studies and thus did not collect any more evidence for whether mordant dye **68** reduced CO_2 or what the reduction products were.

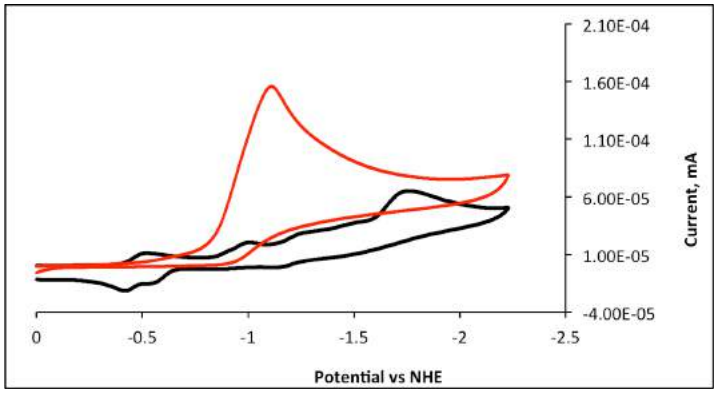

Figure 46. Cyclic voltammograph of mordant dye **68** under N_2 (black) and CO_2 (red) in DMF with 0.1 M Bu_4NPF_6 as electrolyte and a scan rate of 100 mV/s. Ferrocene was used as an internal standard and reference to NHE using the value Fc/Fc^+ = 0.69 vs. NHE reported by Connelly and Geiger.[97] Measured with platinum reference, platinum counter, and glassy carbon working electrode.

EXPERIMENTAL SECTION

See Section 1 of this chapter for General Considerations.

Synthetic Procedures to reach (68)*:*

1:1 Eriochrome Black T : Zn complex (**68**): A flask equipped with a stirbar was charged with Eriochrome Black T (1.0 g, 2.17 mmol), $ZnSO_4$ (0.35 g, 2.17 mmol), H_2O (10 mL), and heated to 100ºC with stirring. After 4h, the reaction mixture was cooled to rt and NaCl (1 g) added. A precipitate formed, was filtered, and was washed with copious H_2O to yield a black solid (0.35 g).

SECTION 6. METHOD DEVELOPMENT FOR THE REDUCTION OF CO_2 AND ANALYTICAL DETECTION OF REDUCTION PRODUCTS.

A key step in catalyst development and reaction optimization is ensuring that the products of a reaction can be accurately and precisely measured once formed (concentrations in the range of <1 turnover number (TON) to levels >1,000 TON). This part of the chapter will focus on the development of reliable reaction parameters for electrochemical and photochemical CO_2 reduction pertaining to everything before and after the chemical reaction occurs (i.e. reaction set-up, general experimental considerations, reaction sampling, and sample analysis). This section is meant to serve as a tutorial for reaction setup and analysis, based on the analytical techniques developed in our lab.

Photochemical Reaction Setup

As is true for any chemical reaction, experiment design is key in CO_2 reduction. This section will walk a user step-by-step in performing a photochemical CO_2 reduction reaction.

1. Choosing a Vessel

The first step in experiment design is to choose the correct reaction vessel as headspace, catalyst/additive concentration, and pressure can be key factors affecting performance. Therefore, it is important to keep the reaction vessel constant through catalyst screening and reaction optimization. In many instances, small screw-cap test tubes work well for this type of screening. Because CO_2 is a gaseous reactant, the choice of septum is important. For this reason,

it is also important to never use a septum that has been used previously, as leakage could occur. The “standard” tubes we have chosen to work with are 17 mL screw cap test tubes that can be fitted with screw cap w/ removable septa (For instance, Chemglass Part No.: CG-4910-02). Larger tubes may also be used if they have sufficiently resilient septa and screw caps. For high-pressure (>1 bar) reactions, heavy walled schlenk flasks (such as ChemGlass UMS-1407-181JS) also work well. For visible light photocatalyses, the reaction vessels do not have to be made of quartz, since glass allows visible light complete transmittance. Examples of vessels for photochemical reaction are shown in Figure 47.

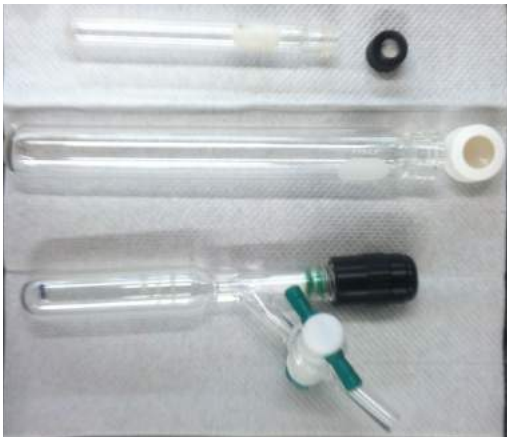

Figure 47. *Top*: 17 mL screw cap vial, *Middle*: 40 mL screw cap vial, and *Bottom*: heavy-walled schlenk flasks for use in photochemical CO_2 reduction.

2. Preparing the Reaction Flask

Once the appropriate vessel has been selected, it is then important to understand the steps required to prepare a reaction for irradiation.

Stirring- Equip a Stirbar

Heterogeneous reactions (involving poorly soluble additives, insoluble catalysts, films, etc.) should certainly be stirred, and it is also a good idea to include stirring for homogeneous reactions in order to reduce the importance of diffusion-mediated processes. Therefore, include a stirbar where possible.

Concentration- Choose a Catalyst Concentration for Initial Screening

Catalyst concentration is a key reaction element that must eventually be optimized; however, it is a good idea to know where to start. For instance, $Re(bpy)(CO)_3X$ type catalysts perform well near 10^{-3} M[18] and Ishitani's (tpy)Ir(ppy)Cl catalyst works well at 5×10^{-4} M.[19a] Another factor to bear in mind when choosing a concentration to start a study with is that non-productive electron transfer processes increase with increasing concentration. This is because with higher concentration comes a higher chance that one excited catalyst/photosensitizer molecule could collide with another catalyst/photosensitizer instead of CO_2. Another factor for consideration is the detection limit of the method being used to analyze the sample. Each method has its own limits of detection, so this will be an important factor in determining catalyst activity, since poor experimental design might lead to incorrect assessment. Figure 48 shows the catalyst TON needed to form 100 parts per million (ppm) of CO for different reaction vessel headspace values. In this figure, the choice of both vessel and catalyst amount are highlighted, in that since ppm is dependent on the headspace sampled, a large headspace or small amount of catalyst means it will take higher TON to achieve higher ppm values. This is important, since the GC (covered later) detects ppm CO.

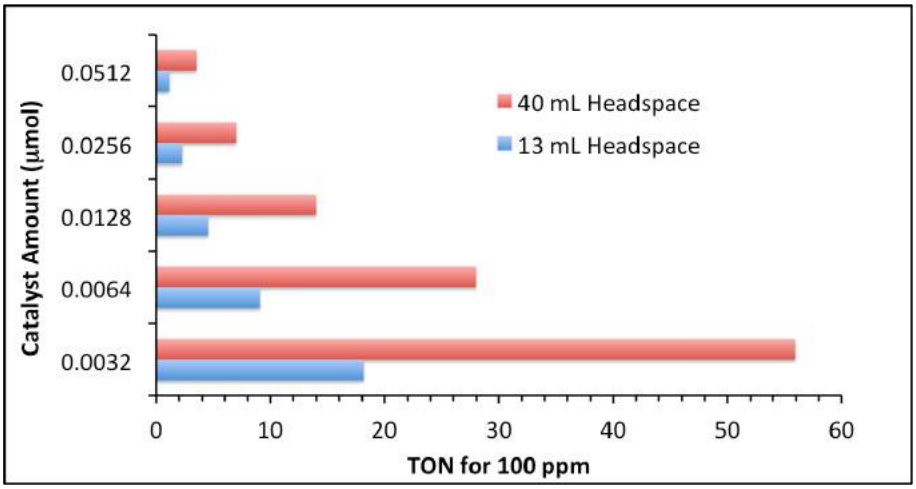

Figure 48. Catalyst amount needed for 100 ppm CO using various vessel headspace values.

Therefore, in order to ensure that catalyst activity is accurately assessed, A good starting point is to choose a catalyst amount that allows for TON = 1 to produce 100 ppm in the given flask.

Solvent- Choose a Suitable Solvent for Initial Screening

The solvent is also subject to optimization; however, it is good to start with a solvent that does not decompose in the reaction conditions to give products. For instance, DMF is often a poor choice of solvent for catalyst screening since it decomposes easily with light and/or acid to give both CO and CO_2H_2. Similarly, dioxane and DMA both decompose to CO with acid, acetone decomposes to methane with light, and DMSO can be reduced with an electron to give methane. The best solvents to try first are MeCN especially, and H_2O if possible, as the only source of CO_2 reduction products are from CO_2.

Electron Source- Choose a Suitable Electron Source for Initial Screening

Many different electron sources have been reported in photosensitized and photochemical CO_2 reduction reactions including TEA, TEOA, BIH, and BNAH to name a few. In choosing an electron source to start catalyst screening, the two most commonly used are TEA and TEOA by far. Since it is not very volatile, TEOA can be added along with solvent. The highly volatile TEA must be degassed with CO_2 prior to addition and addition to the reaction flask should only come after the reaction has been thoroughly degassed, in order to minimize evaporative loss during bubbling.

Electron Source- Choose a Suitable Amount for Initial Screening

Typically, electron sources are included in solvent quantities, so precise measurement and exhaustive optimization screening should not be necessary. A good rule of thumb is to try to follow literature precedent. Typical quantities of electron source are compiled in Table 21.

Table 23. Typical electron source quantities used in photochemical CO_2 reduction reactions.

Electron Source	Commonly Used Amount	Reference
TEA	15 % (v/v)	19a
TEOA	15 % (v/v)	19a
BIH	0.1 M	116e
BNAH	0.1 M	116d

Add any other desired additives

It is typically before degassing that any other (non-volatile) additive be included into the photochemical reaction tube. This is true for photosensitizers, proton sources, and lewis acid additives. The proton sources might be volatile (and thus should be added after degassing as the

case with TEA), however, photosensitizers and lewis acids are almost certainly not volatile. Table 23. shows typical amounts for each type of additive and the references that describe their use.

Table 24. Identity and amount of additive used in catalytic CO_2 reduction.

Additive	Type	Amount	Ref.
$Ir(ppy)_3$	Photosensitizer	1000x cat.	116a,b
$Ru(bpy)_3$	Photosensitizer	1000x cat.	116d
9-CA	Photosensitizer	1000x cat.	116b
p-terphenyl	Photosensitizer	130x cat.	116c
PhOH	Proton Source	0.08 M	113c
F_3CH_2OH	Proton Source	3.5 M	113b
H_2O	Proton Source	2 M	113c
iPrOH	Proton Source	6.5 M	113b
Mg^{2+}	Lewis Acid	15 mM	113a

Degassing the Reaction Flask

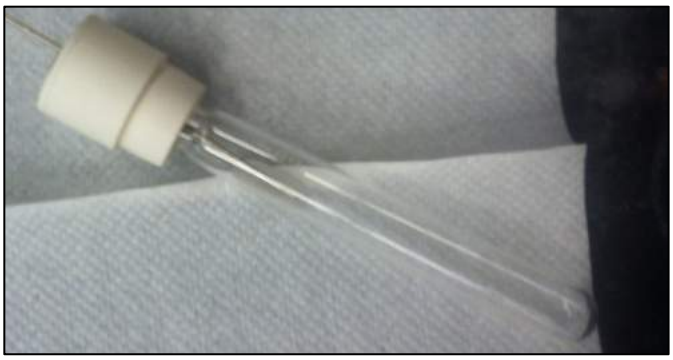

Figure 48. Picture of a 17 mL vial which has been equipped with a 24/40 stopper as septum, long steel needle as inlet needle, and short steel needle as outlet needle.

Upon the judicious selection and addition of each necessary component, the last step is the inclusion of gaseous CO_2 via bubbling (also termed sparging). As in the setup of any other reaction that includes bubbling, the flask needs to be equipped with a septum, inlet needle, and outlet needle (Figure 48). The septum chosen should not be the screw cap and septum to be used

during irradiation. Instead, a septum that fits a 24/40 round bottom flask fits nicely in this regard (Figure 48). Once fitted with the septum, the needle can be placed into the solution until the tip touches the bottom of the tube.

For a satisfactory bubbling rate, it is recommended that the pressure-tuning knob of the CO_2 gas tanks regular be loosed until no gas can be observed bubbling through the solution. Slowly tighten the pressure-tuning knob until satisfactory bubbling is observed. No recommendation is given here about the specific bubbling rate, because the volatility of each solvent is different. For instance, DMF is not volatile and can be bubbled very vigorously, while acetonitrile is volatile enough that its entire volume can be evaporated in 15 min. It is recommended that for volatile solvent, a generous amount of excess solvent be included to account for evaporative loss. For example, 6 mL of MeCN can usually be reduced to nearly 2 mL in 15 min with vigorous bubbling. Using vigorous bubbling for long degassing times can improve reproducibility.

Once a satisfactory bubbling rate has been reached, the timeframe of bubbling then needs to be considered. In general, for non-polar solvents (such as hexane), only 5-10 minutes are needed for bubbling. For mildly polar solvents (such as THF, MeCN, CH_2Cl_2), 15-20 minutes of degassing are sufficient. For very polar solvents (such as DMSO, DMF, H_2O), times up to 30 minutes may need to be utilized. When in doubt about the proper time for degassing, it is advisable to give the solution 30 min.

After bubbling, the tube needs to be sealed without any inclusion of oxygen, which will ruin the reaction. In order to properly seal the tube without inclusion of oxygen, the flow rate of

CO_2 should be turned up to a very high bubbling rate and the long needle pulled out from the solution and ¾ of the way up the tube. To seal the tube, a screw cap with septum (see above) should be readied with one hand and the rubber septum with needles pulled off the top of the tube. The screw cap should be quickly placed so that it covers the open tube, with the long needle tip still under the lip of the tube. After ~15-20 s of allowing the long needle to purge the cap in this manner, the needle should be removed and the septum quickly placed on the tube and screwed down tightly. At this point, the reaction tube is prepared for irradiation.

3. Irradiation

Once prepared, the samples can then be placed in front of the proper light source. Our laboratory has two light sources: the sunbox and the solar simulator (Figure 49). The sunbox contains a merry-go-round apparatus with a 500W Xe lamp at the center in an immersion well. A series of K-2 filters on the merry-go-round stage filters the light from the Xe lamp so that it approximates the solar spectrum. The solar simulator is a 125W Xe lamp that is placed in a dog-kennel that has two black sheets covering the top to exclude light. With a sample 10 cm away from the solar simulator's opening (which has a solar-simulating filter equipped). The light accurately approximates the AM1.5 solar spectrum.

Figure 50. *Left*: A picture of the sunbox. *Right* A picture of the solar simulator.

In general catalyst screening and reaction optimization trials, the sunbox should be utilized. The solar simulator should only be utilized in end-of-study catalyst trials, because the lifetime of the Xe lamp is only ~1000 h. The sunbox has a lifetime of the same magnitude; however, it is meant for general and/or preliminary screening trials.

Operating Procedure for Irradiation in the Sunbox

There are a series of steps required to safely operate the sunbox.

1. Ensure the power is on to each of the sunbox control units: The upconverter, the water alarm system, and the sunbox unit itself. The power to each of these units is controlled by a surge protector, which should be switched to 'ON' before attempted use.

2. Ensure there is a strong flow of water through the quartz Xe lamp well cooling system. Without water, the 500W Xe lamp would surely overheat and explode.

3. Ensure the fan mounted to the top of the sunbox is on. This can be checked by ensuring power to the sunbox unit and switching the fan to ‘ON’ using the control panel inside of the sunbox. Air circulation is important in keeping the sunbox and reaction flasks at a constant temperature.

4. Mount the reaction flask(s) in the box carefully around the stage, being mindful that the glass filters are fragile. A maximum of 15 samples can be irradiated at one time, but only ~4 samples can be stirred at one time.

5. Ensure stirring if needed. A small megnietic stirrer can be placed on the merry-go-round stage to aid in sample stirring. Before continuing, ensure that each sample to be stirred is stirring well.

6. Close the door, latch it, double check that the water is flowing quickly through the well, and turn on the lamp using the switch on the light blue control unit directly under the sunbox. After the allotted time of irradiation has passed, the lamp can be turned off, the sunbox door opened, and the flasks reclaimed.

Operating Procedure for Irradiation with the Solar Simulator

There are a series of steps required to safely operate the solar simulator.

1. Ensure the power is on to the power source. This power source controls the Xe lamp unit as well as the fan.

2. The dial on the right side of the power source control panel should be turned from its resting position at the far left (counter clockwise) position to the marked position nearly 3/5 around the knob (clockwise).

3. Mount the reaction flask(s) in the wire guides that lie 10 cm away from the lamp opening. A maximum of two 17 mL vials, one 40 mL vial, or one pressure flask can be irradiated at a time using this setup.

4. Ensure stirring if needed. A small megnietic stirrer can be placed in the kennel to aid in sample stirring. Before continuing, ensure that each sample to be stirred is stirring well.

6. Close the kennel door, latch it, pull the two lack sheet down around the kennel so that all but the solar simulator is covered, and turn on the lamp using the green initialize buttion. After the allotted time of irradiation has passed, the lamp can be turned off by pressing the red button on the power source control panel, the power control dial turned counter clockwise until it reaches the '0' mark, the sheets lifted, the door opened, and the flasks reclaimed.

4. Analyzing the Reactions for Gaseous and Liquid Products

After irradiation, it is then time to analyze the samples for any reduction products. There are three main methods of analysis that should allow for the reliable separation of the most common products observed in CO_2 photoreduction: Headspace analysis via gas chromatography (GC), solution analysis via high performance liquid chromatography (HPLC), and solution analysis via GC. Each of these methods offer different product detections as shown in Table 24.

Table 25. Instruments needed to detect each of the commonly observed CO_2 reduction products.

Product	Instrument
CO	GC (Headspace)
H_2	GC (Headspace)
CH_4	GC (Headspace)
CO_2H_2	HPLC
HO_2CCO_2H	HPLC
MeOH	GC (Solution)

A picture of each of the instruments is shown in Figure 50.

Figure 51. *Left*: Picture of the GC used for headspace analysis. *Middle*: Picture of the HPLC used for solution analysis analysis. *Right*: Picture of the GC used for solution analysis.

Headspace Analysis

In performing headspace analysis of a reaction, the following series of steps should be followed.

1. Ensure that the GC (Figure 50, *Left*) is turned on at least 1h before the analysis is to take place. This gives the instrument proper equilibration time, which allows for reliable results.

2. Once the instrument has been fully powered on (the flame ionization detector (FID) is on, the oven is at the correct temperature, and the gas has reached the required flow rate), a blank run needs to be initiated. No injection is necessary in this case, just press the 'Run' button on the GC. Performing this blank run is important, as latent materal on the column needs to be cleared away prior to reaction analysis.

3. Using a gas-tight syringe, carefully pierce the reaction flask. Ensure that the valve is set to 'open' and draw the desired volume. It is recommended to draw between 250 and 500 μL. Ensure that the valve is set to 'closed' and remove the needle from the flask.

4. Obtain a vial that has been filled halfway with Et_2O. While the syringe valve is still set to ‘closed,’ depress the syringe plunger to ~halfway of its original value. Place the needle well into the Et_2O and set the syringe valve to ‘open.’ If performed correctly, this should result in an eruption of bubbles from the tip of the needle. Once the initial burst of bubbles have shot from the needle tip, set the valve to ‘closed’ and remove the needle from the Et_2O.

5. After waiting 10-20 s to allow for Et_2O evaporation from the needle tip, ensure that the GC is ‘Ready.’ Once ready, *carefully* place the needle into the GC injector port, set the syringe valve to ‘open,’ and *carefully* depress the plunger. The plunger and needle are both *very* thin and are machined to exactly match the glass syringe. Because they are so thin, it does not take much force to bend either. Once bent, these needles never work as well, so much care should be taken to ensure that both are never bent.

6. Once the syringe has been depressed, press ‘Run’ on the GC and *carefully* remove the needle from the injection port. Ensure that the needle stays attached to the syringe during this removal. If the two separate before the needle is removed, injection port will leak and the run will be ruined.

GC used for headspace analysis

Headspace analysis was performed using an Agilent 7890B Gas Chromatograph (*Column*: Agilent PorapakQ 6 ft, 1/8 O.D.) equipped with FID and TCD detectors.

The temperature program used in the GC should be:

T_o =33 mL/min flow rate, injector = 35ºC, FID = 300ºC, TCD = 200ºC, Oven = 75ºC.

T = 4 min, oven temp ramp to 150 ºC over 5.875 min.

T = 9.875 min, run finished.

Solution Analysis (HPLC)

In performing solution analysis of a reaction in an effort to detect formic acid or oxalic acid, the following series of steps should be followed.

1. Ensure that the HPLC (Figure 50, *Middle*) is turned on at least 1h before the analysis is to take place. This gives the instrument proper equilibration time, which is necessary for reliable results.

2. Once the instrument has been fully powered on (the pumps are on and the instrument response has equilibrated), ensure that the HPLC solvent bottled are refilled and prepare a sample by adding ~1 mL of the solution to be analyzed into a 1 mL vial.

3. Place the vial in one of the vial holders in the autosampling unit. The number of the vial well should be noted, as the instrument needs to know this.

HPLC used for solution analysis

Solution analysis was performed using an Agilent 1100 series HPLC (*Column:*Agilent eclipse plus c-18, 3.5um, 4.5 x 1500 mm).

The program used in the HPLC should be:

T_o =100% H_2O solvent, 0.25 mL/min flow rate, T = 25ºC, detector λ: 180 nm.

T = 1.5 min, flow ramp to 0.30 mL/min

T = 2.5 min, flow ramp to 0.35 mL/min

T = 3.0 min, flow ramp to 0.45 mL/min, solvent to 25% MeOH:H_2O

T = 4.2 min, flow ramp to 0.70 mL/min, solvent to 35% MeOH:H_2O

T = 5.0 min, flow ramp to 1.0 mL/min, solvent to 50% MeOH:H_2O

T = 9.0 min, run finished.

Retention time of HCO_2H: 5.34 min

Retention time of HO_2CCO_2H: 4.0 min

Solution Analysis (GC)

In performing solution analysis of a reaction in an effort to detect methanol, the following series of steps should be followed.

1. Ensure that the GC (Figure 50, *Left*) is turned on at least 1h before the analysis is to take place. This gives the instrument proper equilibration time, which allows for reliable results.

2. Once the instrument has been fully powered on (the flame ionization detector (FID) is on, the oven is at the correct temperature, and the gas has reached the required flow rate), a blank run needs to be initiated. No injection is necessary in this case, just press the 'Run' button on the GC. Performing this blank run is important, as latent materal on the column needs to be cleared away prior to reaction analysis.

3. Place the vial in one of the vial holders in the autosampling unit. The number of the vial well should be noted, as the instrument needs to know this.

GC used for solution analysis

Solution analysis was performed using a Shimadzu GC-2010 Gas Chromatograph equipped with FID detector (*Column*: SHRXI-5MS 15m, 0.25 mm ID).

The temperature program used in the GC should be:

T_o =5.6 mL/min flow rate, injector = 35ºC, FID = 300ºC, Oven = 27ºC.

T = 5 min, oven temp ramp to 57 ºC, then hold 1.0 min.

T = 9 min, oven temp ramp to 200 ºC, then hold 10 min.

T = 27.0 min, run finished.

Electrochemical reaction setup

As is true for any chemical reaction, experiment design is key in CO_2 reduction. This section will walk a user step-by-step in performing a electrochemical CO_2 reduction reaction.

1. Choosing a Vessel

As in the photocatalysis discussion, the first step in experiment design is to choose the correct reaction vessel as solvent, headspace, and catalyst/additive concentration can be key factors affecting performance. Therefore, it is important to keep the reaction vessel constant through catalyst screening and reaction optimization. In some instances, screw-cap test tubes work well for this type of screening, while in others a three-neck conical flask can serve the purpose. The “standard” vessels we have chosen to work with are 40 mL screw vials that can be fitted with screw cap w/ removable septa and a 50 mL three-neck conical vial. For cyclic voltammetry experiments, the three neck conical flask is sufficient, while the screw cap vial should be used in controlled-potential bulk electrolyses. Examples of vessels for electrochemical reaction are shown in Figure 51.

Figure 52. *Left*: A picture of the three-neck conical flask used for CV. *Right* A picture of the bulk electrolysis setup.

2. Preparing the Reaction Flask

Once the appropriate vessel has been selected, it is then important to understand the steps required to prepare a reaction for irradiation.

Stirring- Not Required

Bulk electrolyses and CV experiments do not use stirring, as both are inherently controlled by diffusion rates of products and reactants. Therefore, do not equip the electrochemical reaction flask with a stirbar.

Concentration- Choose a Catalyst Concentration

Catalyst concentration is a key reaction element that must eventually be optimized, however, it is a good idea to know where to start. For instance, an excellent signal/noise ratio can be achieved with 10^{-4} M, in bulk electrolyses 10^{-3} M is advised. As with photocatalysis, another factor for consideration is the detection limit of the method being used to analyze the sample.

Even though each method has its own limits of detection, the reaction flask for each technique should not be changed, so this is not a concern for bulk electrolysis. The best way, then, to ensure more product in solution or headspace is to include more catalyst.

Solvent- Choose a Suitable Solvent

While the solvent is also subject to optimization, the choice of solvent is not nearly as important in electrocatalysis as in photocatalysis. For instance, DMF is often a poor choice of solvent for photocatalyst screening since it decomposes easily with light and/or acid, however electrolytic decomposition is much slower. The best solvents to try first are DMF and MeCN especially, and H_2O if possible, as each is commonly used in catalytic studies.

Degassing the Reaction Flask

Upon the judicious selection and addition of each necessary component, the last step is the inclusion of gaseous CO_2 via bubbling (also termed sparging). Unfortunately, before the solution can be degassed with CO_2, it must first be thoroughly degassed with N_2. This is because when using a Pt reference electrode there can be substantial day-to-day drift. Thus, a scan under nitrogen standardizes the spectrum. Once the spectrum is standardized, gaseous CO_2 can then be thoroughly bubbled into the solution. As in the setup of any other reaction that includes bubbling, the flask needs to be equipped with a septum, inlet needle, and outlet needle (Figure 51). In CV studies, the imperfect seal created from the 14/20 septa in each neck but not folded over is a sufficient outlet, while a long steel needle serves as the inlet. In bulk electrolyses, the inlet needle is a flexible Teflon needle and the outlet is hooked to a bubbler submerged in silicon oil (Figure 48). The same concerns for bubbling rate found in the above section regarding photocatalysis is

valid for electrocatalysis as well. Once the solution has been thoroughly degassed, the needle should be removed from solution and the scan/electrolysis can then begin.

Electrolysis

Electrolyses are performed using a CH instruments electorchemical analyzer. Once the proper time of electrolysis has elapsed, analysis can commence.

Analysis

The techniques for analysis used in electrocatalysis are the same used in photocatalysis. See the instructions in the photocatalysis section for precise techniques.

LIST OF REFERENCES

(1)Kopp, O. C. In *Encyclopaedia Britannica* 2013.

(2) Grätzel, M.; O'Regan, B. *Nature* **1991**, *353*, 737.

(3)(a): MIT; MIT: 2006; Vol. 2014. (b): Green, M. A. *Progress in Photovoltaics: Research and Applications* **2005**, *13*, 447.

(4)Swanson, R. M. *Progress in Photovoltaics: Research and Applications* **2006**, *14*, 443.

(5)Jordan, D. C.; Kurtz, S. R. *Progress in Photovoltaics: Research and Applications* **2013**, *21*, 12.

(6)Grätzel, M.; O'Regan, B. *Nature* **1991**, *353*, 737.

(7)Hagfeldt, A.; Boschloo, G.; Sun, L.; Kloo, L.; Pettersson, H. *Chem. Rev.* **2010**, *110*, 6595.

(8)Gratzel, M. *Journal of Photochemistry and Photobiology C: Photochemistry Reviews* **2003**, *4*, 145.

(9)Matthew, S.; Yella, A.; Gao, P.; Humphry-Baker, R.; ChurchodBasile, F. E.; Tavernelli, I.; Nazeeruddin, M. K.; Gratzel, M. *Nature Chemistry* **2014**, *6*, 242.

(10)Kakiage, K.; Aoyama, Y.; Yano, T.; Otsuka, T.; Kyomen, T.; Unno, M.; Hanaya, M. *Chem. Commun.* **2014**.

(11)Gueymard, C. A.; Myers, D.; Emery, K. *Solar Energy* **2002**, *73*, 443.

(12)Grätzel, M. *Journal of Photochemistry and Photobiology C: Photochemistry Reviews* **2003**, *4*, 145.

(13)Mishra, A.; Fischer, M. K. R.; Bauerle, P. *Angew. Chem. Int. Ed.* **2009**, *48*, 2474.

(14)Oceanography, S. I. o. In *Daily*; Scripps Insitution of Oceanography: 2014.

(15)Trenberth, K. E.; Guillemot, C. J. *Journal of Geophysical Research: Atmospheres* **1994**, *99*, 23079.

(16)Cokoja, M.; Bruckmeier, C.; Rieger, B.; Herrmann, W. A.; Kühn, F. E. *Angew. Chem. Int. Ed.* **2011**, *50*, 8510.

(17)(a): Morris, A. J.; Meyer, G. J.; Fujita, E. *Acc. Chem. Res.* **2009**, *42*, 1983. (b): Kumar, B.; Llorente, M.; Froehlich, J.; Dang, T.; Sathrum, A.; Kubiak, C. P. *Annual Review of Physical Chemistry* **2012**, *63*, 541.

(18)Hawecker, J.; Lehn, J.-M.; Ziessel, R. *J. Chem. Soc., Chem. Commun.* **1983**, 536.

(19) (a): Sato, S.; Morikawa, T.; Kajino, T.; Ishitani, O. *Angew. Chem. Int. Ed.* **2013**, *52*, 988. (b): Yuan, J.-J.; Yu, Z.-T.; Chen, X.-Y.; Zhang, J.-Y.; Zou, Z.-G. *Chem. Eur. J.* **2011**, *17*, 12891-12895.

(20)Hardin, B. E.; Snaith, H. J.; McGehee, M. D. *Nat Photon* **2012**, *6*, 162.

(21)Li, J.-Y.; Chen, C.-Y.; Ho, W.-C.; Chen, S.-H.; Wu, C.-G. *Org. Lett.* **2012**, *14*, 5420.

(22)(a): Yang, J.; Ganesan, P.; Teuscher, J. l.; Moehl, T.; Kim, Y. J.; Yi, C.; Comte, P.; Pei, K.; Holcombe, T. W.; Nazeeruddin, M. K.; Hua, J.; Zakeeruddin, S. M.; Tian, H.; Gratzel, M. *J. Am. Chem. Soc.* **2014**, *136*, 5722. (b): Yum, J.-H.; Holcombe, T. W.; Kim, Y. J.; Rakstys, K.; Moehl, T.; Teuscher, J.; Delcamp, J. H.; Nazeeruddin, M. K.; Gratzel, M. *Scientific Reports* **2013**, 3. (c): Ahmad, S.; Bessho, T.; Kessler, F.; Baranoff, E.; Frey, J.; Yi, C.; Gratzel, M.; Nazeeruddin, M. K. *Physical Chemistry Chemical Physics* **2012**, *14*, 10631. (d): Yella, A.; Humphry-Baker, R.; Curchod, B. F. E.; Ashari Astani, N.; Teuscher, J. l.; Polander, L. E.;

Mathew, S.; Moser, J.-E.; Tavernelli, I.; Rothlisberger, U.; Gratzel, M.; Nazeeruddin, M. K.; Frey, *J. Chem. Mat*. **2013**, *25*, 2733.

(23)(a): Delcamp, J. H.; Yella, A.; Holcombe, T. W.; Nazeeruddin, M. K.; Grätzel, M. Angew. Chem. Int. Ed. 2013, 52, 376. (b): Dualeh, A.; Humphry-Baker, R.; Delcamp, J. H.; Nazeeruddin, M. K.; Grätzel, M. *Advanced Energy Materials* **2013**, *3*, 496.

(24): Koszarna, B.; Matczak, R. Ç.; Krzeszewski, M.; Vakuliuk, O.; Klajn, J.; Tasior, M.; Nowicki, J. T.; Gryko, D. T. *Tetrahedron* **2014**, *70*, 225.

(25)Bury, P. S.; Christiansen, L. B.; Jacobsen, P.; Joergensen, A. S.; Kanstrup, A. **1998**. WO Pat. 055482.

(26)(a): Liu, B.; Wang, Z.; Wu, N.; Li, M.; You, J.; Lan, J. Chem. Eur. J. 2012, 18, 1599. (b): Park, C.-H.; Ryabova, V.; Seregin, I. V.; Sromek, A. W.; Gevorgyan, V. *Org. Lett*. **2004**, *6*, 1159.

(27)Hagberg, D. P.; Marinado, T.; Karlsson, K. M.; Nonomura, K.; Qin, P.; Boschloo, G.; Brinck, T.; Hagfeldt, A.; Sun, L. *J Org Chem* **2007**, *72*, 9550.

(28)Li, R.; Lv, X.; Shi, D.; Zhou, D.; Cheng, Y.; Zhang, G.; Wang, P. *J. Phys. Chem. C*. **2009**, *113*, 7469.

(29)Dentani, T.; Kubota, Y.; Funabiki, K.; Jin, J.; Yoshida, T.; Minoura, H.; Miura, H.; Matsui, M. *New J. Chem*. **2009**, *33*, 93.

(30)Chai, Q.; Li, W.; Zhu, S.; Zhang, Q.; Zhu, W. *ACS Sustainable Chemistry & Engineering* **2013**, *2*, 239.

(31)Yu, Q.-Y.; Liao, J.-Y.; Zhou, S.-M.; Shen, Y.; Liu, J.-M.; Kuang, D.-B.; Su, C.-Y. *J. Phys. Chem. C.* **2011**, *115*, 22002.

(32)Li, W.; Wu, Y.; Zhang, Q.; Tian, H.; Zhu, W. *ACS App. Mat. Int.* **2012**, *4*, 1822.

(33)(a): Zhang, M.; Wang, Y.; Xu, M.; Ma, W.; Li, R.; Wang, P. *Energy & Environmental Science* **2013**, *6*, 2944.

(34)(a): Gabrielsson, E.; Ellis, H.; Feldt, S.; Tian, H.; Boschloo, G.; Hagfeldt, A.; Sun, L. *Advanced Energy Materials* **2013**, *3*, 1647. (b): Feldt, S. M.; Gibson, E. A.; Gabrielsson, E.; Sun, L.; Boschloo, G.; Hagfeldt, A. *J. Am. Chem. Soc*. **2010**, *132*, 16714. (c):Feldt, S. M.; Lohse, P. W.; Kessler, F.; Nazeeruddin, M. K.; Grätzel, M.; Boschloo, G.; Hagfeldt, A. *Phys. Chem. Chem. Phys.* **2013**, *15*, 7087.

(35)(a): Dunlap, B. I. The Journal of Chemical Physics 1983, 78, 3140. (b): Giese, T. J.; York, D. M. *The Journal of Chemical Physics* **2011**, 134.

(36)Frisch, M. J.; Trucks, G. W.; Schlegel, H. B.; Scuseria, G. E.; Robb, M. A.; Cheeseman, J. R.; Scalmani, G.; Barone, V.; Mennucci, B.; Petersson, G. A.; Nakatsuji, H.; Caricato, M.; Li, X.; Hratchian, H. P.; Izmaylov, A. F.; Bloino, J.; Zheng, G.; Sonnenberg, J. L.; Hada, M.; Ehara, M.; Toyota, K.; Fukuda, R.; Hasegawa, J.; Ishida, M.; Nakajima, T.; Honda, Y.; Kitao, O.; Nakai, H.; Vreven, T.; Montgomery Jr., J. A.; Peralta, J. E.; Ogliaro, F. o.; Bearpark, M. J.; Heyd, J.; Brothers, E. N.; Kudin, K. N.; Staroverov, V. N.; Kobayashi, R.; Normand, J.; Raghavachari, K.; Rendell, A. P.; Burant, J. C.; Iyengar, S. S.; Tomasi, J.; Cossi, M.; Rega, N.; Millam, N. J.; Klene, M.; Knox, J. E.; Cross, J. B.; Bakken, V.; Adamo, C.; Jaramillo, J.; Gomperts, R.; Stratmann, R. E.; Yazyev, O.; Austin, A. J.; Cammi, R.; Pomelli, C.;

Ochterski, J. W.; Martin, R. L.; Morokuma, K.; Zakrzewski, V. G.; Voth, G. A.; Salvador, P.; Dannenberg, J. J.; Dapprich, S.; Daniels, A. D.; Farkas, ñ. n.; Foresman, J. B.; Ortiz, J. V.; Cioslowski, J.; Fox, D. J.; Gaussian, Inc.: Wallingford, CT, USA, **2009**.

(37)(a): Becke, A. D. *The Journal of Chemical Physics* **1993**, *98*, 5648. (b): Lee, C.; Yang, W.; Parr, R. G. *Physical Review B* **1988**, *37*, 785.

(38)Van Voorhis, T.; Scuseria, G. E. *The Journal of Chemical Physics* **1998**, 109, 400.

(39)Zhao, Y.; Truhlar, D. G. *The Journal of Chemical Physics* **2006**, 125.

(40)R. Peverati, D. G. Truhlar, *J. Phys. Chem. Lett.* **2012**, *3*, 117.

(41)Peverati, R.; Truhlar, D. G. *Journal of Chemical Theory and Computation* **2012**, *8*, 2310.

(42)Peverati, R.; Truhlar, D. G. *Physical Chemistry Chemical Physics* **2012**, *14*, 13171.

(43)Cossi, M.; Barone, V. *The Journal of Chemical Physics* **2001**, *115*, 4708.

(44)(a): MikoÇajczyk, M. Ç.; Zaleõny, R.; Czynikowska, a.; Toman, P.; Leszczynski, J.; Bartkowiak, W. *J Mol Model* **2011**, *17*, 2143. (b): Vydrov, O. A.; Heyd, J.; Krukau, A. V.; Scuseria, G. E. *The Journal of Chemical Physics* **2006**, 125.

(45)(a): Adamo, C.; Barone, V. The Journal of Chemical Physics 1999, 110, 6158. (b): Ernzerhof, M.; Scuseria, G. E. *The Journal of Chemical Physics* **1999**, *110*, 5029.

(46)Perdew, J. P.; Burke, K.; Ernzerhof, M. *Physical Review Letters* **1996**, *77*, 3865.

(47)Bauernschmitt, R. d.; Ahlrichs, R. *Chemical Physics Letters* **1996**, *256*, 454.

(48)Friedrich, V.; Kivelson, D. *The Journal of Chemical Physics* **1987**, *86*, 6425.

(49)Bode, M. L.; Kaye, P. T. *J. Chem. Soc., Perkin Trans. I* **1993**, 1809.

(50)(a): Soule, J.-F.; Miyamura, H.; Kobayashi, S. *J. Am. Chem. Soc.* **2013**, *135*, 10602. (b): Nunez, A.; Abarca, B.; Cuadro, A. M.; Alvarez-Builla, J.; Vaquero, J. J. *J Org Chem* **2009**, *74*, 4166.

(51)(a): Furstner, A.; Leitner, A.; Mendez, M.; Krause, H. *J. Am. Chem. Soc*. **2002**, *124*, 13856. (b): Benzencon, O.; Bur, D.; Corminboeuf, O.; Dube, D.; Gristomi, C.; Macdonald, D.; McKay, D.; Powell, D.; Remen, L.; Richard-Bildstein, S.; Sheigetz, J.; Therien, M.; Weller, T. U.S., **2007**.

(52)Hamann, T. W.; Ondersma, J. W. *Energy Environ. Sci*. **2011**, *4*, 370.

(53)Urbani, M.; Grätzel, M.; Nazeeruddin, M. K.; Torres, T. *Chem. Rev*. **2014**, *114*, 12330.

(54) (a):Liu, Y.; Lin, H.; Dy, J. T.; Tamaki, K.; Nakazaki, J.; Nishiyama, C.; Uchida, S.; Segawa, H.; Li, J. *J. Phys. Chem. C* **2013**, *118*, 1426. (b): Zhang, C.; Huang, Y.; Huo, Z.; Chen, S.; Dai, S. *J. Phys. Chem. C **2009**, 113*, 21779. (c): (1) Kim, M.-J.; Lee, C.-R.; Jeong, W.-S.; Im, J.-H.; Ryu, T. I.; Park, N.-G. *J. Phys. Chem. C* **2010**, *114*, 19849. (d): Shrestha, M.; Si, L.; Chang, C.-W.; He, H.; Sykes, A.; Lin, C.-Y.; Diau, E. W.-G. *J. Phys. Chem. C* **2012**, *116*, 10451.

(55)Huckaba, A. J.; Giordano, F.; McNamara, L. E.; Dreux, K. M.; Hammer, N. I.; Tschumper, G. S.; Zakeeruddin, S. M.; Grätzel, M.; Nazeeruddin, M. K.; Delcamp, J. H. *Adv. Energy Mater.* **2014**.

(56)Jahangir, A.; Soth, M.; Yang, H.; Lynch, S. WO patent 2011/033053.

(57)Yum, J.-H.; Holcombe, T. W.; Kim, Y.; Yoon, J.; Rakstys, K.; Nazeeruddin, M. K.; Gratzel, M. Chem. Commun. 2012, 48, 10727.

(58)Delcamp, J. H.; Yella, A.; Nazeeruddin, M. K.; Gratzel, M. Chem. Commun. 2012, 48, 2295.

(59)Chen, C.-H.; Hsieh, C.-H.; Dubosc, M.; Cheng, Y.-J.; Hsu, C.-S. Macromolecules 2009, 43, 697.

(60)Morvillo, P.; Parenti, F.; Diana, R.; Fontanesi, C.; Mucci, A.; Tassinari, F.; Schenetti, L. Sol. Energy Mater. Sol. Cells 2012, 104, 45.

(61):Ito, S.; Miura, H.; Uchida, S.; Takata, M.; Sumioka, K.; Liska, P.; Comte, P.; Pechy, P.; Gratzel, M. Chem. Commun. 2008, 5194.

(62):Dentani, T.; Kubota, Y.; Funabiki, K.; Jin, J.; Yoshida, T.; Minoura, H.; Miura, H.; Matsui, M. New J. Chem. 2009, 33, 93.

(63): Kang, X.; Zhang, J.; O'Neil, D.; Rojas, A. J.; Chen, W.; Szymanski, P.; Marder, S. R.; El-Sayed, M. A. *Chem. Mater*. **2014**, *26*, 4486-4493.

(64): Zhang, M.; Wang, Y.; Xu, M.; Ma, W.; Li, R.; Wang, P. *Energy Environ. Sci.* **2013**, *6*, 2944.

(65): Joly, D.; Pelleja † , L.; Narbey, S.; Oswald, F.; Chiron, J.; Clifford, J. N.; Palomares, E.; Demadrille, R. *Sci. Rep*. **2014**, 4.

(66): Steinberger, S.; Mishra, A.; Reinold, E.; Mena-Osteritz, E.; Muller, H.; Uhrich, C.; Pfeiffer, M.; Bauerle, P. *J. Mater. Chem.* **2012**, *22*, 2701.

(67): Guo, J.; Wang, S.; Dai, N.; Teo, Y. N.; Kool, E. T. *Proc. Natl. Acad. Sci.* **2011**, *108*, 3493.

(68): Pramanik, M.; Bhaumik, A. *ACS Appl. Mater. Interfaces* **2013**, *6*, 933.

(69): Kuznetsov, A. G.; Bush, A. a.; Rybakov, V. B.; Babaev, E. V. *Molecules* **2005**, *10*, 1074.

(70): Yao, Z.; Yan, C.; Zhang, M.; Li, R.; Cai, Y.; Wang, P. *Adv. Energy Mater*. **2014**.

(71): Luo, J.; Xu, M.; Li, R.; Huang, K. W.; Jiang, C.; Qi, Q.; Zeng, W.; Zhang, J.; Chi, C.; Wang, P.; Wu, J. *J. Am. Chem. Soc*. **2014**, *136*, 265.

(72): Qi, Q.; Wang, X.; Fan, L.; Zheng, B.; Zeng, W.; Luo, J.; Huang, K.-W.; Wang, Q.; Wu, J. *Org. Lett*. **2015**, *17*, 724.

(73): Hagberg, D. P.; Yum, J.-H.; Lee, H.; De Angelis, F.; Marinado, T.; Karlsson, K. M.; Humphry-Baker, R.; Sun, L.; Hagfeldt, A.; Grazel, M.; Nazeeruddin, M. K. *J. Am. Chem. Soc.* **2008**, *130*, 6259.

(74): Thomas, K. R. J.; Hsu, Y.; Lin, J. T.; Lee, K.; Ho, K.; Lai, C.; Cheng, Y.; Chou, P. *Chem. Mater.* **2008**, *20*, 1830.

(75): Ning, Z.; Zhang, Q.; Wu, W.; Pei, H.; Liu, B.; Tian, H. *J. Org. Chem.* **2008**, *73*, 3791.

(76): Kobin, B.; Grubert, L.; Blumstengel, S.; Henneberger, F.; Hecht, S. *J. Mater. Chem*. **2012**, *22*, 4383.

(77): Heo, N.; Jun, Y.; Park, J. H. *Sci. Rep*. **2013**, 3.

(78): Han, Y. C. and A. I. and Y. W. and R. K. and N. K. and L. *Jpn. J. Appl. Phys*. **2006**, *45*, L638.

(79): Grätzel, M. *Inorg. Chem*. **2005**, *44*, 6841.

(80): Pechy, P.; Renouard, T.; Zakeeruddin, S. M.; Humphry-Baker, R.; Comte, P.; Liska, P.; Cevey, L.; Costa, E.; Shklover, V.; Spiccia, L.; Deacon, G. B.; Bignozzi, C. A.; Gratzel, M. *J. Am. Chem. Soc*. **2001**, *123*, 1613.

(81): Kern, R.; Van Der Burg, N.; Chmiel, G.; Gerber, J.; Hasenhindl, G.; Hinsch, a.; Kinderman, R.; Kroon, J.; Meyer, a.; Meyer, T.; Niepmann, R.; Van Roosmalen, J.; Schill, C.; Sommeling, P.; Spath, M.; Uhlendorf, I. Long term stability of dye sensitized solar cells for large area power applications. *Opto-Electronic Review*, **2000**, *8*, 284–288.

(82): Abbotto, A.; Manfredi, N.; Marinzi, C.; De Angelis, F.; Mosconi, E.; Yum, J.-H.; Xianxi, Z.; Nazeeruddin, M. K.; Grätzel, M. *Energy Environ. Sci*. **2009**, *2*, 1094.

(83): Liu, J.; Zhang, J.; Xu, M.; Zhou, D.; Jing, X.; Wang, P. *Energy Environ. Sci*. **2011**, *4*, 3021.

(84): Su, J.-Y.; Lo, C.-Y.; Tsai, C.-H.; Chen, C.-H.; Chou, S.-H.; Liu, S.-H.; Chou, P.-T.; Wong, K.-T. *Org. Lett***. 2014**, *16*, 3176.

(85): Matsuda, Y.; Kohra, S.; Katou, K.; Itou, T.; uemura, T. *Heterocycles*, **1997**, *11*, 2223.

(86): (a): Liang, F.; Hu, J.; Zhang, L.; Hu, Y.; Hu, H. *J. Heterocyclic Chem.*, **2001**, *38*, 853. (b): Gogoi, S.; Dutta, M.; Gogoi, J.; Boruah, R. C. *Tet. Lett.* **2011**, *52*, 813.

(87): Jessup, M. A.; Leaver, D. *J. chem. Soc. Perkins Trans., I.* **1980**, *6*, 1324.

(88): Piliego, C.; Holcombe, T. W.; Douglas, J. D.; Woo, C. H.; Beaujuge, P. M.; Frechet, J. M. J. *J. Am. Chem. Soc*. **2010**, *132*, 7595.

(89): Matsumoto, S.; Aoki, T; Suzuki, T.; Akazome, M. Betto, A.; Suda, Y. *Bull. Chem. Soc. Jpn.* **2012**, *85*, 1329.

(90): Babin, P.; Dunogues, J. *Tet. Lett.* **1983**, *24*, 3071.

(91): Phipps, E. *Cochineal Red: The Art History of a Color*; 1st ed.; Metropolitan Museum of Art**, 2010**.

(92): *Industrial Dyes: Chemistry, Properties, Applications*; Hunger, K., Ed.; 1st ed.; WILEY-VCH: Darmstadt, Germany, **2003**.

(93): Zhang, L.; Cole, J. M.; Waddell, P. G.; Low, K. S.; Liu, X. *ACS Sustain. Chem. Eng*. **2013**, *1*, 1440.

(94): Boschloo, G.; Hagfeldt, A. *Acc. Chem. Res.* **2009**, *42*, 1819.

(95): (a): Wang, m.; Chamberland, N.; Breau, L.; Moser, J.; Humphry-Baker, R.; Marsan, B.; Zakeeruddin, S. M.; Grätzel, M. *Nat Chem* **2010**, *2*, 385. (b): Zhang, Z.; Chen, P.; Murakami, T. N.; Zakeeruddin, S. M.; Grätzel, M. *Advanced Functional Materials* **2008**, *18*, 341. (c): Wang, P.; Zakeeruddin, S. M.; Moser, J.-E.; Humphry-Baker, R.; Grätzel, M. *J. Am. Chem. Soc.* **2004**, *126*, 7164. (d): Teng, C.; Yang, X.; Yuan, C.; Li, C.; Chen, R.; Tian, H.; Li, S.; Hagfeldt, A.; Sun, L. *Org. Lett.* **2009**, *11*, 5542.

(96): Kuciauskas, D.; Freund, M. S.; Gray, H. B.; Winkler, J. R.; Lewis, N. S. *J. Phys. Chem. B* **2000**, *105*, 392.

(97): Connelly, N. G.; Geiger, W. E. *Chem. Rev.* **1996**, *96*, 877.

(98): Papageorgiou, N.; Grätzel, M.; Infelta, P. P. *Solar Energy Materials and Solar Cells* **1996**, *44*, 405.

(99): Lee, J.-J.; Coia, G. M.; Lewis, N. S. *J. Phys. Chem. B* **2004**, *108*, 5269.

(100): (a): Zistler, M.; Wachter, P.; Wasserscheid, P.; Gerhard, D.; Hinsch, A.; Sastrawan, R.; Gores, H. J. *Electrochimica Acta* **2006**, *52*, 161. (b): Papageorgiou, N.; Athanassov, Y.; Armand, M.; Bonhote, P.; Pettersson, H.; Azam, A.; Gratzel, M. *J. Electrochem. Soc.* **1996**, *143*, 3099.

(101): Nelson, J. J.; Amick, T. J.; Elliott, C. M. *J. Phys. Chem. C*. **2008**, *112*, 18255.

(102): (a): Agarwal, J.; Shaw, T. W.; Stanton, C. J.; Majetich, G. F.; Bocarsly, A. B.; Schaefer, H. F. *Angew. Chemie Int. Ed.* **2014**, *53*, 5152. (b): Antilla, J. C.; Baskin, J. M.; Barder, T. E.; Buchwald, S. L. *J. Org. Chem*. **2004**, *69*, 5578. (c): Grundemann, S.; Kovacevic, A.; Albrecht, M.; Faller, J. W.; Crabtree, R. H.; Gru, S. *J. Am. Chem. Soc.* **2002**, *5*, 10473.

(103): (a): Indumathy, R.; Radhika, S.; Kanthimathi, M.; Weyhermuller, T.; Unni Nair, B. *J. Inorg. Biochem.* **2007**, *101*, 434. (b): Prasad, J.; Peterson, N. C. *Inorg. Chem*. **1969**, *8*, 1622. (c): Sapp, S. A.; Elliott, C. M.; Contado, C.; Caramori, S.; Bignozzi, C. A. *J. Am. Chem. Soc*. **2002**, *124*, 11215.

(104): (a):Leigh, V.; Ghattas, W.; Lalrempuia, R.; Muller-Bunz, H.; Pryce, M. T.; Albrecht, M. *Inorg. Chem*. **2013**, *52*, 5395. (b): Park, H.-J.; Chung, Y. K. *Dalton Trans*. **2012**, *41*, 5678. (c): Kim, H.-M.; Jeong, D.; Noh, H. C.; Kang, Y. K.; Chung, Y. K. *Bull. of the Korean Chem. Soc.* **2014**, *35*, 448.

(105): Aribia, K. B.; Moehl, T.; Zakeeruddin, S. M.; Gratzel, M. *Chem. Sci.* **2013**, *4*, 454.

(106): Hancock, R. D.; Martell, A. E. *Chem. Rev.* **1989**, *89*, 1875.

(107): Kashif, M. K.; Nippe, M.; Duffy, N. W.; Forsyth, C. M.; Chang, C. J.; Long, J. R.; Spiccia, L.; Bach, U. *Angew. Chem. Int. Ed.* **2013**, *52*, 5527.

(108): (a): Aresta, M.; Dibenedetto, A.; Angelini, A. *Chem. Rev*. **2013**, *114*, 1709. (b): Benson, E. E.; Kubiak, C. P.; Sathrum, A. J.; Smieja, J. M. *Chem. Soc. Rev*. **2009**, *38*, 89.

(109): (a): Behr, A. *Carbon dioxide activation by metal complexes*, 1988. (b): Saveant, J.-M. *Chem. Rev.* **2008**, *108*, 2348. (c): Appel, A. M.; Bercaw, J. E.; Bocarsly, A. B.; Dobbek, H.; DuBois, D. L.; Dupuis, M.; Ferry, J. G.; Fujita, E.; Hille, R.; Kenis, P. J. A.; Kerfeld, C. A.; Morris, R. H.; Peden, C. H. F.; Portis, A. R.; Ragsdale, S. W.; Rauchfuss, T. B.; Reek, J. N. H.; Seefeldt, L. C.; Thauer, R. K.; Waldrop, G. L. *Chem. Rev.* **2013**, *113*, 6621. (d): Yui, T.; Tamaki, Y.; Sekizawa, K.; Ishitani, O. *Top. Curr. Chem.* **2011,** *303*, 151. (e): Reithmeier, R.; Bruckmeier, C.; Rieger, B. *Catalysts* **2012**, *2*, 544-571. (f): Xiaoding, X.; Mouijn, J.A. *Energy & Fuels*, **1996**, *10*, 305-325. Mikkelsen, M.; Jorgensen, M.; Krebs, F.C. *Energy & Environmntal Science* **2010**, *3*, 43-81. Schneider, J.; Jia, H.; Muckerman, J. T.; Fujita E. *Chem. Soc. Rev.* **2012**, *41*, 2036-2051.

(110): Smieja, J. M.; Kubiak, C. P. *Inorg. Chem.* **2010**, *49*, 9283.

(111): (a): Ishida, H.; Tanaka, K.; Tanaka, T. *Organometallics* **1987**, *6*, 181. (b): Pugh, J. R.; Bruce, M. R. M.; Sullivan, B. P.; Meyer, T. J. *Inorg. Chem.* **1991**, *30*, 86. (c): Chen, Z.; Chen, C.; Weinberg, D. R.; Kang, P.; Concepcion, J. J.; Harrison, D. P.; Brookhart, M. S.; Meyer, T. J. *Chem. Commun.* **2011**, *47*, 12607. (d): Chen, Z.; Concepcion, J. J.; Brennaman, M. K.; Kang, P.; Norris, M. R.; Hoertz, P. G.; Meyer, T. J. *Proc. Natl Acad. Sci. U.S.A.* **2012**, *109*, 15606.

(112): (a): Meshitsuka, S.; Ichikawa, M.; Tamaru, K. *J. Chem. Soc., Chem. Commun.* **1974**, 158. (c): Lieber, C. M.; Lewis, N. S. *J. Am. Chem. Soc.* **1984**, *106*, 5033. (b):Ogata, T.; Yanagida, S.; Brunschwig, B. S.; Fujita, E. *J. Am. Chem. Soc.* **1995**, *117*, 6708.

(113): (a): Hammouche, M.; Lexa, D.; Momenteau, M.; Saveant, J. M. *J. Am. Chem. Soc.* **1991**, *113*, 8455. (b): Bhugun, I.; Lexa, D.; Saveant, J.-M. *J. Am. Chem. Soc.* **1996**, *118*, 1769. (c): Costentin, C.; Drouet, S.; Robert, M.; Saveaant, J.-M. *Science* **2012**, *338*, 90.

(114): (a): Ratliff, K. S.; Lentz, R. E.; Kubiak, C. P. *Organometallics* **1992**, *11*, 1986. (b): Rakowski Dubois, M.; Dubois, D. L. *Acc. Chem. Res.* **2009**, *42*, 1974. (c): Thoi, V. S.; Chang, C. J. *Chem. Commun.* **2011**, *47*, 6578. (e): Froehlich, J. D.; Kubiak, C. P. *Inorg. Chem.* **2012**, *51*, 3932.

(115): (a): Bolinger, C. M.; Story, N.; Sullivan, B. P.; Meyer, T. J. *Inorg. Chem.* **1988**, *27*, 4582. (b): Angamuthu, R.; Byers, P.; Lutz, M.; Spek, A. L.; Bouwman, E. *Science* **2010**, *327*, 313. (c): Bourrez, M.; Molton, F.; Chardon-Noblat, S.; Deronzier, A. *Angew. Chem. Int. Ed.* **2011**, *50*, 9903. (d): Kauffman, D. R.; Alfonso, D.; Matranga, C.; Qian, H.; Jin, R. *J. Am. Chem. Soc.* **2012**, *134*, 10237. (f): Jupally, V. R.; Dharmaratne, A. C.; Crasto, D.; Huckaba, A. J.; Kumara, C.; Nimmala, P. R.; Kothalawala, N.; Delcamp, J. H.; Dass, A. *Chem. Commun.* **2014**, *50*, 9895. (g): (h): Sampson, M. D.; Nguyen, A. D.; Grice, K. a; Moore, C. E.; Rheingold, A. L.; Kubiak, C. P. *J. Am. Chem. Soc.* **2014**, *136*, 5460. (i): Agarwal, J.; Shaw, T. W.; Stanton, C. J.; Majetich, G. F.; Bocarsly, A. B.; Schaefer, H. F. *Angew. Chemie Int. Ed.* **2014**, *53*, 5152. (j): Raebiger, J. W.; Turner, J. W.; Noll, B. C.; Curtis, C. J.; Miedaner, A.; Cox, B.; DuBois, D. L. *Organometallics* **2006**, *25*, 3345.

(116): (a): Thoi, V. S.; Kornienko, N.; Margarit, C. G.; Yang, P.; Chang, C. J. *J. Am. Chem. Soc.* **2013**, *135*, 14413. (b): Bonin, J.; Robert, M.; Routier, M. *J. Am. Chem. Soc.* **2014**. (c): Dhanasekaran, T.; Grodkowski, J.; Neta, P.; Hambright, P.; Fujita, E. *J. Phys. Chem. A* **1999**, *103*, 7742. (d): V. A.; Takeda, H.; Koizumi, H.; Okamoto, K.; Ishitani, O. *Chem. Commun.* **2014**, *50*, 1491. (e): Tamaki, Y.; Koike, K.; Morimoto, T.; Yamazaki, Y.; Ishitani, O. *Inorg. Chem.* **2013**, *52*, 11902.

(117): (a): Takeda, H.; Koike, K.; Inoue, H.; Ishitani, O. *J. Am. Chem. Soc.* **2008**, *130*, 2023–2031. (b): Kou, Y.; Nabetani, Y.; Masui, D.; Shimada, T.; Takagi, S.; Tachibana, H.; Inoue, H. *J. Am. Chem. Soc.* **2014**, *136*, 6021. (c):Tamaki, Y.; Koike, K.; Morimoto, T.; Yamazaki, Y.; Ishitani, O. *Inorg. Chem.* **2013**, *52*, 11902. (d): Zhao, L.; Odaka, H.; Ono, H.; Kajimoto, S.; Hatanaka, K.; Hobley, J.; Fukumura, H. *Photochem. Photobiol. Sci*. **2005**, *4*, 113.

(118): Nakada, A.; Koike, K.; Nakashima, T.; Morimoto, T.; Ishitani, O. *Inorg. Chem.* **2015**.

(119): (a): Casson, L. A.; Muzzioli, S.; Raiteri, P.; Skelton, B. W.; Stagni, S.; Massi, M.; Brown, D. H. *Dalt. Trans*. **2011**, *40*, 11960. (b):Vaughan, J. G.; Reid, B. L.; Wright, P. J.; Ramchandani, S.; Skelton, B. W.; Raiteri, P.; Muzzioli, S.; Brown, D. H.; Stagni, S.; Massi, M. *Inorg. Chem.* **2014**, *53*, 3629. (c): Casson, L. a; Muzzioli, S.; Raiteri, P.; Skelton, B. W.; Stagni, S.; Massi, M.; Brown, D. H. *Dalton Trans*. **2011**, *40*, 11960. (d): Li, X.-W.; Li, H.-Y.; Wang, G.-F.; Chen, F.; Li, Y.-Z.; Chen, X.-T.; Zheng, Y.-X.; Xue, Z.-L. *Organometallics* **2012**, *31*, 3829.

(120): *For more information about NHC ligands see:* (a): *Herrmann, W. A. A. Angew. Chem. Int. Ed.* ***2002***, *41*, 1290. (b): Herrmann, W. A.; Köcher, C. *Angew. Chem. Int. Ed.* **1997**,

36, 2162. (c): Peris, E.; Crabtree, R. H. *Coord. Chem. Rev.* **2004**, *248*, 2239. (d) Hopkinson, M. N.; Richter, C.; Schedler, M.; Glorius, F. *Nature* **2014**, *510*, 485.

(121): (a): Moya, S. A.; Guerrero, J.; Pastene, R.; Sartori, R.; Schmidt, R.; Sariego, R.; Sanz-Aparicio, J.; Fonseca, I.; Martinez-Ripoll, M. *Inorg. Chem.* **1994**, *33*, 2341. (b): Berger, S.; Klein, A.; Kaim, W.; Fiedler, J. *Inorg. Chem.* **1998**, *37*, 5664.

(122): *For more information about fac-Ir(ppy)$_3$ and other Ir photosensitizers see*: (a): Nguyen, J. D.; D'Amato, E. M.; Narayanam, J. M. R.; Stephenson, C. R. J. *Nat. Chem.* **2012**, *4*, 854. (b): Holzer, W.; Penzkofer, A.; Tsuboi, T. *Chem. Phys*. **2005**, *308*, 93.

(123): *For more information about BIH see:* (a): Naab, B. D.; Guo, S.; Olthof, S.; Evans, E. G. B.; Wei, P.; Millhauser, G. L.; Kahn, A.; Barlow, S.; Marder, S. R.; Bao, Z. *J. Am. Chem. Soc.* **2013**, *135*, 15108. *(b):* Wei, P.; Menke, T.; Naab, B. D.; Leo, K.; Riede, M.; Bao, Z. *J. Am. Chem. Soc*. **2012**, *10*, *3999*. (c): (1) Wei, P.; Oh, J. H.; Dong, G.; Bao, Z. *J. Am. Chem. Soc*. **2010**, *132*, 8852. (d): (1) Zhu, X.-Q.; Zhang, M.-T.; Yu, A.; Wang, C.-H.; Cheng, J.-P. *J. Am. Chem. Soc.* **2008**, *130*, 2501.

(124): Casper, J. V.; Meyer, T. J. *J. Phys. Chem.* **1983**, *6*, 952.

(125): (a): Agarwal, J.; Shaw, T. W.; Stanton, C. J.; Majetich, G. F.; Bocarsly, A. B.; Schaefer, H. F. *Angew. Chemie Int. Ed.* **2014**, *53*, 5152. (b): Antilla, J. C.; Baskin, J. M.; Barder, T. E.; Buchwald, S. L. *J. Org. Chem.* **2004**, *69*, 5578.

(126): Grundemann, S.; Kovacevic, A.; Albrecht, M.; Faller, J. W.; Crabtree, R. H.; Gru, S. *J. Am. Chem. Soc.* **2002**, *5*, 10473.

(127): Li, X.-W.; Li, H.-Y.; Wang, G.-F.; Chen, F.; Li, Y.-Z.; Chen, X.-T.; Zheng, Y.-X.; Xue, Z.-L. *Organometallics* **2012**, *31*, 3829.

(128): Xu, Z.-L.; Li, H.-X.; Ren, Z.-G.; Du, W.-Y.; Xu, W.-C.; Lang, J.-P. *Tetrahedron* **2011**, *67*, 5282.

(129): Vaughan, J. G.; Reid, B. L.; Ramchandani, S.; Wright, P. J.; Muzzioli, S.; Skelton, B. W.; Raiteri, P.; Brown, D. H.; Stagni, S.; Massi, M. *Dalton Trans.* **2013**, *42*, 14100.

(130): Feu, K. S.; Deobald, A. M.; Narayanaperumal, S.; Corrêa, A. G.; Weber Paixão, M. *European J. Org. Chem.* **2013**, *2013*, 5917.

(131): Starkulla, G. F.; Klenk, S.; Butschies, M.; Tussetschlager, S.; Laschat, S. *J. Mater. Chem.* **2012**, *22*, 21987.

(132): Zhu, X.-Q.; Zhang, M.-T.; Yu, A.; Wang, C.-H.; Cheng, J.-P. *J. Am. Chem. Soc.* **2008**, *130*, 2501.

(133): (a): Darensbourg, D. J.; Wiegreffe, H. P.; Wiegreffe, P. W. *J. Am. Chem. Soc.* **1990**, *112*, 9252. (b): Graham, P. M.; Mocella, C. J.; Sabat, M.; Harman, W. D. *Organometallics* **2005**, *24*, 911.

(134): Gonzalez-Baro, A. C.; Pis-Diez, R.; Piro, O. E.; Parajon-Costa, B. S. *Polyhedron* **2008**, *27*, 502.

(135): *For more information on Au nanoparticle synthesis, see:* (a): Jupally, V. R.; Kota, R.; Dornshuld, E. Van; Mattern, D. L.; Tschumper, G. S.; Jiang, D.; Dass, A. *J. Am. Chem. Soc*.

2011, *133*, 20258. (b): Kumara, C.; Dass, A. *Nanoscale* **2011**, *3*, 3064. (c): Nimmala, P. R.; Dass, A. *J. Am. Chem. Soc*. **2011**, *133*, 9175. (d): Dass, A. *J. Am. Chem. Soc*. **2009**, *131*, 11666.

(136): Li, G.; Jin, R. *Acc. Chem. Res*. **2013**, *46*, 1749.

(137): Kauffman, D. R.; Alfonso, D.; Matranga, C.; Qian, H.; Jin, R. *J. Am. Chem. Soc.* **2012**, *134*, 10237.

(138): Zhu, W.; Michalsky, R.; Metin, Ö.; Lv, H.; Guo, S.; Wright, C. J.; Sun, X.; Peterson, A. A.; Sun, S. *J. Am. Chem. Soc*. **2013**, *135*, 16833.

(139): Mistry, H.; Reske, R.; Zeng, Z.; Zhao, Z.-J.; Greeley, J.; Strasser, P.; Cuenya, B. R. *J. Am. Chem. Soc*. **2014**, *136*, 16473.

(140): (a): Huang, X.; Nakanishi, K.; Berova, N. *Chirality* **2000**, *12*, 237. (b): Tanaka, T.; Osuka, A. *Chem. Soc. Rev*. **2015**, *44*, 943. (c): Meunier, B. *Chem. Rev*. **1992**, *92*, 1411.

VITA

EDUCATION

The University of Mississippi, Oxford, MS, Jun 2011-May 2015
PhD in Chemistry
Advisors: T. Keith Hollis (Jun 2011-Jun 2013), Jared Delcamp (Jul 2013-present)

Murray State University, Murray, KY, Aug 2007 – May 2011
B.S. in Chemistry, Departmental Honors, University Honors
Advisor: Kevin Revell

RESEARCH EXPERIENCE

Graduate Research, Jun 2011-Present

- Development of CCC-NHC pincer ligands and the synthesis of transition metal N-heterocyclic carbene complexes as catalysts and/or application in organic light emitting diodes (Hollis).
- Development of CO_2 reduction catalyst systems based on Rhenium and Chromium complexes as well as Au-Nanomolecules (Delcamp).
- Synthesis of novel heterocyclic structures for use in dye-sensitized solar cells (Delcamp).

Undergraduate Research, Jan 2007-Dec 2010

- Progress towards the development of oligo(arylacetylenes) for organic photovoltaic applications.
  -Presented results orally at Kentucky Academy of Sciences Annual Meeting in Highland Heights, KY 2009

- Growth and development analysis of an invasive plant species *Alternanthera philoxeroides* using matrix analysis in order to understand optimal methods for its control.
  -Presented results orally at the Joint (MAA, AMA) Mathematical Meetings in New Orleans, LA 2011.

PUBLICATIONS

Graduate Publications:

1) **Huckaba, A.J.**, Giordano, F. McNamara, L. E., Dreux, K. Hammer, N. I., Tchumper, G. S., Zakeeruddin, S. M., Gratzel, M., Nazeeruddin, M. K., Delcamp, J. H. "Indolizine-Based Donors as Organic Sensitizer Coponents for Dye-Sensitized Solar Cells." *Advanced Energy Materials.* Manuscript Accepted. DOI: 10.1002/aenm.201401629

2) Jupally, V. R., Dharmaratne, A. C., Crasto, D., **Huckaba, A. J.,** Kumara, C., Nimmala, P. R., Kothalawala, N., Delcamp, J. H., Dass, A. "Au137(SR)56 Nanomolecules: Composition, Optical Spectroscopy, Electrochemistry, and Electrocatalytic Reduction of CO2." *Chem. Commun.* **2014**, 50, 9895-9898.

3) **Huckaba**, **A. J.**, Hollis, T. K. "An Efficient Synthesis of Bis-1,3-(3′-aryl-N-heterocycl-1′-yl)arenes as CCC-NHC Pincer Ligand Precursors." Howell, T.O., *Organic Letters* **2014** 16 (9), 2570-2572.

4) **Huckaba, A. J.;** Hollis, T. K.; Reilly, S. W. "Homobimetallic Rh NHC Complexes as Versatile Catalysts for Hydrosilylation of a Multitude of Substrates in the Presence of Ambient Air." *Organometallics* **2013** 32 (21), 6248-6256.

5) **Huckaba, A. J.;** Cao, B.; Hollis, T. K.; Valle, H. U.; Kelly, J. T.; Hammer, N. I.; Oliver, A. G.; Webster, C. E. "Platinum CCC-NHC benzimidazolyl pincer complexes: synthesis, characterization, photostability, and theoretical investigation of a blue-green emitter." *Dalton Trans.* **2013**, 42, 8820.

6) **Huckaba, A. J.;** Hollis, T. K.; Howell, T. O.; Valle, H. U.; Wu, Y. "Synthesis and Characterization of a 1,3-Phenylene-Bridged N-Alkyl Bis(benzimidazole) CCC-NHC Pincer Ligand Precursor: Homobimetallic Silver and Rhodium Complexes and the Catalytic Hydrosilylation of Phenylacetylene." *Organometallics* **2013**, *32*, 63.

Undergraduate Publications:

1) Erwin, S.; **Huckaba, A.;** He, K. S.; McCarthy, M. *Journal of Plant Ecology* **2012**, *6*, 150.

PATENTS

1) **Huckaba, A.J.**, Delcamp, J.H. "Indolizine-Based Dyes for Dye-Sensitized Solar Cells." US. Provisional Patent Award 62031031.

PRESENTATIONS

October 2014. "Indolizine-Based Donors as Organic Sensitizer Coponents for Dye-Sensitized Solar Cells." South Eastern Regional Meeting of the American Chemical Society, Nashville, TN.
January, 2011. "Using matrix analysis to model the spread of an invasive plant, *"alternanthera philoxeroides.""* Joint Mathematics Meeting in New Orleans, LA.
August, 2010. "Correlation and cluster analysis in epidemiology" Mathfest, Pittsburgh, PA.
November, 2009. "Highly conjugated polyphenylene ethynyl oligomers" 95th KAS meeting, Highland Heights, KY.

POSTERS

April 2014. "Dye-Sensitized Solar Cells Utilizing Indolizine Subunits as Donors: An Exceptionally Strong Donor." Mississippi EPSCoR Annual Meeting
February 18, 2014. "Dye-Sensitized Solar Cells Utilizing Indolizine Subunits as Donors: An Exceptionally Strong Donor." Research Day at the Capitol, Jackson, Miss.
October, 2011. "Synthesis and Characterization of benzimidazolyl CCC-NHC pincer complexes." National Center for Natural Products Research Poster Competition.

AWARDS

Undergraduate: Robertah Whitney Scholarship (2009)
Departmental Study Abroad Scholarship (2009)
Most Outstanding Chemistry Major (2011)
Honors Diploma (2011)

TEACHING EXPERIENCE

February 2015 – Guest Lecture, Elementary Organic Chemistry II, Dr. Jared Delcamp. "Fundamentals of Heterogeneous Hydrogenations."
January 2015 – Guest Lecture, Elementary Organic Chemistry II, Dr. Jared Delcamp. "Infrared Spectroscopy."
October 2014 - Guest Lecture, Elementary Organic Chemistry, Dr. Jared Delcamp, "Introduction to Electron Pushing and Acid-Base Reactions"
April 2014 - Guest Lecture, Advanced Organic Synthesis: Structure and Mechanism, Dr. Jared Delcamp, "Determinining Reaction Mechanism using Product Distributions"
March 2014 - Guest Lecture, Advanced Organic Synthesis: Structure and Mechanism, Dr. Jared Delcamp, "Determinining Reaction Mechanism Using Reaction Intermediates"

August 2013 - Guest Lecture, Advanced Organic Synthesis: Structure and Mechanism, Dr. Jared Delcamp, "Carbonyl Reactions and Functional Group Transformations."
August 2012-May 2013, Teaching Assistant, Organic Chemistry Lab I & II, University of Mississippi, Oxford, MS, Dr. Safo Aboaku.

- Instructed two classes of 20+ students in lab technique and data collection.
- Graded student exams and reports.

August 2011-May 2012, Teaching Assistant, General Chemistry Lab I & II, University of Mississippi, Oxford, MS, Dr. John Wigginton.

- Instructed two classes of 20+ students in fundamental chemistry lab technique and data collection
- Graded student exams.

MENTORING EXPERIENCE

Trained and mentored the following students:

Undergraduates

- Drew Puneky (responsible for dyes DP1, DP2, DP3)
- Emily Anne Sharpe (responsible for Hole Transporting Materials HTM2, HTM3)
- Tana Rill (working in DSC sensitizer synthesis)
- Scott Murphy (working in DSC sensitzer synthesis)

Secondary School Students

- Aykeyvius Harris (worked towards CO_2 photocatalysts)
- Keshuna Tables (worked towards CO_2 photocatalysts)